ABSTRACT

Title of Dissertation: PRUSSIAN BLUE NANOIMMUNOTHERAPIES FOR NEUROBLASTOMA

Juliana Cano-Mejia, Doctor of Philosophy, 2019

Dissertation directed by: Adjunct Assistant Professor,
Rohan Fernandes, Ph.D.,
Fischell Department of Bioengineering,
University of Maryland

Neuroblastoma is the most common extracranial solid tumor in children, accounting for 15% of cancer-related deaths. Despite improvements in diagnosis and surgical techniques, neuroblastoma remains challenging to treat due to the heterogeneity of the tumor, low neoantigen expression, immunosuppressive tumor environment, and high recurrence rate. We have therefore engineered a nanoimmunotherapy that combines the advantages of nanotechnology and immunotherapy to combat the aforementioned challenges in treating neuroblastoma. Specifically, our ensemble comprises of Prussian blue nanoparticles (PBNPs) biofunctionalized with the immune adjuvant CpG-oligodeoxynucleotide (CpG). We utilize PBNPs for photothermal therapy (PTT), which ablates tumor cells and releases tumor antigens and adjuvants that increase tumor immunogenicity. Additionally, the PBNPs are biofunctionalized with CpG (CpG-PBNPs) to serve as a depot for local delivery of exogenous immune adjuvants that play an important role in breaking

tolerance to tumor antigens and improving tumor antigen presentation. We hypothesize that this approach of targeting tumor cells, antigen presenting cells, and T cells, may hold the key in converting a non-responsive "cold" tumor such as neuroblastoma into a responsive "hot" tumor, leading to better treatments.

We first describe the synthesis and characterization of CpG-PBNPs using a facile layer-by-layer coating scheme. The resultant nanoparticles exhibit monodisperse size distributions, multiday stability, and are not cytotoxic. The strong, intrinsic absorption of PBNPs in the CpG-PBNPs is leveraged to administer PTT (CpG-PBNP-PTT) that triggers immunogenic tumor cell death releasing tumor antigens, which increases tumor antigenicity. Simultaneously, the CpG coating functions as an exogenous adjuvant that complements the endogenous adjuvants released by the CpG-PBNP-PTT (e.g. ATP, calreticulin, and HMGB1), increasing adjuvanticity. When administered in a murine model of neuroblastoma, CpG-PBNP-PTT results in complete tumor regression in a significantly higher proportion (70%) of treated animals relative to controls. Further, the long-term surviving, CpG-PBNP-PTT-treated animals reject tumor rechallenge suggesting that our nanoimmunotherapy generates immunological memory. When we treat a synchronous model of neuroblastoma, 50% of nanoimmunotherapy-treated mice show complete eradication of both tumors compared to controls, which showed no survival efficacy. Our findings show the importance of simultaneous cytotoxicity, antigenicity, and adjuvanticity in generating robust and persistent antitumor immune responses. The strategies described in this dissertation encompass novel examples of nanoimmunotherapies to be applied in the clinic for the treatment of neuroblastoma.

PRUSSIAN BLUE NANOIMMUNOTHERAPIES FOR NEUROBLASTOMA

By

Juliana Cano-Mejia

Dissertation submitted to the Faculty of the Graduate School of the
University of Maryland, College Park, in partial fulfillment
of the requirements for the degree of
Doctor of Philosophy
2019

Advisory Committee:
Assistant Professor Dr. Rohan Fernandes, Chair
Professor Dr. John P. Fisher, Chair
Professor Dr. William E. Bentley
Assistant Professor Dr. Huang Chiao Huang
Associate Professor Dr. Nam Sun Wang, Dean's Representative

Acknowledgements

I would like to first express my deepest gratitude to my advisor, Dr. Rohan Fernandes. Thank you for supporting me, encouraging me, and challenging me throughout my PhD. Being a member of your lab has been a great honor. I am most grateful for your profound empathy and genuine belief in my success. I will forever consider you a great mentor and friend in my life.

Thank you to my committee members Dr. William Bentley, Dr. John Fisher, Dr. Huang Chiao Huang, Dr. Christopher Jewell, and Dr. Nam Sun Wang for your support throughout my studies and professional development.

I would also like to thank all the lab members (past and present) from the Fernandes Lab. I have enjoyed my time working with you and have learned so much from all of you. I would like to specially thank Dr. Elizabeth Sweeney and Dr. Rachel Burga for all your help and stimulating discussions over the last few years, and specially for you friendship.

I was very lucky to be part of and do research at several institutions over my graduate studies, and I would like to acknowledge all my mentors and colleagues at the Fischell Department of Bioengineering at the University of Maryland, the Sheikh Zayed Institute for Pediatric Surgical Innovation at the Children's National Health System, and the Cancer Center at the George Washington University.

Lastly, I would like to say a heartfelt thank you to my family for always believing in me, and encouraging me in everything I do. I am forever indebted to my

parents for giving me the opportunities and experiences that have allowed me to get to this point.

This work was supported by the National Science Foundation Fellowship (Award Number HRD-1249262) and Alex's Lemonade Stand 'A' Grant Award. Funding and resources were also provided by the Fischell Department of Bioengineering at the University of Maryland, the Sheikh Zayed Institute for Pediatric Surgical Innovation at the Children's National Health System, and the Cancer Center at the George Washington University.

Table of Contents

List of Figures

W for 10 minutes), measured 24 h after treatment. (* significant difference, $p < 0.001$ compared with vehicle).

Figure 2.3. Release of CpG from CpG-PBNPs. (A) Fraction of CpG released from CpG-PBNPs upon addition of ethidium bromide (EtBr) relative to equal concentrations of free CpG added to EtBr (* significant difference, $p < 0.05$). (B) Percent normalized CpG bound in the CpG-PBNPs as a function of time and pH. (C) Fraction of CpG released from CpG-PBNPs after PTT at different laser powers (0.25 – 1.25 W) and different concentrations (0.1 – 0.5 mg/mL). Etbr was added as described above.

Figure 2.4. Photothermal heating curves of CpG-PBNPs. (A) Photothermal heating curves (temperature-time profiles) of varying concentrations (0.025 – 0.5 mg/mL) of CpG-PBNPs irradiated by an 808 nm NIR laser for 10 minutes at a power of 0.75 W (1.875 W/cm^2). (B) Photothermal heating of 1 mg/mL CpG-PBNPs using varying NIR laser powers (0.75 - 1.25 W) for 10 minutes.

Figure 3.1. Prussian blue nanoparticle-based photothermal therapy (PBNP-PTT) generates a thermal window of immunogenic cell death (ICD). A) PBNPs that are administered to tumors and illuminated with a near infrared light trigger tumor cell death by PBNP-PTT. B) (Middle). When an optimal temperature range (thermal dose) of PBNP-PTT is administered to tumors, the tumor cells undergo ICD marked by the release of ATP, HMGB1, and increased expression of surface calreticulin. These effects elicit a potent antitumor immune response that is associated with improved therapeutic outcomes. If the thermal dose of PBNP-PTT is either too low (Bottom) or too high (Top), the tumor cells may still be killed by the effects of PBNP-PTT, but the dying cells do not trigger a favorable antitumor immune response because they do not undergo *bona fide* ICD.

Figure 3.2. PBNP-PTT increases neuroblastoma cell temperature and triggers their death in a temperature (thermal dose)-dependent manner *in vitro* and *in vivo.* A-C) 50,000 Neuro2a cells were seeded in 96-well plates, treated with the listed concentration of PBNPs, and subjected to ten minutes of illumination by an 808 NIR laser at 1.5 W/cm^2. Values represent means ± standard deviation (SD); n = 3/group. A) Temperature-time profiles of the varying PTT conditions as measured by a thermal camera at one-minute intervals. B) Final average temperatures achieved by Neuro2a cells after ten minutes as a function of varying PTT conditions. C) *In vitro* Neuro2a cell viability post-treatment with vehicle or varying doses of PBNPs or PBNP-PTT, measured 24 hours after treatment. *** $p < 0.001$ compared to Vehicle; # $p < 0.05$ compared to 0.05 mg/mL PBNP-PTT+ Laser. (D-E) Mice bearing ~5mm Neuro2a neuroblastoma tumors were treated with varying doses of PBNP-PTT; low, medium, and high PTT, administered by intratumoral injection of PBNPs followed by ten minutes of NIR laser irradiation. Values represent means ± SD; $n \geq 4$/group. D) Average tumor temperatures attained by Neuro2a tumor-bearing mice treated with low thermal dose PBNP-PTT (Low PTT; blue), medium thermal dose PBNP-PTT (Medium PTT; orange), and high thermal dose PBNP-PTT (High PTT; red) as measured by thermal camera. Listed numbers indicate the final average tumor temperatures attained.

E) Survival of Neuro2a tumor-bearing mice treated with Vehicle (black), Low PTT (blue), Medium PTT (orange), and High PTT (red).

Figure 3.3 Neuroblastoma tumor growth after no treatment or treatment with varied levels (doses) of PBNP-PTT. Neuro2a tumor-bearing mice were: A) Untreated, or treated with B) Low-dose PBNP-PTT (Low PTT), C) Medium-dose PBNP-PTT (Medium PTT), and D) High-dose PBNP-PTT (High PTT). Each line represents the tumor growth trajectory of an individual mouse ($n \geq 4$ per group).

Figure 3.4. Neuro2a cells treated with PBNP-PTT *in vitro* exhibit an optimal temperature range for increased expression of ICD markers. A) Temperature-time profiles of samples containing 10 million Neuro2a cells treated 0.75 W laser, > 1 W laser, 0.75 W laser + 0.05 mg/mL PBNP, 0.75 W laser + 0.1 mg/mL PBNP, and > 1 W laser + 0.16 mg/mL PBNP. B) Intracellular ATP in the various treatment groups (as a % of the vehicle-treated group). C) Intracellular HMGB1 in the various treatment groups (as a % of the vehicle-treated group). D) Surface calreticulin expression in the various treatment groups (as a % of the vehicle-treated group). Red boxes indicated the treatment temperatures ranges for which all three markers of ICD are expressed/present (to varied degrees).

Figure 3.5. Effect of treatment with PBNPs only (no heat) on cellular expression of ICD markers *in vitro* as measured by the three ICD hallmarks. Neuroblastoma (Neuro2a) cells (10 million cells/mL in 1.7 mL tubes) were subjected to treatment with vehicle and increasing concentrations of PBNPs, and markers of ICD were then analyzed (ATP release (A), HMGB1 release (B), and calreticulin exposure (C)). Representative histograms of D) HMGB1 and E) calreticulin, analyzed by flow cytometry, are shown.

Figure 3.6. *In vivo* tumor growth after prophylactic vaccination with vehicle-, PBNP-, laser-, or varied PBNP-PTT-treated neuroblastoma cells. Each line represents the tumor growth trajectory of an individual mouse (n=3-9 per group).

Figure 3.7. Animals vaccinated with PBNP-PTT-treated Neuro2a cells within the optimal temperature window (showing increased ICD markers) exhibit significantly increased protection against subsequent Neuro2a challenge. A) Temperature-time profiles of samples containing 10 million Neuro2a cells/mL treated 0.75 W laser, > 1 W laser, 0.75 W laser + 0.05 mg/mL PBNP, 0.75 W laser + 0.1 mg/mL PBNP, and > 1 W laser + 0.16 mg/mL PBNP that were vaccinated in naïve A/J mice (means ±SD; n = 4 replicates/group). B) Survival of mice challenged with 1 million Neuro2a cells that were previously vaccinated with vehicle, PBNP-, laser-, or PBNP-PTT-treated Neuro2a cells. n = 3-9/group; * $p < 0.05$ compared with all groups except 0.05 mg/mL PBNP-PTT.

Figure 3.8. PBNP-PTT-treated Neuro2a cells exhibit a thermal "window" of ICD, which is associated with improved protection against tumor challenge. A)

Expression of ICD markers as a function of thermal dose described in terms of cumulative equivalent minutes at 43 ^{o}C; a thermal dose parameter (CEM43)[38]. The grey shaded area represents the region of increased ICD elicited by PBNP-PTT B) % Survival of mice (at 100 days) challenged with Neuro2a tumors that were vaccinated with PBNP-PTT-treated Neuro2a cells. Improved long-term survival "mirrors" the thermal dose window shown in panel A.

Figure 4.1. Immunostimulatory properties of CpG-PBNPs. (A) Activation of dendritic cells (DCs) upon co-culture with CpG-PBNPs compared to free CpG, PBNPs, and media controls measured by flow cytometry. CD80 (red) and CD86 (blue) MFI of live CD11c+ positive cells (1 – 0.25 mg/mL). CpG concentrations are as follows: 40 μg/mL, 10 μg/mL, and 1 μg/mL. LPS concentration was 1 μg/mL (* significant difference relative to media-treated DCs for both CD80 and CD86 expression, $p < 0.05$). (B) Percent proliferation of CD8+ T cells co-cultured with DCs activated with CpG-PBNPs and controls (free CpG, PBNPs, and media) (1 – 0.25 mg/mL). Groups were treated with and without the antigen Trp2 (1.25 ng/well). (* significant difference relative to media-treated DCs in the presence of Trp2; $p < 0.05$; n.s., not significant relative to media-treated DCs in the presence of Trp2, $p > 0.05$)

Figure 4.2 Immunostimulatory properties of CpG-PBNPs. (A) CD40 MFI amongst CD11c+ positive cells. (B) % live CD11c+ positive cells treated with varying concentrations (1 – 0.25 mg/mL) CpG-PBNPs and controls (Free CpG, PBNPs. (C) % live cells treated with varying concentrations (1x-4x; 1 – 0.25mg/mL) CpG-PBNPs and controls (Free CpG, PBNPs) with and without the antigen Trp2. (D) % CD8+ positive cells treated with varying concentrations (1 – 0.25 mg/mL) CpG-PBNPs and controls (media, free CpG, PBNPs).

Figure 4.3. Induction of immunogenic cell death (ICD) by CpG-PBNP-PTT *in vitro*. (A) Intracellular ATP in the various treatment groups (as a % of the vehicle-treated group) (* significant difference relative to vehicle; $p < 0.05$). (B) Surface calreticulin expression in the various treatment groups (as a % of the vehicle-treated group). (C) Intracellular HMGB1 in the various treatment groups (as a % of the vehicle-treated group). All groups had concentrations of nanoparticles at 0.05 mg/mL. PTT groups were treated with a laser power of 0.75W for 10 minutes. Arrows denote the treatment groups where all 3 markers of ICD are expressed/present. Panels B and C were analyzed using flow cytometry and the trends in ICD markers were consistent across at least three separate studies.

Figure 4.4. Effect of the CpG-PBNP-based nanoimmunotherapy on tumor regression and long-term survival in the Neuro2a neuroblastoma mouse model. (A) Overview of the treatments. Mice bearing ~5 mm diameter Neuro2a neuroblastoma tumors were treated with CpG-PBNP-PTT and corresponding controls. The PTT-treated groups received 50 μL of 1 mg/mL CpG-PBNPs or PBNPs intratumorally (i.t.), and were irradiated by an 808 nm laser at 0.75 W for 10 minutes. Additionally, the

CpG-PBNP-PTT received two boosters with CpG-PBNP on Days 2 and 5. The CpG-PBNP-treated groups received 2 μg of conjugated CpG per dose by i.t. injection (Days 0, 2, and 5). CpG-treated groups received 10 μg of free CpG per dose by i.t. injection (Days 0, 2, and 5). (B) Temperature-time profiles of Neuro2a bearing mice treated intratumorally with 1mg/mL CpG-PBNPs (red) or PBNPs (blue) and irradiated with a NIR laser at 0.75 W for 10 minutes. (C) Kaplan-Meier survival plots of neuroblastoma tumor-bearing mice that were treated with CpG-PBNP-PTT, PBNP-PTT, Free CpG-PBNPs, Free CpG, or vehicle. Mice receiving CpG-PBNP-PTT showed significantly higher long-term survival (>100 days) compared with mice in the other groups (* significant difference compared to all other groups, $p < 0.05$, long-rank test, n=10/group).

Figure 4.5. Tumor growth curves for individual mice in the various treatment groups: (A) Vehicle, (B) CpG-treated, (C) CpG-PBNP-treated, (D) PBNP-PTT-treated, (E) CpG-PBNP-PTT-treated. Each line represents tumor growth measured in one mouse (numbers in parentheses in each panel A-E indicate number of long-term surviving mice in each group i.e. >60 day survival).

Figure 5.1. Effect of the CpG-PBNP-based nanoimmunotherapy on Neuro2a rechallenge of surviving mice. Long-term surviving mice rechallenged with Neuro2a cells 60-90 days after treatment showed complete tumor rejection (* significant difference compared to naïve mice, $p < 0.05$, n>=7/group).

Figure 5.2. Effect of the CpG-PBNP-based nanoimmunotherapy on tumor regression and long-term survival in the distal Neuro2a neuroblastoma mouse model. (A) Overview of the treatments. Mice bearing ~5 mm diameter Neuro2a neuroblastoma tumors were treated with CpG-PBNP-PTT + anti-CTLA-4 and corresponding controls. The PTT-treated groups received 50 μL of 1 mg/mL CpG-PBNPs or PBNPs intratumorally (i.t.), and were irradiated by an 808 nm laser at 0.75 W for 10 minutes. Additionally, the CpG-PBNP-PTT received two boosters with CpG-PBNP on Days 2 and 5 i.t. (black arrows). The groups that received anti-CTLA-4 got 150 μg of antibody on days 1, 5, and 8 intraperitoneally (i.p) (pink arrows) (B) Temperature-time profiles of Neuro2a bearing mice treated intratumorally with 1mg/mL CpG-PBNPs or PBNPs and irradiated with a NIR laser at 0.75 W for 10 minutes. (C) Kaplan-Meier survival plots of neuroblastoma tumor-bearing mice that were treated with PBNP-PTT, CpG-PBNP-PTT, PBNP-PTT + anti-CTLA-4, CpG-PBNP-PTT + anti-CTLA-4, or vehicle. Mice receiving CpG-PBNP-PTT + anti-CTLA-4 showed significantly higher long-term survival compared with mice in the other groups. (D) Long-term surviving mice rechallenged with Neuro2a cells 65 days after treatment showed complete tumor rejection (* significant difference compared to naïve mice, $p < 0.05$, n>=3/group).

Figure 5.3. Tumor growth curves for individual mice in the various treatment groups: (A,B) Vehicle, (C,D) PBNP-PTT-treated, (E,F) CpG-PBNP-PTT-treated,

(G,H) PBNP-PTT + anti-CTLA-4 - treated, (I,J) CpG-PBNP-PTT + anti-CTLA-4 - treated. Each line represents tumor growth measured in one mouse

Figure 6.1. Heating capabilities of of PTT vs iPTT *in vitro*. Photothermal heating curves (time-temperature profiles) of 200uL of 1 mg/mL PBNPs in water using NIR laser powers at (A) 80 mW, (B) 140 mW, and (C) 200 mW. Laser power was delivered using an 808 nm NIR laser (PTT; blue), or an 808 nm NIR laser through a spherical diffuser (iPTT; red).

Figure 6.2. Schematic illustration of PTT vs iPTT *in vivo* pilot study. Neuroblastoma tumor-bearing mice were intratumorally injected with 1 mg/mL PBNPs and treated with PTT or iPTT using an 808 nm NIR laser at a power of 200 mW for 10 minutes.

Figure 6.3. Heating capabilities of PTT vs iPTT *in vivo*. Photothermal heating curves (time-temperature profiles) of mice treated with iPTT or PTT. Mice bearing ~17 mm Neuro2a neuroblastoma tumors were treated with iPTT or PTT for 10 minutes after intratumoral (i.t) injection of PBNPs (50 uL of 1 mg/mL); laser power: 200 mV (n=3/group).

Figure 6.4. Characterization of 9464D cells. A) Expression of neuroblastoma-associated genes in the MYCN transgenic cell line 9464D. Total RNA was isolated and reverse transcribed to cDNA. Quantitative expression was determined for hMYCN (the human *MYCN* cDNA transgene used in the TH-MYCN transgenic mouse), *GD2 synthase*, *survivin*, *S100A6*, and *ODC* and related to the expression of the household gene PBGD. B) GD2 is greatly expressed in 9464D cells compared to Neuro2a cells.

Figure 6.5. Heating capabilities of 9464D cells after PBNP-PTT. A) Photothermal heating curves (temperature-time profiles) of 1.5 mg/mL PBNPs using varying NIR laser powers (0.2 – 1.5 W) for 10 minutes. B) Thermal dose after PBNP-PTT described in terms of cumulative equivalent minutes at 43 ^{o}C; a thermal dose parameter (CEM43).

Figure 6.6. Induction of immunogenic cell death (ICD) by PBNP-PTT in 9464D cells. A) Intracellular ATP in the various treatment groups (as a % of the vehicle-treated group). (B) Intracellular HMGB1 in the various treatment groups (as a % of the vehicle-treated group). (C) Surface calreticulin expression in the various treatment groups (as a % of the vehicle-treated group). Vehicle groups were treated with 10 μL of distilled water. All groups had concentration of nanoparticles of 1.5 mg/mL.

Figure 6.7. Effect of CpG-PBNP-based nanoimmunotherapy on tumor regression and survival in the 9464D neuroblastoma mouse model. Mice bearing ~5 mm diameter 9464D neuroblastoma tumors were treated with CpG-PBNP-PTT and corresponding controls. The PTT-treated groups received 50 μL of 1 mg/mL CpG-PBNPs or PBNPs intratumorally (i.t.), and were irradiated by an 808 nm laser at 0.75

W for 10 minutes. Additionally, the CpG-PBNP-PTT received two boosters with CpG-PBNP on Days 2 and 5 i.t. (A) Temperature-time profiles of 9464D bearing mice treated intratumorally with 1mg/mL CpG-PBNPs or PBNPs and irradiated with a NIR laser at 0.75 W for 10 minutes. (B-D) Tumor growth curves for individual mice in the various treatment groups. Each line represents tumor growth measured in one mouse (E) Kaplan-Meier survival plots of 9464D tumor-bearing mice that were treated with PBNP-PTT, CpG-PBNP-PTT, or left untreated. Mice receiving CpG-PBNP-PTT showed significantly higher long-term survival compared with the other groups. Ongoing study.

Figure 6.8: A hypothesized mechanism of action of the CpG-PBNP-PTT + anti-CLTA-4 nanoimmunotherapy is presented. 1) PTT-based destruction of tumors in a minimally invasive manner, 2) Release of tumor antigens and danger signals post-PTT providing an immunostimulatory, multi-antigen local effect, and 3) the use of CpG-PBNPs that improves the uptake and antigen presentation of DCs to T cells, activating them and unleashing a potent antitumor immune response. 4) I.p (systemically) administered anti-CTLA-4 reverses immunosuppression, unleashing the antitumor immune responses of endogenous immune cells, particularly T cells. The above processes combine to yield improved tumor responses and development of immunity against tumor rechallenge and distal tumors in a mouse model of neuroblastoma.

Appendix 1: PBNPs work as effective PTT agents. A) Photothermal heating of varying concentrations of PBNPs irradiated with a 808 nm NIR laser for 10 minutes at 1.875 W/cm^2 showing heating of the nanoparticles. B) PTT with 0.05 mg/mL PBNPs + 1.875 W/cm^2 laser fluence (using 808nm laser) results in significantly decreased proliferation of Neuro2a cells relative to controls using nanoparticles alone, laser alone, and left untreated (**$p<0.01$).

Appendix 2: Effect of PBNP-PTT on Neuro2a tumor growth. Representative photographs of Neuro2a tumor-bearing mice treated with: A) PBNP-PTT and B) remaining untreated. Representative, temporal images (Day 0, 2, and 6) of bioluminescent Neuro2a tumor-bearing mice that are C) PBNP-PTT treated and D) untreated (Scale bar = tumor bioluminescence intensity; $p/s/cm^2/sr$). E) Normalized tumor volume showing a marked reduction in Neuro2a tumor growth rate in PBNP-PTT treated mice relative to Untreated and Laser alone controls (**indicates significant decrease; $p< 0.001$).

Appendix 3. Immunostimulatory effects of PBNP-based PTT. Representative scatter plots of CD45+ cells in tumors of: A) Untreated and B) PTT-treated mice. C) %CD45+ cells in the tumors of untreated and PTT-treated mice showing significantly higher percentage of CD45+ cells in tumors of PTT-treated vs. untreated mice ($p=0.0294$). Representative scatter plots of CD3+ cells in tumors of: D) Untreated and E) PTT-treated mice. F) %CD3+ cells in the tumors of untreated and PTT-treated mice showing significantly higher percentage of CD3+ cells in tumors of PTT-treated vs. untreated mice ($p=0.0424$).

Appendix 4. Effect of photothermal immunotherapy (PTT+anti-CTLA-4 therapy) on tumor regression and long-term survival in the neuroblastoma mouse model. A) Representative image of a long-term surviving mouse treated with PTT+anti-CTLA-4 showing complete tumor regression (scale bar = bioluminescent intensity; p/s/cm^2/sr). B) Normalized tumor growth curves for tumor-bearing mice treated with PTT+anti-CTLA-4 (violet) or left untreated (black). C) Kaplan-Meier survival plots of neuroblastoma mice that were treated with PTT+anti-CTLA-4, anti-CLTA-4 alone, PTT alone, or untreated. Mice receiving photothermal immunotherapy showed significantly higher long-term survival (> 100 days) compared with mice in the other groups (log-rank test; $p<0.05$).

Appendix 5: Effect of PBNP-PTT+anti-CTLA-4 nanoimmunotherapy on tumor regression and long-term survival in a mouse model of neuroblastoma. A) Kaplan-Meier survival plots of Neuro2a tumor-bearing mice that were treated with PBNP-PTT + anti-CTLA-4, anti-CTLA-4 alone, PBNP-PTT alone, PBNPs alone, or untreated. Mice receiving PBNP-PTT + anti-CTLA-4 showed significantly higher long-term survival (<100 days) compared with mice in the other groups (log-rank test $p<0.05$, n>=5 per group). B) Kaplan-Meier survival plots of Neuro2a tumor-bearing mice depleted in CD4+ and CD8+ T cells. Depletion of CD4+ and CD8+ T cells (n=5 per group) effectively abrogated the therapeutic responses of the PBNP-PTT + anti-CTLA-4 nanoimmunotherapy (log-rank test, $p<0.005$).

Appendix 6. Effect of tumor rechallenge in combination photothermal immunotherapy-treated, long-term surviving mice. (A-B) Representative images showing protection against tumor rechallenge in A) photothermal immunotherapy-treated mice and B) tumor progression in naïve, untreated mice (scale bars = bioluminescent intensity; p/s/cm^2/sr). C) Tumor growth curves after challenge with 10^6 Neuro2a cells in untreated mice (naïve, black; n=3) and long-term surviving photothermal immunotherapy-treated mice (rechallenged, blue ; n=3) showing protection in the rechallenged group compared to progression in the naïve group. D) Kaplan-Meier survival plots showing significantly higher long-term survival in the rechallenged group compared to naïve mice (log-rank test, $p<0.05$).

Appendix 7: Representative image of an H&E stained tumor excised from a Neuro2a tumor-bearing mouse. Inset: representative photograph of a tumor excised from a tumor-bearing mouse. Both images demonstrate that the tumors are well vascularized and not a loose collection of tumor cells.

Appendix 8: Synthesis and characterization of HMGB1-coated PBNPs. (A) Dynamic light scattering (DLS). (B) HMGB1 encapsulation onto the PBNPs, showing 81% encapsulation efficiency. (C) Cytotoxicity of varying concentrations (0.001-0.1 mg/mL) PBNPs and HMGB1-PBNPs on Neuro2a cells, measured by a cell viability assay. (D) Cytotoxicity of 50,000 Neuro2a cells after PBNP-PTT or HMGB1-PBNP (nanoparticle concentration was 0.05 – 0.1 mg/mL, 0.75 W laser, 10 minutes).

List of Abbreviations

%EE Percent entrapment efficiency

APC Antigen presenting cell

ATP Adenosine triphosphate

CD40 Cluster of differentiation 40

CD80 Cluster of differentiation 80

CD86 Cluster of differentiation 86

cDNA Complementary DNA

CEM43 cumulative equivalent minutes at 43 ^{o}C

CpG cytosine-phosphate-guanine oligodeoxynucleotide

CpG-PBNP CpG-coated Prussian blue nanoparticles

CpG-PBNP-PTT CpG oligodeoxynucleotide-coated Prussian blue nanoparticles-based photothermal therapy

CTLA-4 Cytotoxic T-lymphocyte-associated protein 4

DAMPs Danger-associated molecular patterns

DAPI 4′,6-diamidino-2-phenylindole

DC Dendritic cell

DLS dynamic light scattering

DMEM Dulbecco's Modified Eagle Medium

EMEM Eagle's Minimum Essential Medium

EtBr Ethidium bromide

FACS Fluorescence-activated cell sorting

FBS Fetal bovine serum

FDA Food and Drug Administration

$Fe(Cl)_3 \cdot 6H_2O$ Iron (III) chloride hexahydrate

HEPES (4-(2-hydroxyethyl)-1-piperazineethanesulfonic acid)

HMGB1 High motility group box 1

i.p. Intraperitoneally

i.t. Intratumorally

IACUC Institutional Animal Care and Use Committee

ICD Immunogenic cell death

IFN□γ Interferon□γ

iPTT Interstitial photothermal therapy

$K_4[Fe(CN)_6] \cdot 3H_2O$ Potassium hexacyanoferrate (II) trihydrate

mRNA microRNA or messenger RNA

mW milliwatt

MW molecular weight

NIR Near infrared

NK cell Natural killer cell

NP nanoparticle

OD optical density

ODC ornithine decarboxylase

ODN oligodexynucleotides

PBGD Porphobilinogen deaminase

PBNP-PTT Prussian blue nanoparticle-based photothermal therapy

PBNPs Prussian blue nanoparticles

PBS Phosphate buffered saline

PEI Poly(ethylenimine)

PEI-PBNPs Poly(ethylenimine)-coated Prussian blue nanoparticles

PTT Photothermal therapy

RPMI 1640 Roswell Park Memorial Institute 1640

RT-PCR Reverse transcription polymerase chain reaction

TEM Transmission electron microscopy

TLR Toll-like receptor

Trp2 Tyrosinase-related protein 2

Vis-NIR Ultraviolet-visible spectroscopy or ultraviolet-visible spectrophotometry

W watt

W/v Weight/volume

Chapter 1: Introduction

1.1 Background and significance

1.1.1 Neuroblastoma is a significant pediatric health concern

Neuroblastoma is the third most common pediatric cancer and the most common extracranial solid tumor in children accounting for 15% of cancer-related deaths in the pediatric age group [1, 2]. More than 50% of neuroblastoma patients present with regional or distant-stage disease at initial diagnosis [3]. Even though progress has been made over the last 20 years in the management and treatment of low-risk and intermediate-risk neuroblastoma patients, the prognosis for patients with high-risk neuroblastoma has remained low [4]. The overall survival rate in this patient population is at 30-40% [3, 5]. Various treatment modalities such as surgery, chemotherapy, radiation therapy, retinoid therapy, and high dose radio/chemotherapy with stem cell transplant have made incremental but limited progress in treating patients with high-risk neuroblastoma [4]. Hence, there is an urgent need to develop novel and effective therapies for patients with this resistant and advanced tumor.

1.1.2 Key challenges in treating neuroblastoma

Despite being a prevalent tumor, the etiology of neuroblastoma is not well understood. There are no known risk factors and there is no clear genetic predisposition for developing the disease. The low survival rate of neuroblastoma is due to neuroblastoma's characteristics of being heterogeneous [4, 6, 7], immunosuppressive [8-10], exhibiting low neoantigen expression levels [11, 12], and high relapse rates [13].

Tumor heterogeneity in neuroblastoma results in a diverse collection of cells harboring distinct molecular signatures with differential levels of sensitivity to treatment [14]. This heterogeneity might result in a no-uniform distribution of genetically distinct tumor-cell subpopulations across and within disease sites or temporal variations in the molecular makeup of cancer cells [7]. Heterogeneity means that neuroblastoma presents with different characteristics from one patient to another [14], making therapies that are one size fits all very inefficient for this type of cancer.

Another main challenge in treating neuroblastoma is that it exhibits low neoantigen expression [11]. Neoantigens are newly formed antigens that have not been previously recognized by the immune system. They can arise from altered peptides as a result of tumor mutations. Neoantigens can be recognized by the immune system and elicit an immune response. Neoantigen-specific T cells have been identified in several human cancers [15]. Therefore, tumors with high neoantigen expression have been shown to be more sensitive to immunotherapies [15]. Not only does neuroblastoma not express neoantigens, making it “hide” from the immune system, but it is also a immunosuppressive tumor [8]. Tumor cells that are targeted and destroyed are highly immunogenic, meaning they have an antigenic profile that is easily visible to the immune system [9]. Neuroblastoma cells which are poorly immunogenic may escape extrinsic tumor suppression and enter a phase of equilibrium, in which the immune system can control the growth of these cells without eliminating them [16, 17].

Lastly, neuroblastoma is a cancer that has a high recurrence rate. Despite improvements in diagnosis and surgical techniques, most deaths from neuroblastoma are due to advanced cancers that have metastasized or are resistant to conventional therapies [3, 13]. The continued challenges facing treatments for this patient population highlight a need for better control over the treatments and the immune responses they generate. Therefore, an ideal treatment for neuroblastoma consists of one that can take advantage of the heterogeneity of the disease, reverses its low neoantigen expression and immunosuppressive nature, and is able to treat not only the primary tumor in an effective way, but also introduce strategies to treat distal or metastatic tumors. **An important goal in this dissertation is to engineer a strategy that meets all the design criteria for overcoming the challenges of treating neuroblastoma using a combination treatment comprising of Prussian blue nanoparticles (PBNPs) with immunotherapies.** Prussian blue nanoparticles will be used for photothermal therapy of tumors, which both reduces tumor burden through ablation, and modifies the tumor cells to die in an immunogenic cell way, reversing the low neoantigen expression and immunosuppressive tumor environment by engaging the immune system. These effects will be further complemented by immunotherapies, which further activate immune cell subsets such as dendritic cells (DCs) and T cells, leading to antitumor memory effects that can combat recurring or metastatic tumors. The therapeutic advantages of combining photothermal therapy with immunotherapies can eliminate primary

tumors as well as upregulate an antitumor immune response that can overcome the challenges of treating neuroblastoma.

1.1.3 Prussian blue nanoparticles as photothermal immunotherapy agents

Recent advances in nanotechnology have facilitated the synthesis of multifunctional nanoparticles that exhibit properties that make them attractive candidates for use in the treatment of neuroblastoma [18-23]. These properties, not observed in the current therapies for neuroblastoma, include: 1) 10-200 nm size ranges that enable them to extravasate into tumors with poorly differentiated vasculature and lack of functional lymphatics via the enhanced permeability and retention (EPR) effect, [24, 25] 2) High surface area-to-volume ratios for biofunctionalizing the nanoparticles for long circulation, added immunotherapies, or for attaching ligands that target receptors overexpressed on tumor cells, and 3) The ability to carry or be used themselves as therapeutic agents at the tumor sites (e.g. photothermal therapies and photothermal immunotherapies) [18-21, 23]. Motivated by the ideal properties of nanoparticles for cancer therapies, we use Prussian blue nanoparticles as our choice of photothermal immunotherapy agents.

Prussian Blue (PB) was one of the first synthetic pigments synthesized and is a mixed-valence iron hexacyanoferrate with the general formula $AFe^{III}[Fe^{II}(CN)_6].yH_2O$ (where y = 1-5 and A is a monovalent cation such as K^+, Na^+, or NH_4^+) [26]. PBNPs have a lattice structure comprised of repeating units of the iron (III) hexacyanoferrate (II) lattice (**Figure 1.1A**) [18]. The UV−vis spectrum of the PB NPs shows a wide absorption band from 650 – 900 nm (λ_{max} = 705 nm), corresponding to the energy of

the metal-to-metal charge transfer between Fe^{II} and Fe^{III} through the cyanide-bridge (**Figure 1.1B**) [18, 27, 28]. On account of this strong near-infrared (NIR) absorption, the PBNPs are photothermally heated when irradiated with an NIR laser.

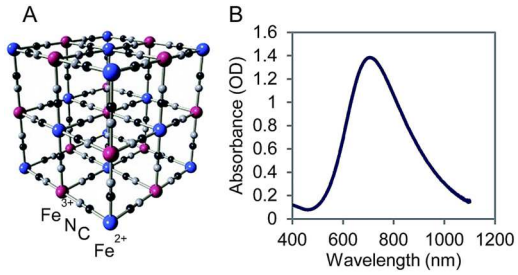

Figure 1.1: A) PBNPs consist of many repeating units of the iron (III) hexacyanoferrate (II) lattice. B) UV-vis spectrum of the PBNPs showing broad NIR absorption that enables photothermal heating upon irradiation by a NIR laser.

PBNPs offer several advantages compared to other NP-based photothermal agents (gold nanorods, copper sulfides, carbon nanotubes): They are easily synthesized in a single, scalable step at low costs, they are already FDA approved for human oral use (as Radiogardase)[29], and are easily and safely degraded in the body [19]. We have previously demonstrated the successful use of PBNPs for PTT of tumors *in vivo* and as multimodal imaging agents for *in vitro* and in *vivo* settings [27, 28, 30, 31]. PTT, in which NIR light-responsive PBNPs are used to thermally ablate tumors, is an appealing addition to cancer treatment regiments. This is because PTT offers unique features such as the ability to locally ablate tumors in a minimally invasive manner [18,

19]. Furthermore, recent studies have demonstrated antitumor immune effects as a result of stimulation by PTT [19-21, 23, 32]. Compared with other tumor shrinking approaches including radiation therapy, RF ablation, oncolytic viruses, etc. that are being investigated in combination with immunotherapie, nanoparticles offer the potential to serve as a sone-stop platform for ablating tumors, capturing (and stabilizing) the released antigens, and locally delivering immune adjuvants – effects important for maximizing their therapeutic and abscopal effects. The immune stimulation elicited by PTT has been a motivator to combine PTT-based cancer therapies with immunotherapies, leading to more potent antitumor responses.

1.1.4 Cancer immunotherapies

Cancer immunotherapy – treatments that harness and enhance the innate powers of the immune system to fight cancer – represent one of the most promising new cancer treatments [33]. Immunotherapies have revolutionized the treatment of cancer because they offer the potential to elicit robust and persistent treatment responses [34]. The novelty of immunotherapy relies on the fact that it aims to treat cancer in a completely different way- by targeting the immune system, not the tumor itself. These therapies enable the immune system to recognize, target, and eliminate cancer cells. Immunotherapy is an effective treatment for patients with certain types of cancer that have been resistant to chemotherapy and radiation treatment, and has also been approved as a first line of treatment in several cancers [35-38]. It may be given alone or in combination with other cancer treatments.

Several types of immunotherapy are currently being used or studied to treat cancer. Checkpoint inhibitors marked the beginning of increased enthusiasm for cancer immunotherapies due to their increased and continuous success in treating cancer patients [35, 36, 38, 39]. Checkpoint inhibitors use monoclonal antibodies to target key immune checkpoints such as CTLA-4 and PD-1 in order to reverse immune suppression, unleashing potent antitumor immune responses by activating endogenous immune cells (e.g. T cells) [40-43]. Adoptive cell therapies have also burgeoned to the field of cancer therapeutics as a therapy strategy that has dramatically influenced cancer patient care [44, 45]. It involves an initial phase of obtaining and enriching a population of patient-derived effector cells *ex vivo*, followed by subsequent re-infusion of the expanded cells into the patient in order to target and kill cancer cells [46]. Cancer vaccines are also currently being studied as powerful immunotherapies. Cancer vaccines aim to treat cancer by upregulating the immune system to recognize and attack tumor cells. These vaccines can be made from dead cancer cells, proteins or peptides from cancer cells, or immune system cells [11, 47]. Finally, immune adjuvants such as toll-like receptors agonists (TLRs) have gradually emerged as potential targets for newer immunotherapies. TLR agonists target TLRs on the surface of immune cells such as DCs and enhance their antigen presentation and activation [48-50].

Despite advances in immunotherapies, clinical responses have been restricted to modest subsets of patients [51]. The heterogeneity of responses to immunotherapies observed in patients suggests the existence of additional immunomodulatory mechanisms employed by tumors. More specifically, tumors evade the immune system by a variety of mechanisms including loss of immunogenicity, loss of antigenicity, and

maintenance of an immnosuppressive tumor environment [9, 10]. Therefore the key to improving therapeutic outcomes for immunotherapies is developing strategies to circumvent these immune evasion mechanisms. To this end, we have designed an ensemble ***nanoimmunotherapy*** that combines state-of-the-art advances in the field of nanotechnology with immunotherapies for treating neuroblastoma. Our nanoimmunotherapy comprises various components: 1) Prussian blue nanoparticles, 2) immune adjuvants, specifically TLR agonists, and 3) immune checkpoint inhibitors, specifically anti-CTLA-4. This combination nanoimmunotherapy approach offers the potential for a robust and persistent therapeutic, which can be applied to different cancers.

1.1.5 Nanoimmunotherapies

The term nanoimmunotherapy refers to an emerging niche field that combines the multifunctional capabilities of nanoparticles with immune-based therapies. The aim of nanoimmunotherapies is to apply and further nanotechnology to solve the limitations encountered in immunotherapy [52]. Nanoparticles can be used for immune functions such as deliver cancer vaccine antigens and adjuvants to DCs, stimulate T cells directly as artificial APCs, concentrate stimulatory compounds in the immunosuppressive tumor environment, or deliver drugs to T cells in circulation [52]. In this dissertation, we have designed a nanoimmunotherapy comprised of PBNPs coated with a TLR for photothermal tumor ablation, local delivery of antigens and adjuvants, and an upregulation of an antitumor immune response.

The robustness of this combination therapy as an engineering strategy is based on its customizable nature across multiple nanoparticle and immunotherapy platforms. By using a customizable nanoimmunotherapy, the nanoparticle element can be adjusted accordingly, to target the features of the disease that the immunotherapeutic alone cannot achieve. Our group and others have demonstrated the advantages of combining nanoparticle-based PTT with immunotherapies for the treatment of cancers. The synergistic therapeutic effects of nanoparticles and immunotherapies continue to show improved therapeutic effects than each component alone.

The therapy strategy pursued in this dissertation (CpG-coated PBNPs) builds on my Master of Science thesis work [19] where we demonstrated that PBNP-PTT can be used for effective tumor ablation in a syngeneic mouse model of neuroblastoma (**Appendix 1**). We show that PBNP-PTT is not only able to ablate tumors (**Appendix 2**), but also cause an upregulation of an immune response marked by the infiltration of lymphocytes and T cells to the local tumor area (**Appendix 3**). We also demonstrated that PBNP-PTT combined with anti-CLTA-4 therapy resulted in complete tumor regression (**Appendix 4**) and long-term survival in a majority (56%) of Neuro2a tumor-bearing mice compared to either single therapy by itself and untreated mice (**Appendix 5**). Further, long-term surviving, PBNP-PTT + anti-CTLA-4-treated mice exhibited protection against tumor rechallenge suggesting the development of immunological memory (**Appendix 6**). Our work shows that nanoimmunotherapies comprising of PTT and immunotherapies are able to act synergistically to ablate tumors and increase the antitumor immune effects elicited by PTT using checkpoint inhibitors, leading to better treatments and long-term immune memory against tumors.

We build on these findings by engineering nanoimmunotherapies using PBNPs that can be combined with immunotherapies that target not only T cells (anti-CTLA-4), but also dendritic cells (DCs) (CpG). It is well known that tumor cells usually do not induce potent antitumor immune responses because of their ineffective expression of molecules important for antigen processing and presentation. PBNP-PTT tumor cell death, on the other hand, can release tumor antigens into the local environment. Furthermore, immunoadjuvants for cancer immunotherapy promote antigen uptake and presentation by professional antigen-presenting cells, thus triggering specific antitumor immunity. Therefore, PTT can act synergistically with immunotherapies such as CpG to enhance immune responses, rendering the tumor residues and metastasis more susceptible to immune-mediated killing.

1.1.6 CpG-PBNP-PTT as a novel nanoimmunotherapy

In this dissertation, we address the limitations of existing therapeutics and develop a nanoimmunotherapy treatment modality that is applicable for the treatment of neuroblastoma. We aim to use PBNP-PTT in combination with immune signals to improve the potency of PTT. Specifically, in this body of work we use nanoimmunotherapy techniques that combine PBNPs coated with a molecular adjuvant, CpG oligodeoxynucleotides (CpG-PBNPs) to increase the antigenicity and adjuvanticity of treated neuroblastoma tumors. PBNP-PTT can be combined with several different immune signals and adjuvants. However, we have used CpG based on the ground-breaking findings of Carpentier et al. that shows that CpG can induce rejection of neuroblastoma in mice [53].

Toll-like receptors (TLRs) have gradually emerged as potential targets of newer immunotherapies [49, 50]. TLR-9 is preferentially expressed on endosome membranes of B-cells and DCs, and it is known for its ability to stimulate specific immune reactions through the activation of inflammation-like immune responses [54]. Several synthetic CpG oligonucleotides (CpG-ODNs, CpG) have been developed as TLR-9 agonists with the aim of enhancing cancer immune surveillance [53]. In many preclinical models, CpG found to suppress tumor growth and proliferation both in monotherapy and in addition to chemotherapies [49, 50, 55-60]. These agents showed good tolerability and usually met activity endpoints in early phase trials. However, they have not yet been demonstrated to significantly impact survival, neither as single agent treatments, nor in combination with chemotherapies or cancer vaccines.

We utilize the PBNPs in CpG-PBNPs for PTT of tumors leveraging their inherent absorption in the near infrared (NIR) spectrum [18, 61]. PBNP-PTT not only elicits tumor cell death but increases antigenicity by releasing antigens from dying tumor cells[62]. The CpG oligodeoxynucleotides coated on the CpG-PBNPs are TLR-9 agonists that function as adjuvants to enhance the CpG-PBNPs-based nanoimmunotherapy [48, 53, 55, 60]. PTT using CpG-PBNPs (CpG-PBNP-PTT) therefore serves as a dual treatment modality, wherein tumors are killed by PTT and a robust antitumor immune response is elicited through the release of tumor antigens in the presence of exogenously administered adjuvant (**Figure 1.2**).

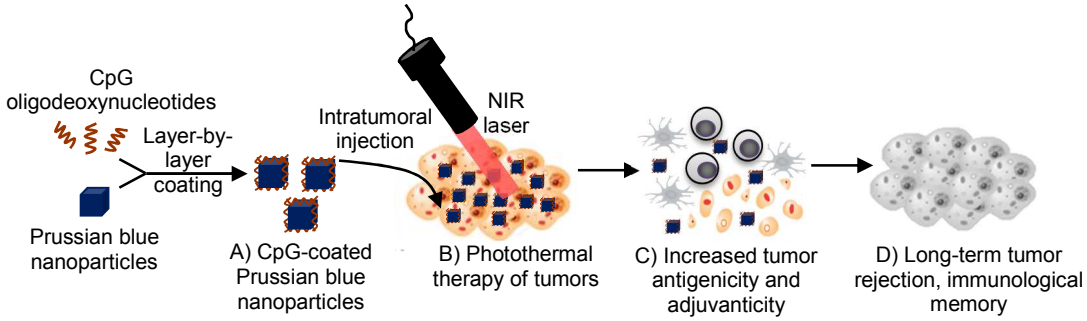

Figure 1.2. CpG oligodeoxynucleotide-coated Prussian blue nanoparticles (CpG-PBNPs)-mediated nanoimmunotherapy for neuroblastoma. (A) CpG-PBNPs are synthesized via a layer-by-layer coating strategy. (B) The synthesized CpG-PBNPs are intratumorally injected into syngeneic neuroblastoma tumors and activated using a near infrared (NIR) laser effecting photothermal therapy-based ablation of the tumors. (C) The conditions utilized for tumor ablation elicits immunogenic cell death (ICD) in dying tumor cells marked by increased antigenicity and adjuvanticity. (D) The CpG-PBNPs-mediated cell death occurring concurrently with increased antigenicity and adjuvanticity triggers long-term tumor regression and rejection of tumor-rechallenge, suggestive of the generation of immunological memory as a result of the nanoimmunotherapy.

1.2 Innovation

The innovative aspects of our nanoimmunotherapy, which combines biofunctionalized PBNPs with a TLR agonist to treat neuroblastoma tumors in syngeneic mouse models of disease include:

1.2.1 The use of PBNP-PTT for tumor eradication and to elicit an *O* vaccine effect

PBNP-PTT is a minimally invasive *in situ* method for destroying (ablating) cancer cells and reducing tumor burden. In this treatment modality, NIR light-absorbing PBNPs are injected into tumors and irradiated with a low-power NIR laser, resulting in rapid heating of the nanoparticles and destruction of the tumor. In this dissertation, we leverage the property of PBNPs to be used as PTT agents to eradicate Neuro2a neuroblastoma tumors by ablation. We have the ability to synthesize PBNPs with controllable sizes (from as low as 10 nm to 200-300 nm), porosities (solid vs hollow), surface biofunctionalization (uncoated, layer-by-layer coated, etc), and biodegradability (**Figure 1.3**) [18, 19, 27, 28, 30, 31, 63, 64]. This biodegradability mitigates concerns associated with the long-term fate and toxicity of these nanoparticles within the body, a feature not offered by other types of nanoparticles used for PTT [18, 27]. Further, PBNPs can be easily synthesized in a single, scalable step at extremely low costs, and are already FDA approved for human oral consumption (to treat radioactive poisoning)[29], which suggests the potential safety of using this PBNP platform

for PTT of tumors. Additionally, the release of key tumor antigens and "danger signals" by PBNP-PTT-based destruction of tumor cells is expected to provide an immunostimulatory, multi-antigen "PTT vaccine" effect without the need for knowledge of specific tumor antigen targets, as required for standard vaccines. This PTT vaccine is expected to play a role in triggering ICD, which is important for eradicating tumors, conferring immunity, and preventing relapse.

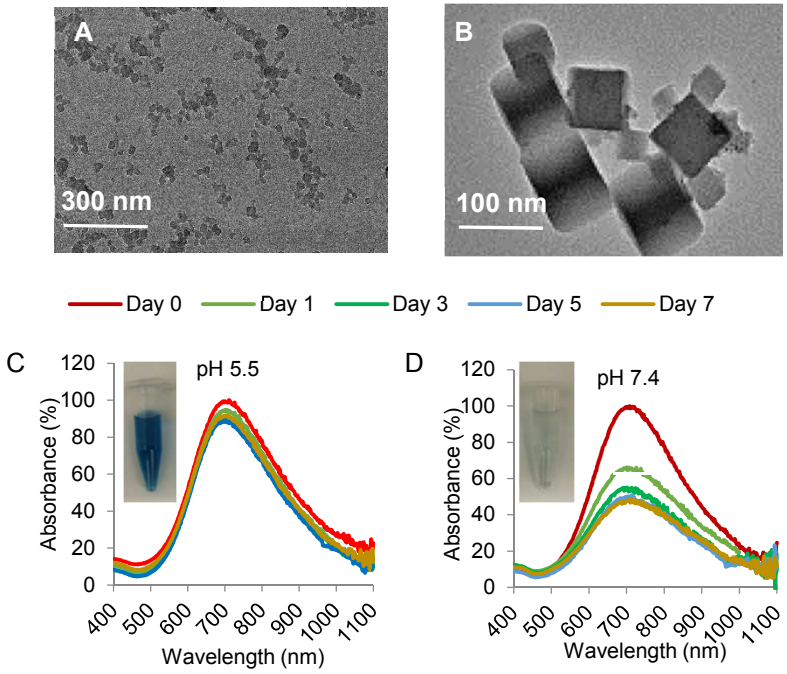

Figure 1.3: Controllable sizes, morphologies, and degradation of PBNPs. A-B) Cuboidal PBNPs synthesized using a one-pot synthesis scheme and by controlling nanoparticle growth. C) pH 5.5 and D) pH 7.4, exhibiting PBNP stability at mildly acidic pH (5.5), and decreased PBNP stability at mildly alkaline pH (7.4). Insets: PBNP photographs on Day 7 at a pH of 5.5 and 7.5, respectively.

1.2.2 The use of PBNPs as a depot for immune adjuvants

Several reports have conclusively demonstrated the benefits of using nanoparticle depots to locally administer immune adjuvants compared to direct intratumoral injection or systemic administration [20, 21, 23]. We conducted electrostatic coating of PBNPs with a potent TLR agonist, CpG, to play a key role in breaking tolerance to tumor antigens and improving tumor antigen presentation. From this perspective, PBNP-PTT offers advantages over other tumor ablation technologies such as high-intensity focused ultrasound, radiofrequency ablation, and cryoablation [32, 65, 66], because the nanoparticles themselves are modified to carry the immunostimulatory molecules [20, 58] as compared to the other ablation technologies which would necessitate the administration of the immune adjuvants separately.

1.3 Overview of thesis work

In this dissertation, we addressed the limitations of existing therapies and challenges in treating neuroblastoma, and engineer a novel therapy comprising of PBNPs and immunotherapies. By focusing on the key challenges in treating neuroblastoma (low neoantigen expression, heterogeneity, immunosuppression, high recurrence rate), we utilize nanotechnological and immunological based solutions to develop enhanced nanoimmunotherapies. Nanoimmunotherapy refers to the marriage of nanomedicine and immunotherapy approaches in order to promote the development of a robust and persistent therapeutic. In principle, a successful nanoimmunotherapy should allow the therapeutic efficacies of each

treatment modality to persist, all while supplementing and overcoming the limitations of each platform alone. Through both PBNP-based photothermal therapy and combination with toll like-receptor agonists and checkpoint inhibitors, we have demonstrated multiple approaches to developing an enhanced therapeutic, that is capable of robust antitumor efficacy against neuroblastoma.

The overall objective of this dissertation is to successfully engineer a combination therapy to treat neuroblastoma using PBNPs in combination with immunotherapies. We hypothesize that by biofunctionalizing PBNPs with CpG, our nanoimmunotherapy (CpG-PBNP-PTT) elicits immunogenic cell death (ICD) and improved antigen presentation, which combines with immune checkpoint inhibition to effectively eradicate neuroblastoma tumors, prevent relapse, and trigger antitumor effects against disseminated disease.

To accomplish this, our first objective was to synthesize and characterize PBNPs biofunctionalized with CpG. In **Chapter 2**, the properties of CpG-PBNPs were characterized for size, stability, absorption spectrum, and cytotoxicity compared to PBNPs to confirm that layer-by-layer coating with CpG was not affecting the intrinsic properties of PBNPs. We then present the photothermal heating characteristics of the nanoparticles as well as their immunostimulatory properties *in vitro* and *ex vivo* to ensure that CpG-PBNPs are suitable for administration of PTT.

Chapter 3 describes a thermal "window" of immunogenic cell death (ICD) elicited by PTT in an animal model of neuroblastoma. We demonstrate tunable immune responses to heat generated by PBNP-PTT, which should be critically engaged in the administration of PTT for maximizing its therapeutic effects. After characterizing CpG-PBNPs, as well as their ability for PTT and eliciting ICD, we tested the ability of our nanoimmunotherapy to upregulate an immune response by activating DCs and T cells *in vitro* (**Chapter 4**). We then evaluated the efficacy of CpG-PBNP in treating a syngeneic mouse model of neuroblastoma.

An effective nanoimmunotherapy for neuroblastoma should be capable of treating both primary tumors as well as preventing recurrence, and treat disseminated disease. In **Chapter 5** we therefore tested the ability of our therapy in protecting long-term surviving mice from neuroblastoma rechallenge, as well as the ability of our therapy to treat a disseminated model of neuroblastoma. Finally, in **Chapter 6**, we discuss future studies to continue the improvement of PBNP-based nanoimmunotherapies for the treatment of neuroblastoma.

Chapter 2: Layer-by-layer coating of PBNPs with CpG yield stable and functional CpG-PBNPs[1]

2.1 Abstract

Nanoparticle-based photothermal therapy (PTT) has been widely investigated in cancer therapy as a rapid and minimally invasive tumor ablation technique. An emerging area of interest is the effect of PTT on the immune system during tumor therapy, since PTT not only causes tumor cell death, but can also release tumor antigens and endogenous adjuvants under certain conditions. We describe biofunctionalized PBNPs as an enhanced *photothermal immunotherapy* wherein PBNP-based PTT is used for tumor ablation and *in situ* vaccine effects, complemented by adjuvant CpG biofunctionalization that increases antigen-processing and presentation. Here, we describe the synthesis and characterization of CpG oligodeoxynucleotide-coated Prussian blue nanoparticles (CpG-PBNPs) that function as a nanoimmunotherapy for neuroblastoma, a common childhood cancer. These CpG-PBNPs increase the antigenicity and adjuvanticity of treated tumors, ultimately driving robust antitumor immunity through a multi-pronged mechanism. CpG-PBNPs are synthesized using a facile layer-by-layer coating scheme resulting in nanoparticles that exhibit monodisperse size distributions and multiday stability without cytotoxicity. The strong, intrinsic absorption of PBNPs in the CpG-PBNPs enables ablative photothermal therapy (CpG-PBNP-PTT) that triggers tumor cell death, as well as release of tumor

[1] This chapter was adapted from Cano-Mejia, J. et al, *Prussian blue nanoparticle-based antigenicity and adjuvanticity trigger robust antitumor immune responses against neuroblastoma.* Biomaterials Science, 2019. doi: 10.1039/c8bm01553h

antigens to increase antigenicity. Lastly, the high encapsulation efficiency and tightness of CpG bound to PBNPs allows for a more bioavailable antigen in the local tumor environment. CpG-PBNPs are therefore effective nanoimmunotherapy agents for photothermal immunotherapy of cancers. PTT-elicited cell death combined with released antigens and added adjuvants will result in a stronger engagement of an antitumor immune response.

2.2 Introduction

Treatments that recruit the immune system have emerged as attractive options for cancer as they offer the potential for more specific and persistent antitumor effects. As a representative immunotherapy method, nanoimmunotherapies show tremendous potential in cancer immunotherapy owing to the antigen-specific immune responses and the long-term immunological memory induced by them [67]. Among them, protein- or peptide- based vaccines show more advantages in terms of safety, stability, specificity, or reproducibility[68-71]. Nevertheless, the insufficient immunogenicity of some of these treatments leads to the difficulty of eliciting robust immune effects for immune clearance. With the development of adjuvants, co-delivery of antigens and adjuvants can significantly promote the effectiveness of cancer treatments and even overcome the body's immune tolerance. Reports have indicated that sustained release of the antigen and adjuvant from a delivery system can generate an "antigen reservoir" effect that further enhances tumor-specific cytotoxic T lymphocyte responses [72]. Co-delivery of antigens and adjuvants has achieved a positive role for cancer immunotherapy [22]. The application of carrier systems for co-delivery of antigens and

adjuvants would provide a suitable strategy for further enhancing the tumor therapy effect [59, 60, 68-70]. To this end, we have designed an ensemble nanoimmunotherapy that combines state-of-the art advances in the field of nanotechnology with immunotherapy for treating advanced tumors such as neuroblastoma. Specifically, our ensemble comprises: 1) PBNPs biofunctionalized with 2) the immune adjuvant CpG.

We utilize the PBNPs for photothermal therapy (PBNP-PTT) by irradiating them with a low power, NIR laser. PBNP-PTT serves as a method for tumor ablation and decreasing tumor burden[18, 19]. In addition, PBNP-PTT releases tumor antigens and endogenous adjuvants particularly damage-associated molecular patterns (DAMPS) such as ATP and HMGB1 that can increase tumor immunogenicity [62]. Therefore PBNP-PTT functions as an *in situ* vaccine. An advantage of using PBNP-PTT is that it can elicit a multi-antigen vaccination effect without the need for a *priori* knowledge of the tumor antigens, which may be difficult to acquire for less immunogenic tumors[6, 7]. Additionally, an *in situ* vaccine obviates the need for synthesis, purification, and processing steps for exogenous vaccines, which can be complex, time-consuming, and costly.

The PBNPs also function as a depot for immune adjuvants, improving antigen presentation and processing. Synthetic oligodeoxynucleotides (ODNs) containing the unmethylated cytosine-phosphate-guanine (CpG) motif are potent stimulants of the innate immune system [50]. These sequences bind to TLR-9 in the endosome of antigen presenting cells (APCs), this promoting the expression of co-stimulatory molecules, and the development of CD8+T cell responses[9]. As a result, CpG has shown great promise as a monotherapy and vaccine adjuvant for the treatment of cancer. Our

motivation for employing a depot approach for administering the immune adjuvants is premised on several published reports that have conclusively demonstrated the benefits of using nanoparticle depots to deliver immune adjuvants compared with direct injection of these agents [20, 21, 23]. Direct injection at the tumor site causes rapid clearance of the adjuvants, and systemic administration is associated with non-specific immune activation/toxicity effects. Additionally, PBNPs serve as a source for *in situ* vaccination and a depot for immune adjuvants using a single platform that is easily assembled, a clear advantage over other techniques to co-administer these agents. A co-delivery system including PBNP-PTT and CpG introduces the antigen and adjuvant to the local tumor environment and its surrounding and infiltrating immune cells, executing a dual function of antigen by means of the dying tumor cells, as well as the CpG adjuvant. PTT using CpG-PBNPs (CpG-PBNP-PTT) will serve as a dual treatment modality, where tumors are killed by ablation and enhancement of the immune response through the delivery of both antigens and adjuvants locally. Photothermal immunotherapy using CpG-PBNPs therefore have the potential of greatly improving the treatments and responses of cancers.

We present a layer-by-layer scheme for the generation of the CpG-PBNPs, leveraging our expertise in generating polyelectrolyte multilayers. The properties of the resultant CpG-PBNPs were characterized for size, stability, absorption spectrum, and cytotoxicity. Next, we present the photothermal heating characteristics of the nanoparticles as well their immunostimulatory properties *in vitro* and *ex vivo* to ensure that the CpG coating is not affecting the intrinsic characteristics and properties of PBNPs, and the CpG-PBNPs are suitable for administration of PTT.

2.3 Materials and Methods

2.3.1 Materials and chemicals

All synthesis procedures were conducted using ultrapure water obtained from a Milli-Q system (Millipore Corporation, Billerica, MA) with resistivity of 18.2 MΩ·cm. Potassium hexacyanoferrate (II) trihydrate (Mw 422.39; $K_4[Fe(CN)_6]\cdot 3H_2O$), iron (III) chloride hexahydrate (Mw 270.3; $Fe(Cl)_3\cdot 6H_2O$), and citric acid were purchased from Sigma-Aldrich (St. Louis, MO, USA), and were used as supplied. Acetone, ethanol, and ethidium bromide (EtBr) solution were obtained from Sigma-Aldrich. Poly(ethylenimine) (PEI, Mw 2,000, Mn 1,800, 50% w/v in H_2O) was purchased from Sigma-Aldrich, and diluted in acetate buffer (pH 5.2, Sigma-Aldrich). Murine CpG oligodeoxynucleotide (CpG) TLR9 ligand (ODN 1585; Class A)) was purchased from InVivoGen (San Diego, CA, USA).

2.3.2 Cells and cell culture

The murine neuroblastoma cell line Neuro2a was obtained from ATCC (Manassas, VA, USA) and cultured in Eagle's Minimum Essential Medium (EMEM) (Gibco, Carlsbad, CA, USA) containing 10% fetal bovine serum (FBS, Gibco) and 1% penicillin/streptomycin (Sigma-Aldrich).

2.3.3 Synthesis of PBNPs

PBNPs were synthesized using a one-pot synthesis scheme as previously described by us with minor modifications [18, 19, 31, 64]. Briefly, an aqueous solution of 1.0 mM $FeCl_3 \cdot 6H_2O$ and 0.5 mmol citric acid in 20 mL of MilliQ water was added under vigorous stirring to an aqueous 20 mL solution containing 1 mM $K_4Fe(CN)_6 \cdot 3H_2O$ and 0.5 mmol citric acid at 60 °C. After stirring for 1 minute, the solution was allowed to come to room temperature, and the precipitate containing PBNPs was isolated by the addition of equal volumes of acetone followed by centrifugation (10,400 ×g for 10 minutes). The collected PBNPs were rinsed and resuspended by sonication for 5 s using a Q500 sonicator (QSonica LLC, Newton, CT, USA) at high power in Milli-Q water. The isolation and rinsing steps were repeated 3× before the stock nanoparticles were finally resuspended by sonication in Milli-Q water. The concentration of the PBNPs was determined by measuring the absorbance of the nanoparticle suspensions at 680 nm using a calibration curve plotting OD_{680} versus concentration of PBNPs in mg/mL. These calculations were confirmed by weighing a known volume of the PBNPs before and after drying in an oven.

2.3.4 Synthesis of CpG-PBNPs

To generate the CpG-PBNPs, we adopted a layer-by-layer coating strategy where PEI was first coated on to the PBNPs. PBNPs at a concentration of (3 mg/mL) were contacted with equal volumes of PEI (12 mg/mL) in acetate buffer (pH 5.2) at room temperature for 1 hour on an orbital shaker. The resultant

PEI-coated PBNPs (PEI-PBNPs) were collected by centrifugation at 10,400 ×g for 10 minutes with the addition of equal volumes of ethanol. After 4 washes with the 50%-50% Milli-Q water-ethanol mixture, the PEI-PBNPs were resuspended by sonication in Milli-Q water. The concentration of the PEI-PBNPs was determined as described above. Next, CpG was assembled on the PEI-PBNPs. Accordingly, 300 μL of an aqueous solution of CpG (containing 100 μg CpG in endotoxin-free water) was added to 500 μL of the above PEI-PBNP suspension (at a concentration of 2 mg/mL) under stirring at room temperature for 15 minutes. The mixture was centrifuged at 21,000 ×g for 15 minutes to collect the CpG-PBNPs. The amount of CpG loaded on to the nanoparticles was calculated by measuring the difference in absorbance (at 260 nm) between the CpG added to the nanoparticles and the CpG detected in the nanoparticle-free supernatant, using a NanoDrop spectrophotometer (Thermo Fisher Scientific). Based on these measurements, we calculated the entrapment efficiency (%EE) = (Amount of CpG added – Amount of CpG measured in the supernatant)/(Amount of CpG added).

2.3.5 Nanoparticle characterization

The size (hydrodynamic diameter) and charge (zeta potential) distributions of PBNPs, PEI-PBNPs and CpG-PBNPs were measured using dynamic light scattering (DLS) on a Zetasizer Nano ZS (Malvern Instruments, Malvern, UK). The visible-NIR (Vis-NIR) absorbance spectra of the nanoparticles were measured on the Genesys 10S spectrophotometer using the

VISIONlite software (Thermo Fisher Scientific). Transmission electron microscopy (TEM) images of the PBNPs, PEI-PBNPs, and CpG-PBNPs were prepared by loading 5 μL of the nanoparticle suspensions on to formvar carbon coated copper grids (Ted Pella, Inc., Reading CA) and dried overnight. The samples were imaged in a Talos F200X Transmission Electron Microscope (TEM) (Thermo Fisher) at 200 KV. The Velox software (Thermo Fisher) captured images at 200X magnification with a Ceta 4k x 4k camera. Multiday stability of the nanoparticles in ultrapure water was assessed by measuring their hydrodynamic size distributions, zeta potentials, and Vis-NIR spectra every 24 hours over 7 days.

2.3.6 Release of CpG from CpG-PBNPs

To quantify if CpG is tightly bound on the layer-by-layer-assembled CpG-PBNPs, EtBr was added to CpG-PBNPs or dose-matched free CpG at a 1:5 mass ratio and allowed to equilibrate for 1 hour. Fluorescence was measured on a Gemini XPS plate reader (Molecular Devices LLC, San Jose, CA, USA) at an excitation wavelength of 520 nm and an emission wavelength of 590 nm. The intensity ratio was calculated by comparing the fluorescence of the CpG-PBNPs with EtBr to the fluorescence of CpG and EtBr alone. To determine the multi-day release of CpG from the nanoparticles at varying physiological pHs (4.6, 7.0, and 8.0), the appropriate amounts of mild acid or base were added to the CpG-PBNP suspensions (0.8 mg/mL) in Milli-Q water until the desired, stable pH was obtained. The amount of CpG released was measured using a NanoDrop

spectrophotometer. To determine the amount of CpG released from the particles, PTT was conducted as a function of concentration (0.1 mg/mL and 0.5 mg/mL) at a fixed laser power of 0.75 W for 10 minutes. The PTT capabilities were also tested as a function of laser power (0.25, 0.75, and 1.25 W) by irradiating CpG-PBNPs at a fixed concentration of 1 mg/mL. EtBr was added to the nanoparticles after PTT or dose-matched free CpG as described above.

2.3.7 Cell viability assays

Intrinsic and PTT-induced cytotoxicity of the CpG-PBNPs *in vitro* was measured using the murine neuroblastoma cell line Neuro2a. Briefly, Neuro2a was seeded in a 96-well plate at a cell density of 50,000 cells per well, and incubated with either vehicle or varying concentrations of nanoparticles (0.001-0.5 mg/mL) with or without laser irradiation using an 808 nm NIR continuous wave, collimated diode laser (Laserglow Technologies, Toronto, ON, Canada) at 1.5 W/cm^2 for 10 minutes. Twenty-four hours after the treatment, cell viability was assessed using the CellTiter-Glo luminescent cell viability assay (Promega Corporation, Madison, WI, USA). Each treatment was conducted with at least three replicates.

2.3.8 *In vitro* PTT

The photothermal capabilities of CpG-PBNPs were tested *in vitro* as a function of concentration by varying the concentration of the nanoparticles from 0.025 mg/mL to 0.5 mg/mL at a fixed laser power of 0.75 W for 10 minutes. The

PTT capabilities were also measured as a function of laser power (0.25W – 1.25W) by irradiating CpG-PBNPs at a fixed concentration of 1 mg/mL for 10 minutes. The stability of the nanoparticles as a photothermal agent was assessed by a cyclic heating/cooling study where 1 mg/mL CpG-PBNPs were irradiated by the NIR laser at 0.75 W (laser on/off times = 10 minutes each). The laser power administered in each study was confirmed using a power meter (Thorlabs, Newton, NJ, USA). Temporal temperature measurements were taken using an i7 thermal imaging camera (FLIR, Arlington, VA, USA).

2.4 Results

2.4.1 Layer-by-layer coating yields CpG-PBNPs with stable, monodisperse size distributions that retain the absorption properties of PBNPs and are not cytotoxic

We employed a layer-by-layer coating scheme to generate the CpG-PBNPs by sequentially coating the PBNPs with PEI and then CpG. Using this coating scheme, the yield of PEI-PBNPs was 92% on a mass/mass basis (gram of PEI-PBNPs obtained per gram PBNPs used in the coating) and the yield of CpG-PBNPs was 99.5% (gram of CpG-PBNPs obtained per gram of PEI-PBNPs used in the coating) resulting in an overall process yield of approximately 91.5% (g CpG-PBNP/g PBNP). We measured the size, zeta potential, and Vis-NIR spectrum of the resultant CpG-PBNPs to assess their properties relative to unmodified PBNPs and PEI-PBNPs, to ensure that coating PBNPs with CpG did not affect the intrinsic characteristics of PBNPs. DLS measurements yielded CpG-PBNP size distributions that were similar to PBNPs and intermediate PEI-

PBNPs (mean diameter ~ 190 nm; **Figure 2.1A**). Further, we were able to verify that the layer-by-layer coating was able to successfully coat the PBNPs with PEI and then CpG using zeta potential measurements (**Figure 2.1B**). Specifically, the intrinsic negative charge of PBNPs (average zeta potential -34 mV) changed to a net positive charge upon addition of positively charged PEI (+42 mV) and then back to a net negative charge after subsequent addition of the negatively charged CpG (-32 mV). The Vis-NIR spectrum of CpG-PBNPs demonstrated an absorption band between 650 and 900 nm (λmax = 705 nm; **Figure 2.1C**), which is similar to the absorption band of unmodified PBNPs [18, 19, 61]. This absorption band corresponds to the energy of the metal-to-metal charge transfer between Fe^{II} and Fe^{III} through the cyanide bridge and confers photothermal heating capabilities to the nanoparticles (upon NIR laser irradiation). TEM images of PBNPs, PEI-PBNPs, and CpG-PBNPs showed the characteristic cuboidal morphology of PBNPs (**Figure 2.1D**). In contrast, the crystallinity of the PEI-PBNPs and CpG-PBNPs were less well-defined and diffuse compared with PBNPs. This could be attributed to the presence of the polymer layers on the PEI-PBNPs and CpG-PBNPs that were likely affected and/or damaged by exposure to the electron beam during the TEM imaging (**Figures 2.1E** and **F**). Using these synthesis conditions, the entrapment efficiency (%EE) for CpG in the CpG-PBNPs was approximately 25%, which corresponded to approximately 40 μg CpG/mg of nanoparticles.

We conducted a temporal DLS study to assess nanoparticle size distributions as a function of time. The nanoparticles (PBNPs, PEI-PBNPs, and CpG-PBNPs)

were stable over 7 days as measured by consistent size distributions over the study (**Figures 2.1G, 2H**). The addition of varying concentrations of PBNPs, PEI-PBNPs, or CpG-PBNPs (0.001-0.1 mg/mL) to Neuro2a cells did not significantly affect their cellular viability (**Figures 2.1I**), indicating biocompatibility of the nanoparticles within these concentration ranges. These results demonstrate that our synthesis scheme yields stable CpG-PBNPs with monodisperse size distributions that retain the Vis-NIR absorption properties and biocompatibility of uncoated PBNPs.

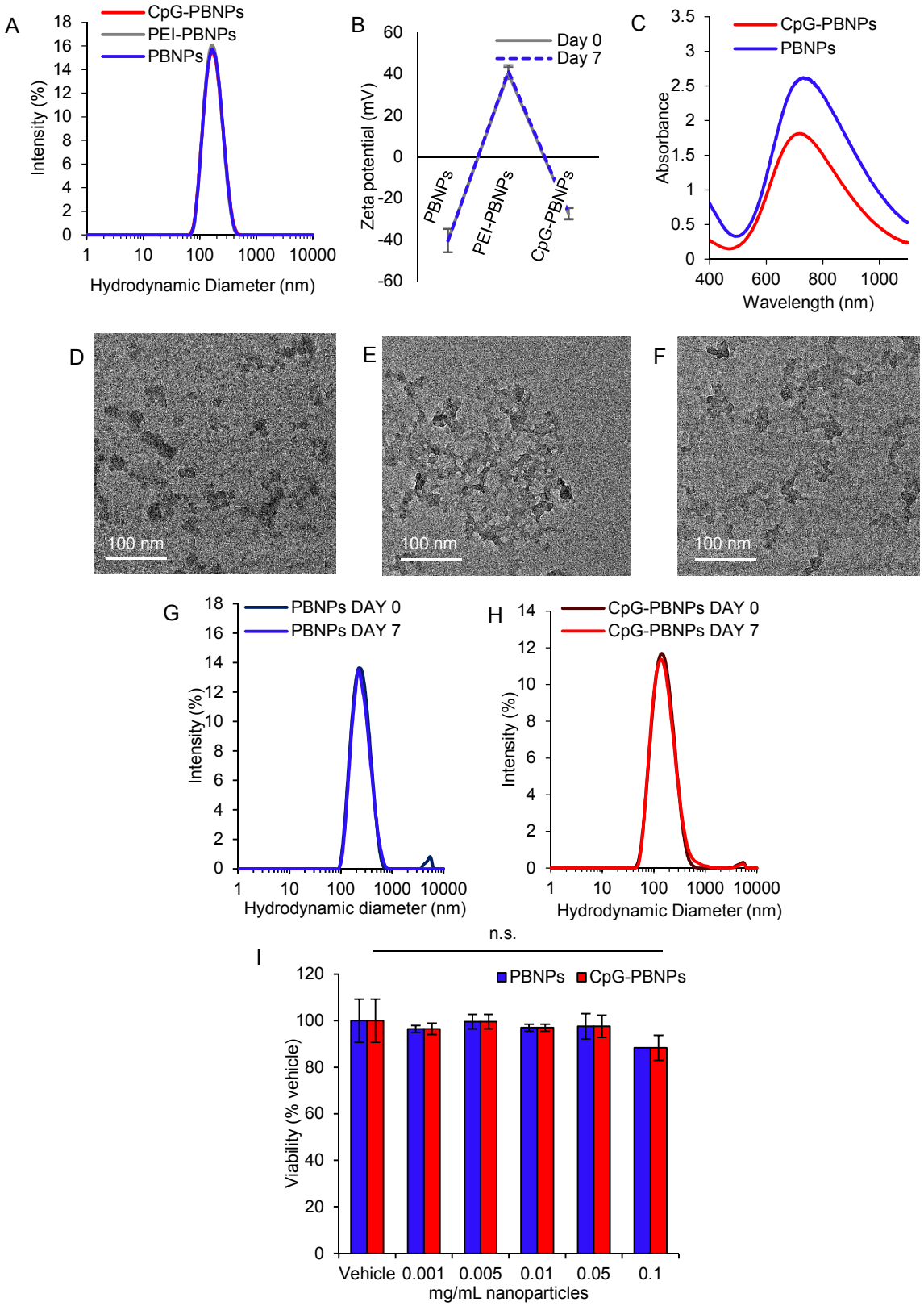
A
CpG-PBNPs
PEI-PBNPs
PBNPs
Intensity (%)
Hydrodynamic Diameter (nm)
B
Day 0
Day 7
Zeta potential (mV)
PBNPs
PEI-PBNPs
CpG-PBNPs
C
CpG-PBNPs
PBNPs
Absorbance
Wavelength (nm)
D
E
F
100 nm
G
PBNPs DAY 0
PBNPs DAY 7
Intensity (%)
Hydrodynamic diameter (nm)
H
CpG-PBNPs DAY 0
CpG-PBNPs DAY 7
Intensity (%)
Hydrodynamic Diameter (nm)
I
n.s.
PBNPs
CpG-PBNPs
Viability (% vehicle)
Vehicle
0.001
0.005
0.01
0.05
0.1
mg/mL nanoparticles

Figure 2.1. Size distribution, zeta potential, absorbance, multi-day stability, and cytotoxicity of CpG-PBNPs. CpG-PBNPs, as well as the starting (PBNPs) and intermediate nanoparticles (PEI-PBNPs), were characterized using: (A) Dynamic light scattering (DLS), (B) Zeta potential measurements after each step of the synthesis (Days 0 and 7), and (C) Vis-NIR spectra. TEM images of (D) PBNPs, (E) PEI-PBNPs, and (F) CpG-PBNPs. Nanoparticle stability was measured over the course of a week for the (G) PBNPs and (H) CpG-PBNPs using DLS. (I) Cytotoxicity of varying concentrations (0.001 – 0.1 mg/mL) PBNPs and CpG-PBNPs on Neuro2a cells, measured by a cell viability assay (n.s.; no statistical significant difference in viability between both types of nanoparticles and concentrations; $p > 0.05$).

2.4.2 CpG-PBNPs retain the photothermal therapy capabilities of PBNPs after CpG coating

To assess the effect of the CpG coating on the photothermal heating properties of the resultant CpG-PBNPs, we conducted photothermal heating studies *in vitro* as a function of nanoparticle concentration, laser power, and cyclic heating (**Figure 2.2**). The photothermal heating effect was concentration-dependent (**Figure 2.2A**) and laser power-dependent (**Figure 2.2B**). The temperatures increased with increasing CpG-PBNP concentrations (0.025 to 0.5 mg/mL CpG-PBNPs) reaching a maximum temperature around 80 ^{o}C at 10 minutes at a concentration of 0.5 mg/mL CpG-PBNPs (laser power 0.75 W). The photothermal heating effect was also dependent on incident laser power, and was observed to increase with increasing laser powers (0.25 to 1.25 W) reaching a maximum temperature around 80 ^{o}C (for 1 mg/mL CpG-PBNPs) at 1.25 W at 10 minutes. Furthermore, we demonstrated the stability of CpG-PBNPs as PTT agents through a cyclic heating study (1 mg/mL CpG-PBNPs, 0.75 W laser power). CpG-PBNPs showed consistent photothermal heating tracing similar heating-cooling curves over three consecutive heating and cooling cycles indicating stability of the CpG-PBNPs as PTT agents (**Figure 2.2C**). To test the

efficacy of CpG-PBNPs to induce Neuro2a killing, we tested cell viability at different concentrations of CpG-PBNPs with and without laser. Neuro2a cell viability significantly decreased as temperatures induced by CpG-PBNP-PTT increased (**Figure 2.2D**). These results show that coating PBNPs with CpG does not affect their photothermal heating abilities and indicate their suitability for use at PTT agents.

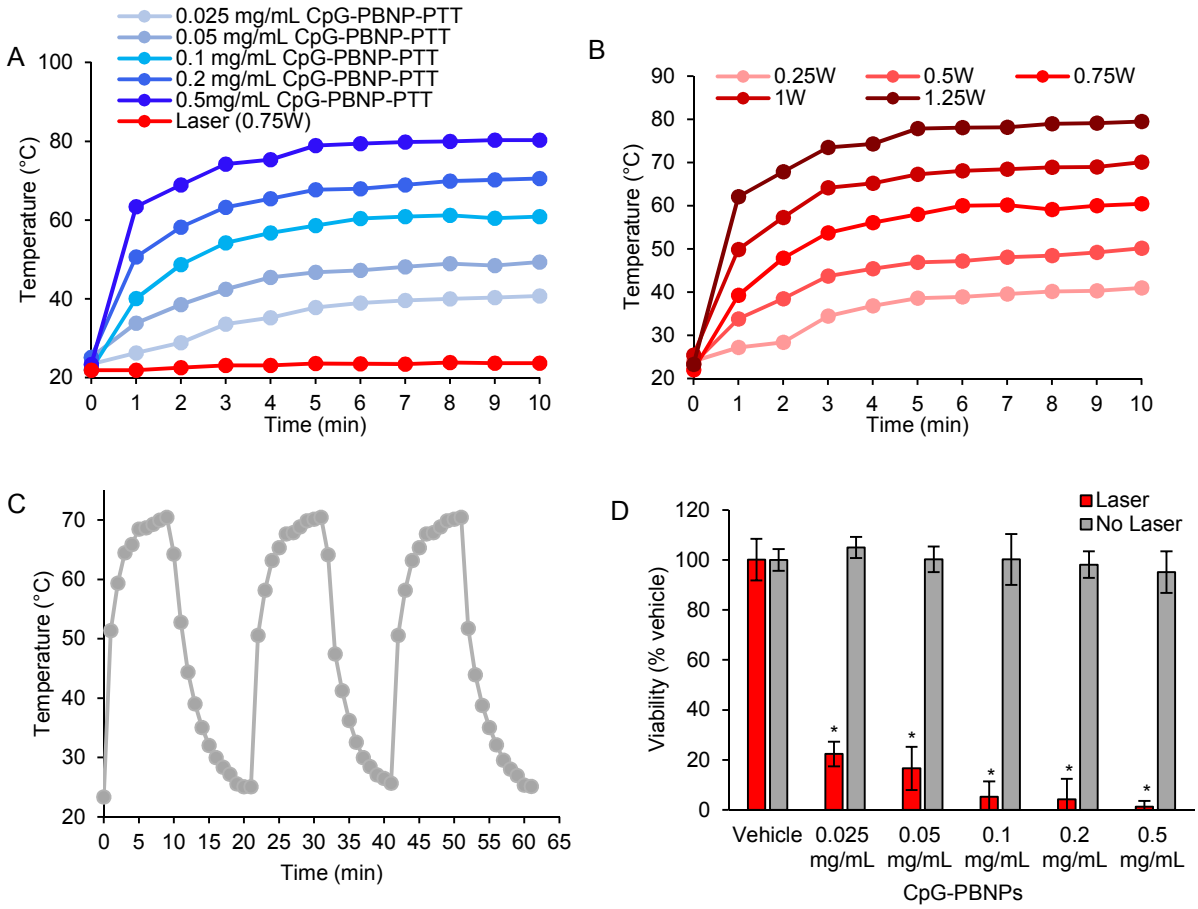

Figure 2.2. Photothermal properties of CpG-PBNPs. (A) Photothermal heating curves (temperature-time profiles) of varying concentrations (0.025 – 0.5 mg/mL) of CpG-PBNPs irradiated by an 808 nm NIR laser for 10 minutes at a power of 0.75 W (1.875 W/cm^2). (B) Photothermal heating of 1 mg/mL CpG-PBNPs using varying NIR laser powers (0.25 - 1.25 W) for 10 minutes. (C) Temperature profiles during cyclic heating of 1 mg/mL CpG-PBNPs using an 808nm NIR laser at 0.75 W (laser on/off time: 10 minutes each). (D) Neuro2a cell viability *in vitro* post-treatment with vehicle or varying doses of CpG-PBNPs (in the absence or presence of the NIR laser at 0.75 W for 10 minutes), measured 24 h after treatment. (* significant difference, $p < 0.001$ compared with vehicle).

2.4.3 CpG-PBNPs contain tightly bound CpG and exhibit pH-dependent CpG release

We conducted studies to quantify the release of CpG from CpG-PBNPs because the release (or retention) of this immunological adjuvant from the nanoparticles directly impacts tumor adjuvanticity. An EtBr assay conducted to determine the binding affinity of CpG and the PBNPs demonstrated that only 6.75% of bound CpG in the CpG-PBNPs could complex with EtBr when compared with equivalent concentrations of free CpG (**Figure 2.3A**). This finding suggests that greater than 93% of CpG is tightly bound in the CpG-PBNPs post-synthesis.

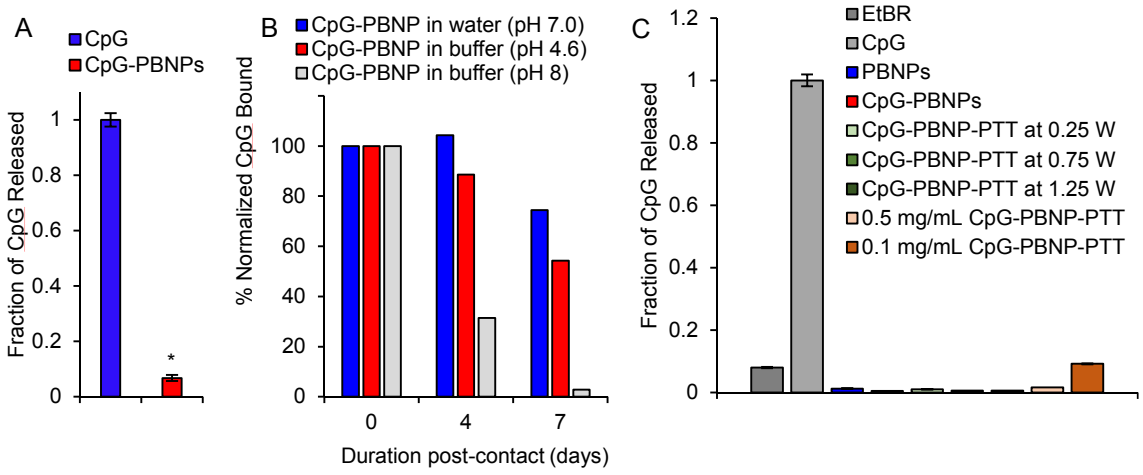

Figure 2.3. Release of CpG from CpG-PBNPs. (A) Fraction of CpG released from CpG-PBNPs upon addition of ethidium bromide (EtBr) relative to equal concentrations of free CpG added to EtBr (* significant difference, $p < 0.05$). (B) Percent normalized CpG bound in the CpG-PBNPs as a function of time and pH. (C) Fraction of CpG released from CpG-PBNPs after PTT at different laser powers (0.25 – 1.25 W) and different concentrations (0.1 – 0.5 mg/mL). Etbr was added as described above.

Complementary to these studies, we assessed the percentage of CpG that remained bound on the CpG-PBNPs as a function of varying pH and duration of contact. This is because we administer the CpG-PBNPs intratumorally for PTT and both tumor insterstitia and endosomal compartments - potential loci for the nanoparticles after intratumoral injection - exhibit mildly acidic pH compared to neutral, physiological pH observed in the serum and cytosol [73, 74]. At a neutral pH (7.0), the percent of bound CpG remained constant for up to 4 days and then decreased slightly (to 74.5%; **Figure 2.3B**). At a mildly acidic pH (4.6), the percent of bound CpG decreased slightly to 88.6% by Day 4 and down to 54.3% by Day 7. In contrast, at a mildly basic pH (8.0), the bound CpG decreased rapidly to 31.4% by Day 4 and was almost completely released by Day 7 at this pH. We can attribute this CpG release at mildly basic pHs to the well-described attack of the characteristic Fe^{II}-CN-Fe^{III} bonds of PBNPs (and CpG-PBNPs) by the slight excess of hydroxyl ions, previously described by us and others [19, 75, 76]. To test the fraction of CpG released from the nanoparticles after PTT, we conducted PTT at varying laser powers (0.25 W – 1.25 W), as well as different concentrations (0.1 mg/mL – 0.5 mg/mL), reaching final temperatures of around 40°C, 60°C, and 80°C (**Figure 2.4**). EtBr was added as described above. Our results showed that CpG remained bound to the nanoparticles after PTT, regardless of temperatures attained under the various PTT conditions suggesting that heat did not cause the de-complexation of CpG from the nanoparticles (**Figure 2.3C**). Together, these studies demonstrate that CpG in the CpG-PBNPs, as synthesized, is tightly bound and remains tightly bound in the pH 4.6-7.0 range

for up to 4 days, and after PTT, thus establishing the conditions for the retention of this adjuvant after intratumoral administration.

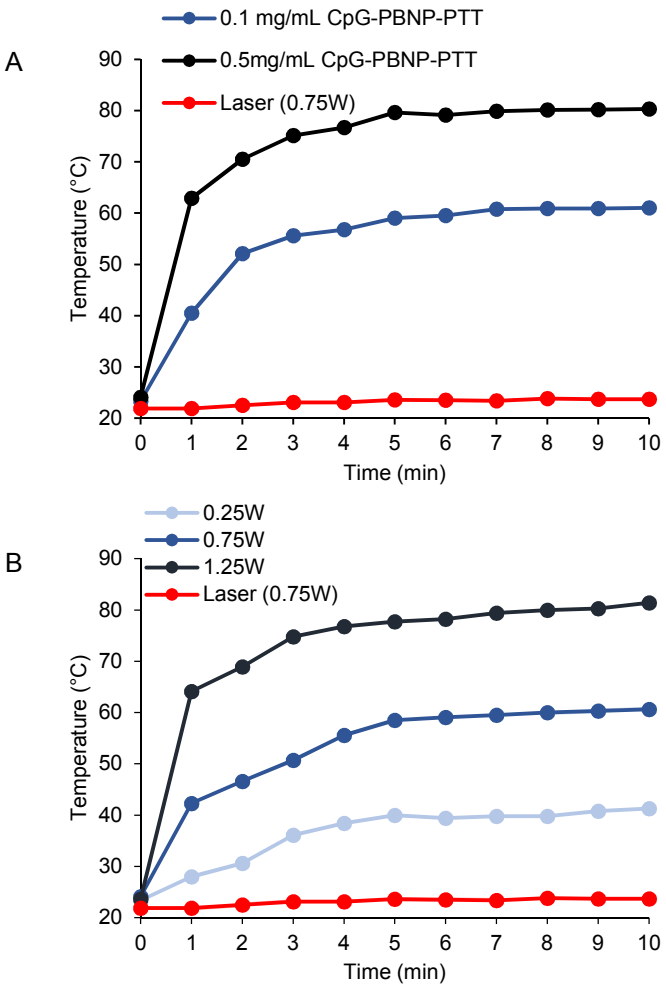

Figure 2.4. Photothermal heating curves of CpG-PBNPs. (A) Photothermal heating curves (temperature-time profiles) of varying concentrations (0.025 – 0.5 mg/mL) of CpG-PBNPs irradiated by an 808 nm NIR laser for 10 minutes at a power of 0.75 W (1.875 W/cm^2). (B) Photothermal heating of 1 mg/mL CpG-PBNPs using varying NIR laser powers (0.75 - 1.25 W) for 10 minutes.

2.5 Discussion

We have described a novel CpG-PBNPs nanoimmunotherapy that triggers robust antitumor immune responses in a syngeneic model of neuroblastoma by combining the effects of nanoparticle-based photothermal therapy with increased tumor antigenicity and adjuvanticity. We employed a layer-by-layer coating scheme to generate stable, monodisperse, and biocompatible CpG-PBNPs wherein CpG was tightly bound to the nanoparticles (**Figures 2.1** and **2.3A**).

CpG-PBNPs exhibited inherent pH-dependent stability (**Figure 2.3B**) where they are stable at an acidic pH mimicking conditions observed in the tumor interstitium, and exhibited incipient degradation at higher pHs mimicking the blood/lymph. The pH-dependent stability of CpG-PBNPs suggest their potential use in delivering tumor-specific therapies, where the nanoparticles remain intact intratumorally, while rapidly degrading when they enter the bloodstream or lymphatic system. This pH-dependent stability also minimizes potential toxicities associated with the long-term persistence of the nanoparticles *in vivo*- an important consideration in the field of nanomedicine for clinical translation.

The CpG-PBNPs retained the PTT properties of PBNPs (**Figure 2.2**), which is important for eliciting ICD in treated Neuro2a cells, and an upregulation of an immune response. CpG-PBNPs heat up in a concentration-dependent (**Figure 2.2A**) and laser power-dependent (**Figure 2.2B**) manner, allowing for precise control of temperatures reached during PTT. Furthermore CpG-PBNPs are able to undergo cyclic heating (**Figure 2.2C**), alluding to the stability of the crystal structure after PTT. This

phenomenon is further demonstrated through the lack of release of CpG from the CpG-PBNPs after PTT at different temperatures (**Figure 2.3C**). This is an important characteristic of our therapy, since the PBNP stability post-PTT allows for a multi-treatment strategy of tumor cell death to occur via: 1) local tumor heating, 2) release of tumor neoantigens, 3) ICD of neuroblastoma cells, 4) infiltration of immune cells, and 5) activation of a tumor-specific immune response that is upregulated through the 6) local bioavailability of CpG. The upregulation of tumor antigenicity and adjuvanticity via the CpG-PBNP-PTT nanoimmunotherapy is therefore a crucial step in the design of functional nanoparticles for the treatment of neuroblastoma.

Layer-by layer assembly has been used to coat a wide range of substrates with polyelectrolyte multilayers consisting of antigens, adjuvants, or both antigen and adjuvant.[69, 77-82] Similarly, the synthesis and coating scheme described here can be easily modified to coat PBNPs with other immune signals consisting of tumor antigen, immunological adjuvants, and/or other antigen-adjuvants combinations. This tripartite PTT-based cell death-antigenicity-adjuvanticity can, in principle, be applied for the treatment of other solid tumors that employ similar immune evasion mechanisms.

Chapter 3: Photothermal therapy generates a thermal window of immunogenic cell death in neuroblastoma[2]

3.1 Abstract

We describe a thermal "window" of immunogenic cell death (ICD) elicited by nanoparticle-based photothermal therapy (PTT) in an animal model of neuroblastoma. In studies using PBNPs to administer photothermal therapy (PBNP-PTT) to established localized tumors in the neuroblastoma model, we observed that PBNP-PTT conformed to the "more is better" paradigm, wherein higher doses of PBNP-PTT generated higher cell/local heating and thereby more cell death, and consequently improved animal survival. However, *in vitro* analysis of the biochemical correlates of ICD (ATP, HMGB1, calreticulin) elicited by PBNP-PTT demonstrated that PBNP-PTT triggered a thermal window of ICD. ICD markers were highly expressed within an optimal temperature (thermal dose) window of PBNP-PTT (63.3-66.4 ^{o}C) as compared with higher (83.0-83.5 ^{o}C) and lower PBNP-PTT (50.7-52.7 ^{o}C) temperatures, which both yielded lower expression. Subsequent vaccination studies in the neuroblastoma model confirmed our *in vitro* findings wherein PBNP-PTT administered within the optimal temperature window resulted in long-term survival (33.3% at 100 days) compared with PBNP-PTT administered within the higher (0%) and lower (20%) temperature ranges, and controls (0%). Our findings demonstrate a tunable immune response to heat

[2] This chapter was adapted from Sweeney EE, Cano-Mejia J, and Fernandes R, *Photothermal therapy generates a thermal window of immunogenic cell death in neuroblastoma.* Small, 2018. doi: 10.1002/smll.201800678

generated by PBNP-PTT, which should be critically engaged in the administration of PTT for maximizing its therapeutic benefits.

3.2 Introduction

Nanoparticle-based photothermal therapy (PTT) has been widely investigated in cancer therapy as a rapid and minimally invasive tumor ablation technique [19, 83]. In this treatment modality, the intrinsic photothermal conversion property of synthesized nanoparticles is used for tumor control [18, 30, 84]. This property allows the conversion of incident light into heat, which generates cell temperature increases, thereby killing cancer cells in contact with the nanoparticles. Over the past two decades, several reports utilizing nanoparticles for PTT of diverse tumor types *in vitro* and *in vivo* have been described [18, 30, 64, 85-94].

An emerging area of interest is the effect of PTT on the immune system during tumor therapy, since PTT not only causes tumor cell death, but can also release tumor antigens and endogenous adjuvants (e.g. heat shock proteins, DAMPs) under certain conditions [21, 23]. These endogenous adjuvants have the potential to increase tumor immunogenicity, which can result in improved therapeutic responses. Engaging the immune system during PTT is favorable as if offers the potential for persistent treatment responses and immunological memory. Earlier studies have described the use of PTT in combination with immunotherapies such as checkpoint inhibitors and adoptively transferred T cells [19, 21, 23], and studies wherein the nanoparticles themselves were modified to deliver immune adjuvants (e.g. TLR agonists) [20, 57, 59,

95]. While these findings suggest that PTT engages the immune system, both by itself and/or in combination with immune adjuvants/immunotherapies, it is still unclear if PTT elicits *bona fide* ICD [96] - a cell death phenotype that engages the immune response and is associated with favorable therapeutic implications. Further, the effect of increasing levels of heat, specifically through PTT, on ICD is still unclear.

In this study, we seek to answer whether nanoparticle-based PTT elicits ICD. ICD is associated with several endogenous biochemical correlates including (but not limited to) the release of ATP and high-motility group box 1 (HMGB1) from dying cells, and increased exposure of surface calreticulin on the surface of dying cells [96-100]. We use these molecular markers to indicate ICD, but we further confirm its presence by demonstrating the effect on immunological memory through a vaccination model. It is important to note that the ICD markers may be present without *bona fide* ICD; a cytotoxic component is required in order for both benefits of ICD, the cell killing and immune cell engagement, to occur [101-103]. Additionally, we determine if PTT elicits ICD under all temperature regimes (thermal doses), or if ICD occurs under only certain favorable conditions of PTT.

To answer these questions, we utilize PBNPs for PTT (PBNP-PTT) (**Figure 3.1A**). PBNPs are biodegradable, FDA-approved nanoparticles [26, 104, 105] that we have previously used for photothermal therapy of tumors, both alone [18] and in combination with chemotherapy [64] and immunotherapies [19, 106]. Specifically, we administer varying thermal doses of PBNP-PTT to tumor cells *in vitro* and *in vivo* by varying the PBNP concentrations and the laser power. For *in vivo* studies, we use Neuro2a cells in a hard-to-treat, syngeneic animal model of neuroblastoma [107-109]

- the third leading cause of cancer-related death in children in the United States [2, 110]. Neuroblastoma evades the immune system as it typically exhibits a lower neoantigen load [11] and therefore serves as a suitable model to test the effect of PBNP-PTT on generating ICD. Our findings demonstrate a tunable immune response to heat generated by PBNP-PTT, which has important implications for eliciting potent and persistent antitumor immune responses for maximizing its therapeutic benefits (**Figure 3.1B)**.

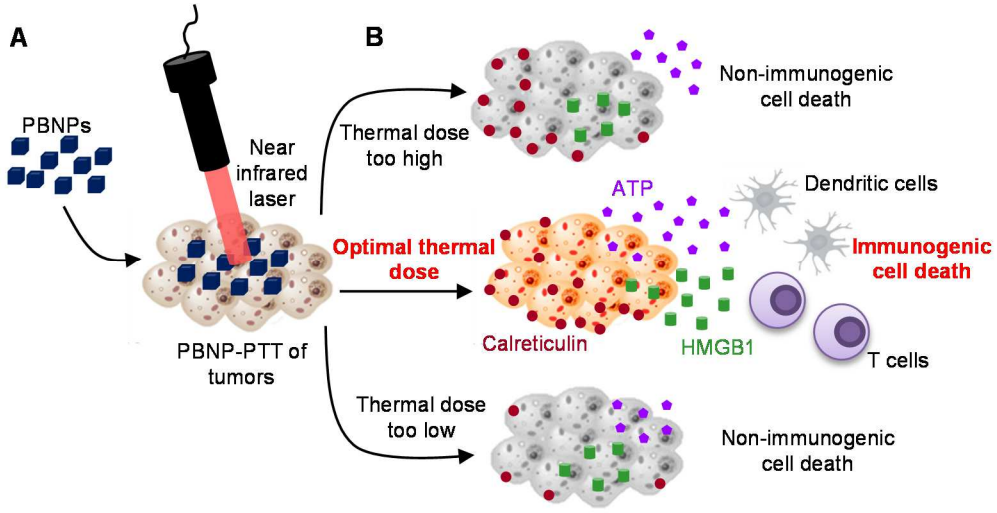

Figure 3.1. Prussian blue nanoparticle-based photothermal therapy (PBNP-PTT) generates a thermal window of immunogenic cell death (ICD). A) PBNPs that are administered to tumors and illuminated with a near infrared light trigger tumor cell death by PBNP-PTT. B) (Middle). When an optimal temperature range (thermal dose) of PBNP-PTT is administered to tumors, the tumor cells undergo ICD marked by the release of ATP, HMGB1, and increased expression of surface calreticulin. These effects elicit a potent antitumor immune response that is associated with improved therapeutic outcomes. If the thermal dose of PBNP-PTT is either too low (Bottom) or too high (Top), the tumor cells may still be killed by the effects of PBNP-PTT, but the dying cells do not trigger a favorable antitumor immune response because they do not undergo *bona fide* ICD.

3.3 Materials and Methods

3.3.1 Cells

The murine neuroblastoma cell line Neuro2a was originally obtained from American Type Culture Collections (ATCC, Manassas, VA) and cultured under recommended conditions. Cells were subcultured in DMEM (Gibco, Carlsbad, CA) containing 10% fetal bovine serum (FBS, Gibco, Carlsbad, CA) and 1% penicillin/streptomycin (Sigma-Aldrich, St. Louis, MO).

3.3.2 Animals

Four-to-five-week old female A/J mice were purchased from Jackson Laboratory (Bar Harbor, ME). The animals were acclimated for 3-4 days prior to any injections. All procedures were approved by the Institutional Animal Care and Use Committee of Children's National Health System (CNHS), Washington, DC (Protocol # 00030439), and are in accordance with the humane care of research animals. Tumor volumes were monitored every other day by caliper measurement. A tumor size of 15 mm diameter in any dimension, or 13 mm if two tumors were present, was designated as the endpoint and mice were euthanized at that time. Euthanasia was achieved through cervical dislocation after CO_2 narcosis. If the tumor impaired mobility of the animal, became ulcerated or appeared infected, or if the mice displayed signs of distress by sick mouse posture, the mouse was euthanized.

3.3.3 PBNP synthesis

PBNPs were synthesized using a scheme as described previously [18, 27, 31, 111]. Briefly, an aqueous solution of 6.8 mg $FeCl_3 \cdot 6H_2O$ (2.5×10^{-5} mol) in 5 mL of Milli-Q water was added under vigorous stirring to an aqueous solution containing 10.6 mg of $K_4Fe(CN)_6 \cdot 3H_2O$ (2.5×10^{-5} mol) in 5 mL of Milli-Q water. After stirring for 15 min, the precipitate was isolated by centrifugation (20,000g for 10 min) and rinsed by sonication (5 s, high power) in Milli-Q water. The isolation and rinsing steps were repeated three times before the particles were resuspended by sonication in Milli-Q water. All synthetic procedures were conducted using ultrapure water obtained from a Milli-Q system (Millipore Corporation, Billerica, MA) with resistivity of 18.2 MΩ·cm. Potassium hexacyanoferrate (II) trihydrate (MW 422.39; $K_4[Fe(CN)_6] \cdot 3H_2O$), iron (III) chloride hexahydrate (MW 270.3; $Fe(Cl)_3 \cdot 6H_2O$), were all purchased from Sigma-Aldrich (St. Louis, MO).

3.3.4 *In vitro* PBNP-PTT

In vitro PBNP-PTT was performed using an 808 nm NIR laser from Laserglow Technologies (Toronto, ON, Canada). Either 50,000 Neuro2a neuroblastoma cells were seeded overnight in 96-well plates, or ten million Neuro2a cells were suspended in 1 mL PBS in a 1.7 mL microcentrifuge tube. Varied concentrations of PBNPs were added to the cells, and the cells were then illuminated by the NIR laser. Power was confirmed by a power meter (Thorlabs, Newton, NJ). Temporal temperature measurements were taken using a thermal camera (FLIR, Arlington, VA).

3.3.5 *In vivo* PBNP-PTT

1 million Neuro2a cells in 100 μL PBS were subcutaneously injected into the backs of previously shaved A/J mice. Treatment began when tumor volumes reached ~60 mm^3. Visual as well as histological examination of the tumors excised from these tumor-bearing mice confirmed that the tumors are well vascularized and not a loose collection of cells (**Appendix 7**). Mice were anesthetized prior to treatment using 5% isoflurane. They were then intratumorally injected with 50 μL of PBNPs (varied concentrations). After injection, tumors were irradiated with NIR light (808 nm) from Laserglow Technologies (Toronto, ON, Canada) (varied power) for 10 minutes. Their eyes were covered with opaque black cardboard during treatment to avoid eye damage. Temperatures reached during PBNP-PTT were measured using a FLIR thermal camera (Arlington, VA).

3.3.6 ICD marker analysis

In vitro PBNP-PTT was performed as described above. Cell suspensions were then washed and stained with fluorescent antibodies against HMGB1 (intracellular) and calreticulin (extracellular) and flow cytometry was performed. Antibodies were purchased from Abcam (Cambridge, UK), flow cytometry was performed on the BD Biosciences FACSCaliber (Franklin Lakes, NJ), and analysis was done using FlowJo (Ashland, OR) software. For intracellular ATP presence, cells were washed after *in vitro* PBNP-PTT and the ATP-based CellTiter-Glo (Promega, Madison, WI) Luminescent Cell Viability Assay was performed.

3.3.7 Vaccination model

In vitro PBNP-PTT was performed as described above in the 1.7 mL microcentrifuge tube. Resulting cell/nanoparticle suspensions (1 million cells in 100 μL per mouse) were injected subcutaneously into the right side of the backs of previously shaved A/J mice. Four days later, this was repeated. Three days later (seven days from first injection), mice were subcutaneously inoculated with 1 million Neuro2a cells in 100 μL PBS into the backs on the opposing (left) side. Tumor growth was measured by calipers, and survival was analyzed over time.

3.3.8 CEM43 calculations

Thermal doses administered to the various groups was expressed in terms of CEM43 (cumulative equivalent minutes at 43 ^{o}C). CEM43 was calculated using the equation described by Sapareto and Dewey:[112]

$$CEM43 = \Delta t \times R^{(43-T)}$$

Where Δt signifies summation over the length of exposure, T is the average temperature during time interval t, and R is a constant equal to 0.25 for T<43°C and 0.5 for T>43°C.

3.3.9 Statistical analysis

Statistical significance was determined from a two-tailed Student's *t* test and values with $p<0.05$ qualified as statistically significant. Survival results were analyzed

according to a Kaplan-Meier curve. The log-rank test was used to determine statistically significant differences in survival between the various groups.

3.4 Results

3.4.1 Higher doses of PBNP-PTT results in improved tumor eradication and survival for mice with localized focal Neuro2a tumors

To begin PBNP-PTT dosage studies, we first demonstrated PBNP concentration-dependent temperature increases of Neuro2a neuroblastoma cells *in vitro* (**Figure 3.2A-B**). We show that cell viability significantly decreases as temperatures induced by PBNP-PTT rise above ~48 °C (**Figure 3.2C**). As a step toward illustrating the effects of varied doses of PBNP-PTT on primary neuroblastoma tumors, we conducted studies on local Neuro2a tumor eradication. Specifically, Neuro2a tumor-bearing mice (~ 5 mm tumor sizes; $n \geq 4$/group) were treated with: 1) vehicle (PBS), 2) low-dose PBNP-PTT (low PTT; attaining an average tumor temperature < 40 °C), 3) medium-dose PTT (medium PTT; average tumor temperature < 60 °C), and 4) high-dose PTT (high PTT; average tumor temperature ~ 90 °C) (**Figure 3.2D**). Our studies demonstrate that for a localized tumor, higher PTT was more effective in tumor eradication as evidenced by slower tumor growth (**Figure 3.3**) and 100% survival at 40 days, compared with medium PTT (50% survival), low PTT (20% survival), and vehicle treated controls (0% survival) (**Figure 3.2E**). These results demonstrate that higher-dose PBNP-PTT generates the highest cell heating and is most effective for localized tumor eradication *in vitro* and *in vivo*.

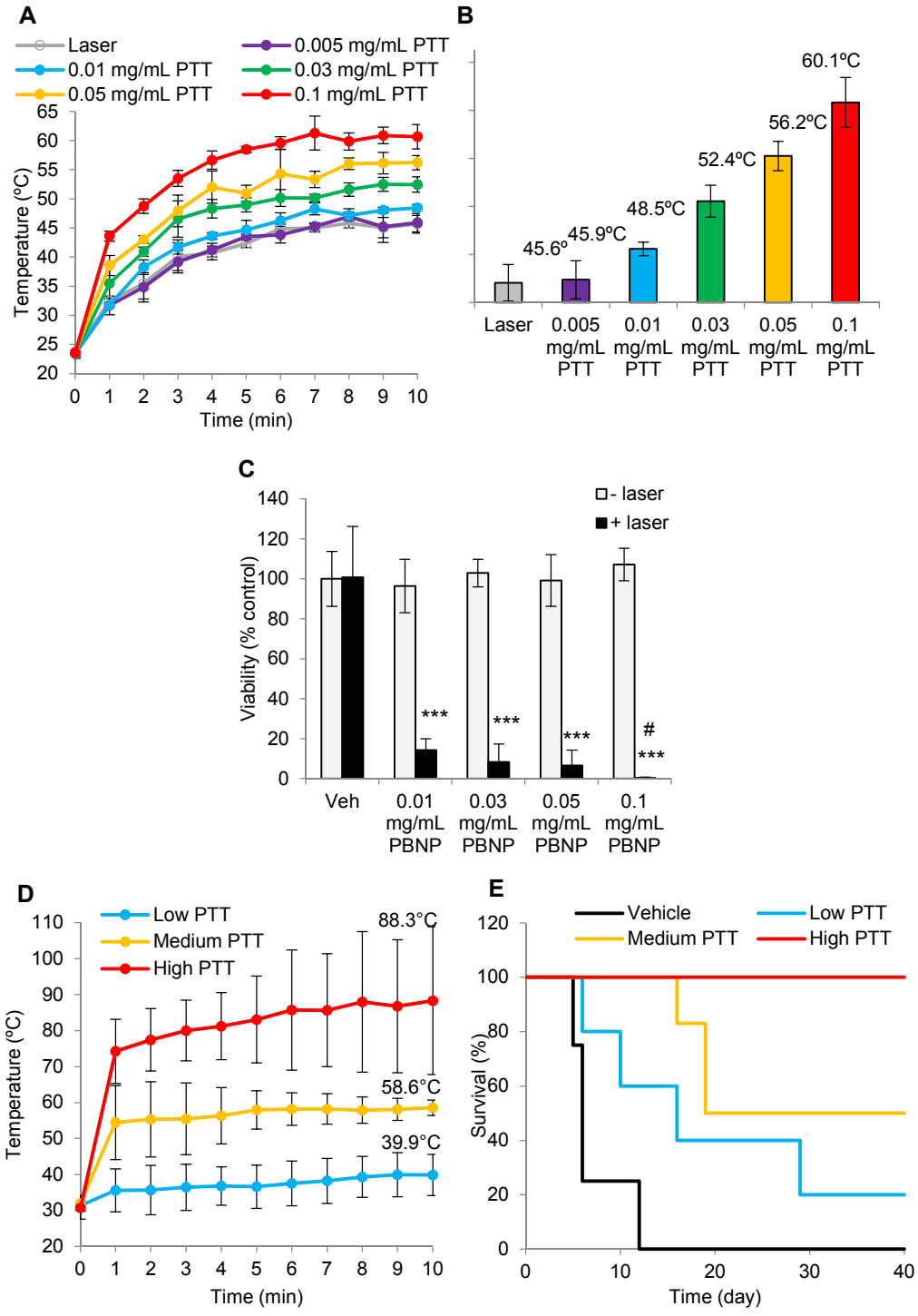

Figure 3.2. PBNP-PTT increases neuroblastoma cell temperature and triggers their death in a temperature (thermal dose)-dependent manner *in vitro* and *in vivo.* A-C) 50,000 Neuro2a cells were seeded in 96-well plates, treated with the listed concentration of PBNPs, and subjected to ten minutes of illumination by an 808 NIR laser at 1.5 W/cm^2. Values represent means ± standard deviation (SD); n = 3/group. A) Temperature-time profiles of the varying

PTT conditions as measured by a thermal camera at one-minute intervals. B) Final average temperatures achieved by Neuro2a cells after ten minutes as a function of varying PTT conditions. C) *In vitro* Neuro2a cell viability post-treatment with vehicle or varying doses of PBNPs or PBNP-PTT, measured 24 hours after treatment. *** $p < 0.001$ compared to Vehicle; # $p < 0.05$ compared to 0.05 mg/mL PBNP-PTT+ Laser. (D-E) Mice bearing ~5mm Neuro2a neuroblastoma tumors were treated with varying doses of PBNP-PTT; low, medium, and high PTT, administered by intratumoral injection of PBNPs followed by ten minutes of NIR laser irradiation. Values represent means ± SD; $n \geq 4$/group. D) Average tumor temperatures attained by Neuro2a tumor-bearing mice treated with low thermal dose PBNP-PTT (Low PTT; blue), medium thermal dose PBNP-PTT (Medium PTT; orange), and high thermal dose PBNP-PTT (High PTT; red) as measured by thermal camera. Listed numbers indicate the final average tumor temperatures attained. E) Survival of Neuro2a tumor-bearing mice treated with Vehicle (black), Low PTT (blue), Medium PTT (orange), and High PTT (red).

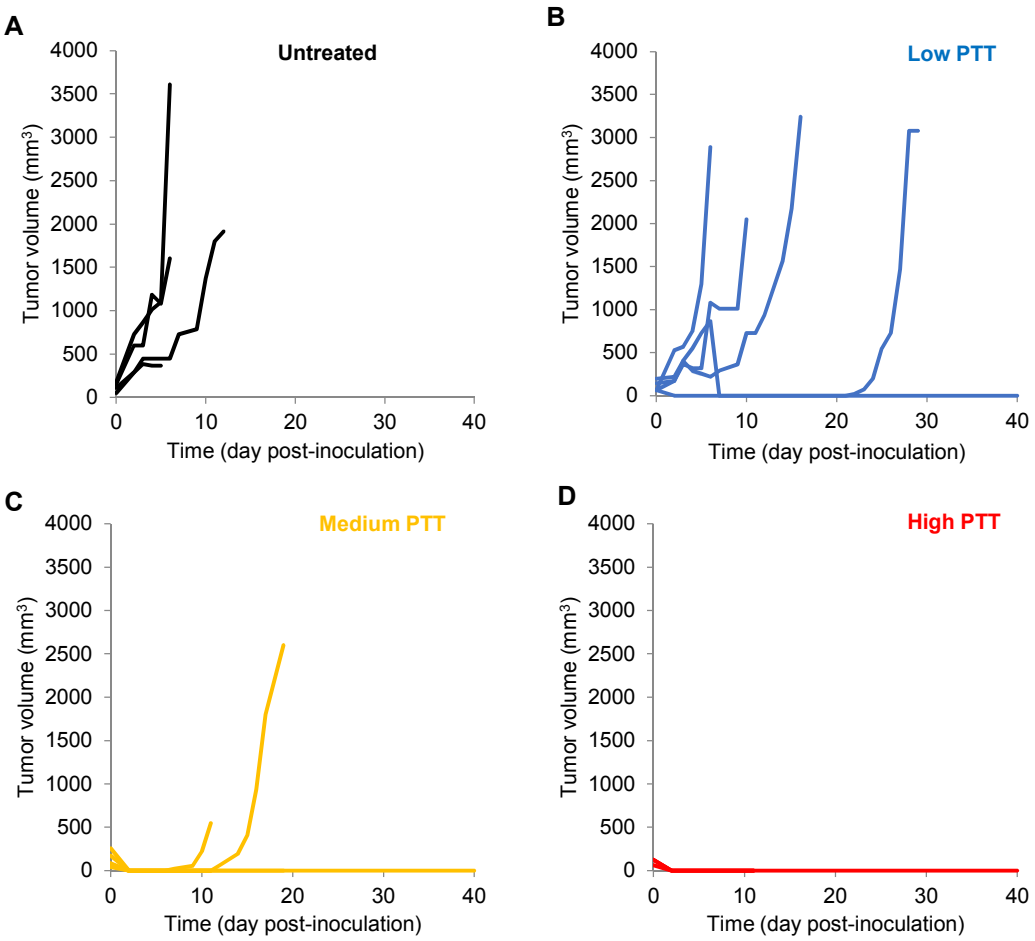

Figure 3.3 Neuroblastoma tumor growth after no treatment or treatment with varied levels (doses) of PBNP-PTT. Neuro2a tumor-bearing mice were: A) Untreated, or treated with B) Low-dose PBNP-PTT (Low PTT), C) Medium-dose PBNP-PTT (Medium PTT), and D) High-dose PBNP-PTT (High PTT). Each line represents the tumor growth trajectory of an individual mouse ($n \geq 4$ per group).

3.4.2. Neuro2a cells treated with PBNP-PTT *in vitro* exhibit an optimal temperature range for increased expression of ICD markers

In the context of engaging a robust antitumor response needed for treating locally advanced or disseminated tumors (as is typically seen in high-risk neuroblastoma), we sought to determine if the "more is better" trend observed for local tumor eradication held for engaging a robust antitumor immune response. Accordingly, we treated Neuro2a cells *in vitro* with varying thermal doses of PBNP-PTT and assessed the effects of temperature on the tumor cells (**Figure 3.4A**). Specifically, we looked at the expression of ICD markers (ATP release, HMGB1 release, and surface calreticulin expression) on the PBNP-PTT-treated Neuro2a cells (based on consensus guidelines previously described by Kepp *et al.*)[99] (**Figure 3.4B-D**). Briefly, in order to suggest that the treated cells are undergoing ICD, intracellular ATP and HMGB1 should be decreased, and surface calreticulin expression should be increased, when compared to untreated controls. All three markers should be present in order to classify the cells are undergoing ICD. Here, in terms of ATP secretion and surface calreticulin expression, all temperatures/thermal doses above 50 $^{\circ}$C showed notably lower intracellular ATP and higher surface calreticulin expression as compared to controls. However, in terms of HMGB1 release, only the 50.7 $^{\circ}$C group and 61.1 $^{\circ}$C group exhibited > 30% change in intracellular HMGB1 compared with untreated controls. Cells heated to 84.3 $^{\circ}$C did not exhibit a marked decrease in intracellular HMGB1 suggesting that this higher temperature may not elicit ICD when compared to the lower temperature groups (i.e. the 50.7 $^{\circ}$C and 61.1 $^{\circ}$C groups). PBNP alone-treated cells did not show induction of ICD (**Figure 3.5**). These observations suggest that PBNP-PTT-

treated Neuro2a cells exhibit a window of ICD, i.e. ICD increases as temperature rises to an average temperature of ~60 °C, and then it decreases as temperature rises further to 80 °C and higher (**Figure 3.4**). This indicates that more is not necessarily better in this context, and that an optimal temperature window exists for eliciting ICD by PBNP-PTT.

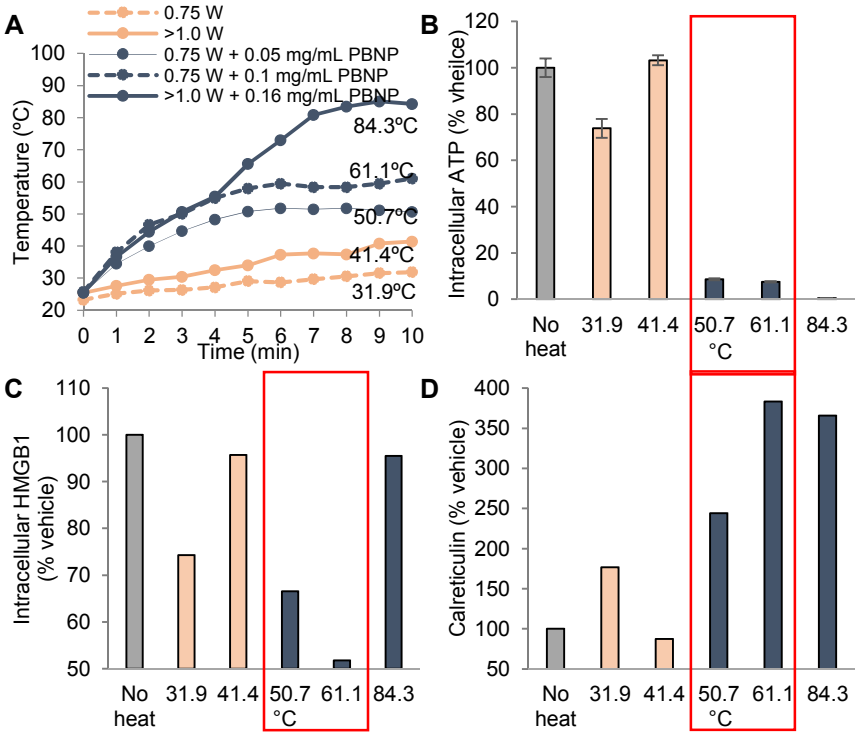

Figure 3.4. Neuro2a cells treated with PBNP-PTT *in vitro* exhibit an optimal temperature range for increased expression of ICD markers. A) Temperature-time profiles of samples containing 10 million Neuro2a cells treated 0.75 W laser, > 1 W laser, 0.75 W laser + 0.05 mg/mL PBNP, 0.75 W laser + 0.1 mg/mL PBNP, and > 1 W laser + 0.16 mg/mL PBNP. B) Intracellular ATP in the various treatment groups (as a % of the vehicle-treated group). C) Intracellular HMGB1 in the various treatment groups (as a % of the vehicle-treated group). D) Surface calreticulin expression in the various treatment groups (as a % of the vehicle-treated group). Red boxes indicated the treatment temperatures ranges for which all three markers of ICD are expressed/present (to varied degrees).

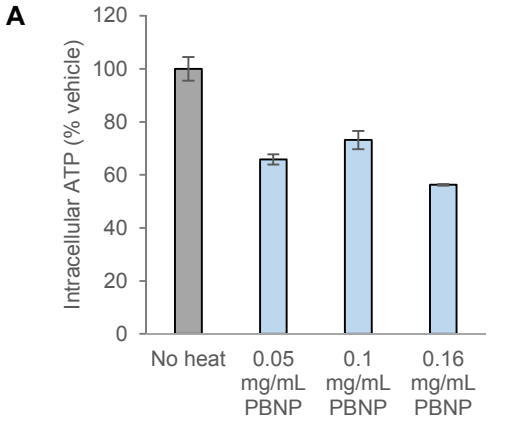
A
Intracellular ATP (% vehicle)
120
100
80
60
40
20
0
No heat
0.05 mg/mL PBNP
0.1 mg/mL PBNP
0.16 mg/mL PBNP

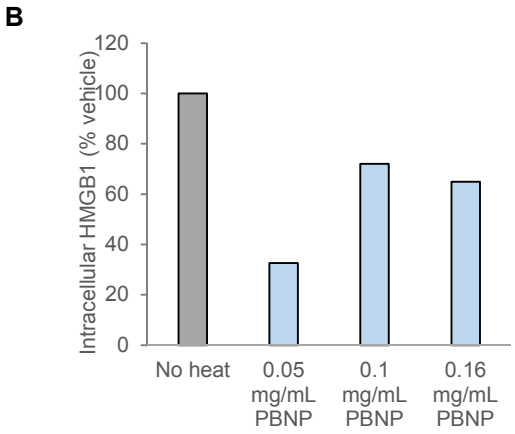
B
Intracellular HMGB1 (% vehicle)
120
100
80
60
40
20
0
No heat
0.05 mg/mL PBNP
0.1 mg/mL PBNP
0.16 mg/mL PBNP

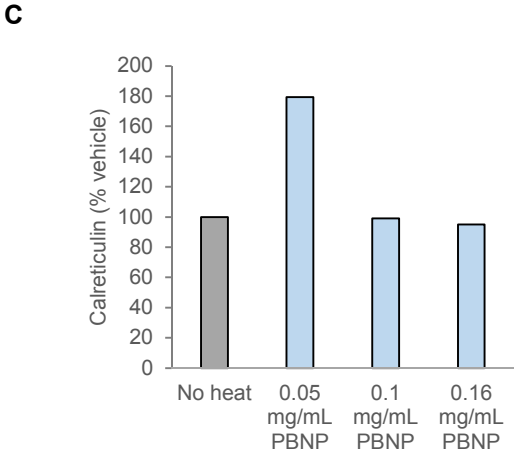
C
Calreticulin (% vehicle)
200
180
160
140
120
100
80
60
40
20
0
No heat
0.05 mg/mL PBNP
0.1 mg/mL PBNP
0.16 mg/mL PBNP

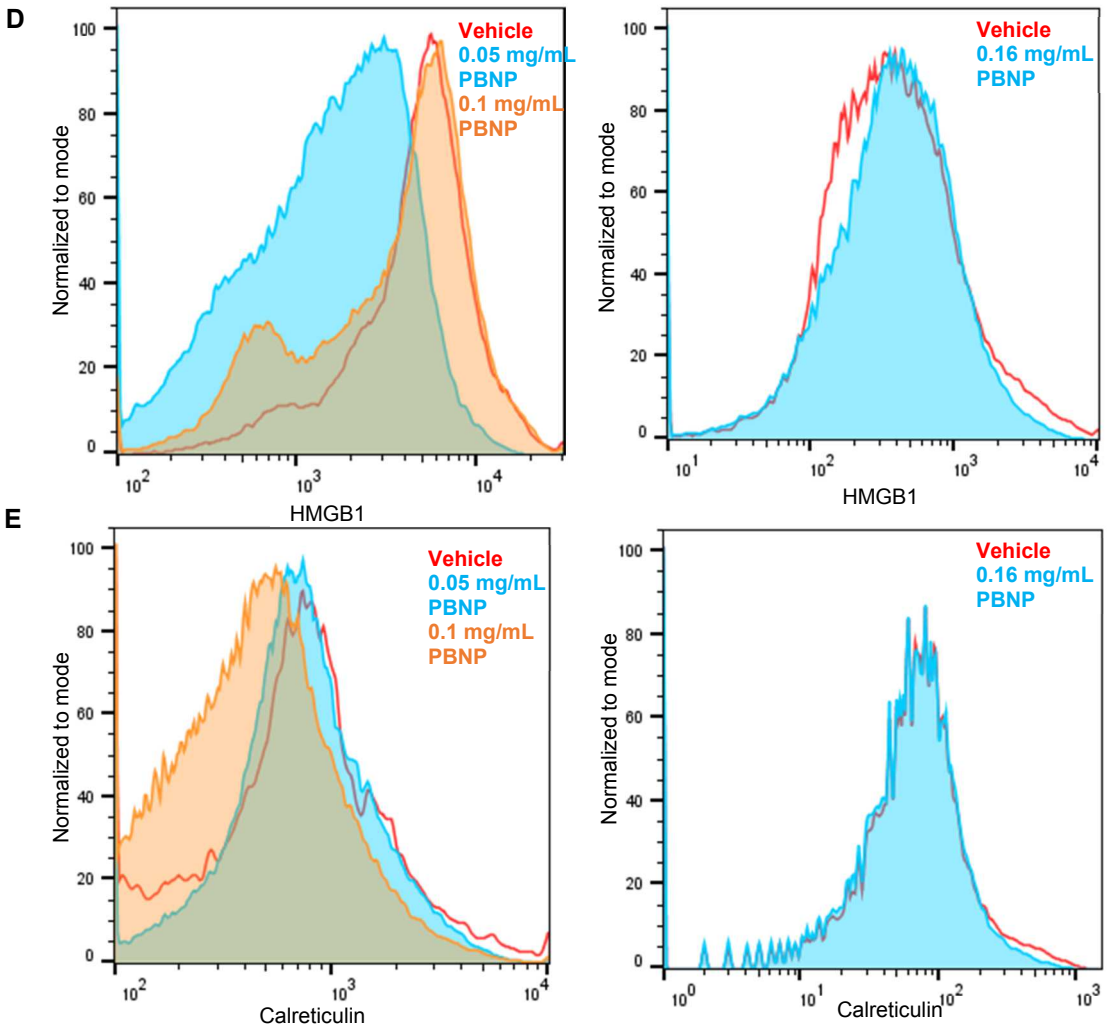

Figure 3.5. Effect of treatment with PBNPs only (no heat) on cellular expression of ICD markers *in vitro* as measured by the three ICD hallmarks. Neuroblastoma (Neuro2a) cells (10 million cells/mL in 1.7 mL tubes) were subjected to treatment with vehicle and increasing concentrations of PBNPs, and markers of ICD were then analyzed (ATP release (A), HMGB1 release (B), and calreticulin exposure (C)). Representative histograms of D) HMGB1 and E) calreticulin, analyzed by flow cytometry, are shown.

3.4.3 Animals vaccinated with PBNP-PTT-treated Neuro2a cells within the optimal temperature window (showing increased ICD markers) exhibit significantly increased protection against subsequent Neuro2a challenge

We next tested if our observations of a window of ICD *in vitro* and had implications for engaging an immune response *in vivo*. Therefore, we performed a vaccination study wherein Neuro2a cells were treated with different doses of PBNP-PTT (0.05-0.16 mg/mL PBNP + 0.75-1 W laser) and controls (0.75 laser alone or 0.16 mg/mL PBNP alone) *in vitro* and then injected into naïve A/J mice (2×, 7 days apart). Vehicle-treated mice were given PBS alone (no cells). Subsequently, these "vaccinated" animals were challenged with 1 million Neuro2a cells and tumor growth and animal survival was monitored. Our studies demonstrate that animals vaccinated with PBNP-PTT-treated Neuro2a cells within the thermal window of ICD resulted in slower tumor progression (**Figure 3.6**) and higher long-term survival compared to animals in the other treatment groups (**Figure 3.7**)**.** Specifically, animals in the 65.3 $^{\circ}$C and 52.3 $^{\circ}$C average final temperature groups exhibited higher long-term survival than animals in the higher (83.3 $^{\circ}$C) and lower (32.5 $^{\circ}$C) average final temperature groups. The group showing the most dramatic ICD markers, the 65.3 $^{\circ}$C group, showed significantly longer survival than all groups except the 52.3 $^{\circ}$C group. This suggests that at the optimal thermal dose, ICD is present and effective in Neuro2a cell killing and endogenous adjuvant release, causing immune cell engagement and thus neuroblastoma tumor challenge rejection.

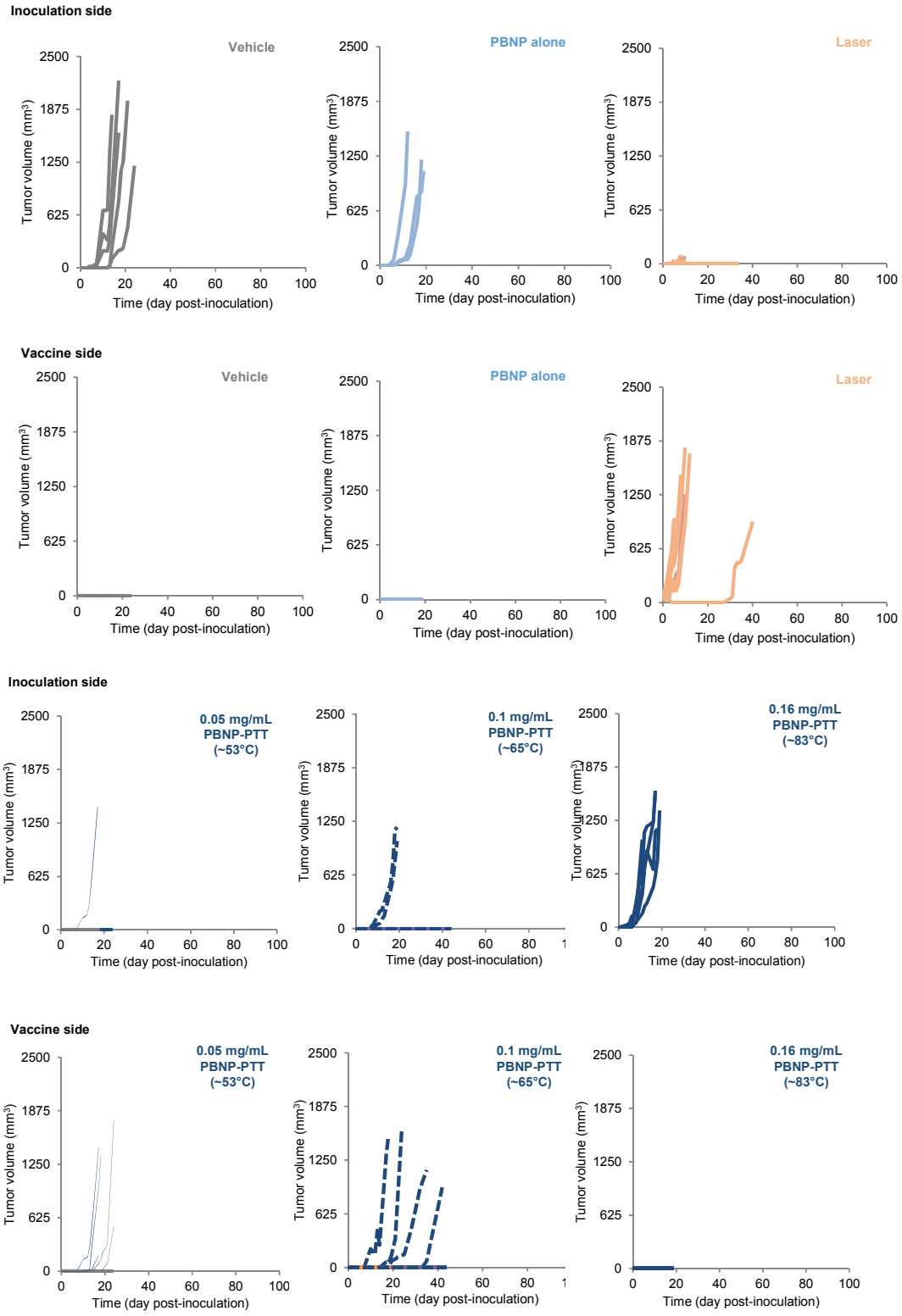

Figure 3.6. *In vivo* tumor growth after prophylactic vaccination with vehicle-, PBNP-, laser-, or varied PBNP-PTT-treated neuroblastoma cells. Each line represents the tumor growth trajectory of an individual mouse (n=3-9 per group).

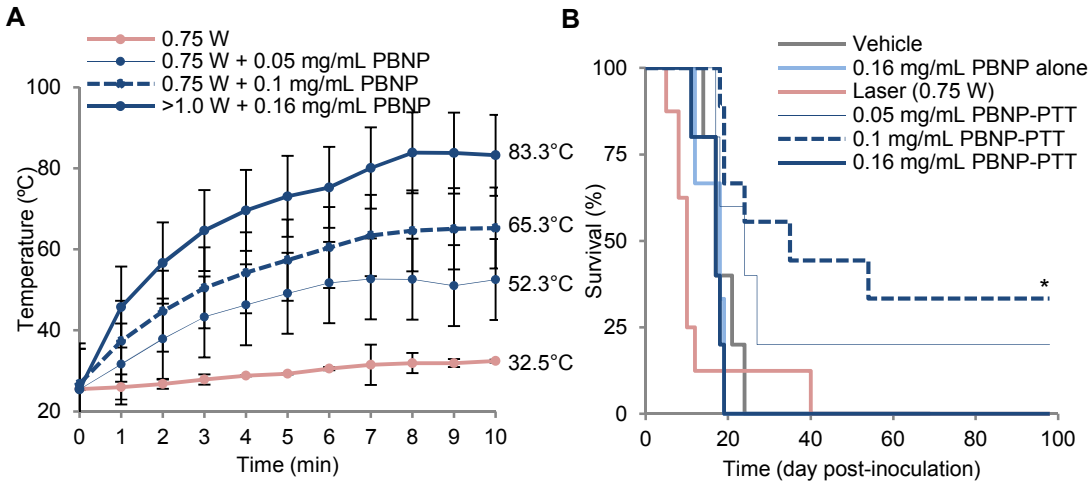

Figure 3.7. Animals vaccinated with PBNP-PTT-treated Neuro2a cells within the optimal temperature window (showing increased ICD markers) exhibit significantly increased protection against subsequent Neuro2a challenge. A) Temperature-time profiles of samples containing 10 million Neuro2a cells/mL treated 0.75 W laser, > 1 W laser, 0.75 W laser + 0.05 mg/mL PBNP, 0.75 W laser + 0.1 mg/mL PBNP, and > 1 W laser + 0.16 mg/mL PBNP that were vaccinated in naïve A/J mice (means ±SD; n = 4 replicates/group). B) Survival of mice challenged with 1 million Neuro2a cells that were previously vaccinated with vehicle, PBNP-, laser-, or PBNP-PTT-treated Neuro2a cells. n = 3-9/group; * $p < 0.05$ compared with all groups except 0.05 mg/mL PBNP-PTT.

3.4.4 PBNP-PTT-treated Neuro2a cells exhibit a thermal "window" of ICD, which is associated with improved protection against tumor challenge

Based on our findings, we calculated the expression of ICD markers (**Figure 3.8A**) and long-term survival (% survival at 100 days post-treatment) (**Figure 3.8B**) as a function of thermal dose expressed as CEM43 (cumulative equivalent minutes at 43 °C) [112, 113]. CEM43 analysis allows for a generalizable comparison of biological effect across different thermal therapies and serves as an objective metric for thermal injury [112]; it has been used extensively in the literature for measuring the effects of heat on different tissues [114-116]. Our results demonstrate that PBNP-PTT exhibits a thermal window of ICD between 3.3 and 5.6 log(CEM43) (**Figure 3.8A**) wherein the

ICD markers of interest, decreased intracellular ATP and HMGB1 and increased surface calreticulin, were most highly expressed. We found this thermal window (3.3 – 5.6 log(CEM43)) to be associated with improved protection against tumor challenge compared to animals in other sub-optimal treatment groups (**Figure 3.8B**). The thermal dose maximizing ICD correlates (5.6 log(CEM43)) resulted in the highest long-term survival (33.3%), suggesting the importance of ICD in generating an antitumor immune response and the requirement of the three biochemical correlates in eliciting ICD and subsequent immune effects.

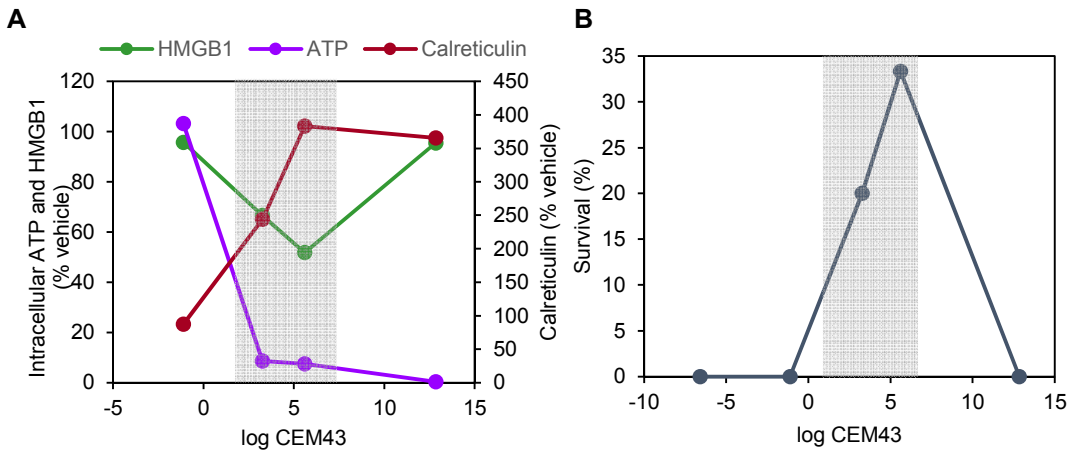

Figure 3.8. PBNP-PTT-treated Neuro2a cells exhibit a thermal "window" of ICD, which is associated with improved protection against tumor challenge. A) Expression of ICD markers as a function of thermal dose described in terms of cumulative equivalent minutes at 43 ºC; a thermal dose parameter (CEM43)[38]. The grey shaded area represents the region of increased ICD elicited by PBNP-PTT B) % Survival of mice (at 100 days) challenged with Neuro2a tumors that were vaccinated with PBNP-PTT-treated Neuro2a cells. Improved long-term survival "mirrors" the thermal dose window shown in panel A.

3.5 Discussion

Here, we illustrate the discovery of an optimal thermal dose window, wherein cancer cells subjected to optimized conditions of PBNP-PTT undergo ICD and are able to reject future tumor challenge. Despite a direct correlation of increased temperature to survival in a localized primary neuroblastoma tumor model (**Figure 3.2E**), in the context of a secondary or disseminated tumor model, as modeled by our vaccination studies, the temperatures achieved by PBNP-PTT must be in the range of ~50-60 $^{\circ}$C in order to effect improved survival (**Figure 3.7**). Thus, the "more is better" paradigm may be inappropriate for tumors that have already spread, or tumors that cannot be sufficiently treated with monotherapy. Despite being the most cytotoxic thermal dose, the highest thermal dose is not the most effective in generating an antitumor immune response.

To our knowledge, this is the first description of a thermal dose-dependent induction of ICD in cancer. We present a simple and generalizable method to test ICD by measuring three biochemical correlates as measured against a CEM43 thermal dose value. While we have described the effective thermal doses for the Neuro2a neuroblastoma model, the observations described here may be applicable across other cancer types. Other types of tumors will need to be considered individually, as disease-specific characteristics such as location of tumor, extent of angiogenesis and vasculature, and intrinsic immunogenicity may alter the effect of a given thermal dose on eliciting ICD. It is important to consider the cytotoxic effect of the heat as well,

since the primary tumor cells must be adequately killed while simultaneously engaging an immune response [96].

In vitro flow cytometry reveals HMGB1 to perhaps play the most integral role in effective ICD in our model. Although the mice treated with the ~80 °C vaccine increased surface calreticulin and released ATP, HMGB1 levels were similar to vehicle-treated cells (**Figure 3.4**), and no survival benefit was conferred, suggesting that HMGB1 secretion is required for improved outcome. HMGB1 has been described in the literature as a critical DAMP for initiating the innate and adaptive immune responses [117, 118] and may be required for DC-mediated responses [119]. Our data mirrors these observations and further points to HMGB1 being essential for ICD. We recognize that at high temperatures, HMGB1 would still be predicted to release from necrotic cells; however, HMGB1 may be unstable at such temperatures and thus be rendered non-functional and ineffective.

The tunable nature of ICD induction presented in this context may also apply to other ICD-inducing cancer therapies; perhaps a "more is better" approach is inappropriate for these therapies and treatment-specific optimal windows may exist. Ongoing studies will further elucidate the phenomenon of PBNP-PTT-generated ICD and its effect on secondary or metachronous tumors in the vaccination as well as therapeutic settings. Further, these findings suggest the potential of combining PBNP-PTT with exogenous adjuvants or other immunotherapies to augment and/or complement the effects of ICD.

These studies describe a thermal "window" of ICD elicited by PBNP-PTT in an animal model of neuroblastoma. *In vitro* analysis of the biochemical markers of ICD

elicited by PBNP-PTT demonstrate an optimal temperature range of ~65 °C and correlative thermal dose of 6.5 log(CEM43) to elicit ICD. Importantly, we noted the maximum long-term survival (33.3%) in mice vaccinated with Neuro2a cells treated with the same thermal dose optimal for ICD markers. These observations should guide the application of nanoparticle-based PTT in the future, and point to a new paradigm of "moderate is better" in the context of antitumor immune responses to thermal cancer therapy.

Chapter 4: Prussian blue nanoparticles-based antigenicity and adjuvanticity trigger robust antitumor immune responses against neuroblastoma[3]

4.1 Abstract

We have described the synthesis and characterization of PBNPs coated with a molecular adjuvant, CpG oligodeoxynucleotides (CpG-PBNPs) as a nanoimmunotherapy to increase the antigenicity and adjuvanticity of treated tumors. The CpG coating functions as an exogenous molecular adjuvant that complements the endogenous adjuvants released by the CpG-PBNP-PTT (e.g. ATP, calreticulin, and HMGB1). In cell culture, coating nanoparticles with CpG increases immunogenicity while maintaining the photothermal activity of PBNPs. CpG-PBNPs are able to activate DCs in the same manner as free CpG at equal concentrations *in vitro*. Furthermore, when CpG-PBNP-activated DCs are co-cultured with exogenous CD8+T cells, they are activated due to the improved activation and antigen presentation of the DCs. These findings demonstrate the potential of the modified PBNPs to overcome immune tolerance by increasing DC activation and T cell proliferation.When administered in a syngeneic, Neuro2a-based, murine model of neuroblastoma, CpG-PBNP-PTT results in complete tumor regression in a significantly higher proportion (70% at 60 days) of treated animals relative to controls. Our findings point to the importance of

[3] This chapter was adapted from Cano-Mejia, J. et al.., *Prussian blue nanoparticle-based antigenicity and adjuvanticity trigger robust antitumor immune responses against neuroblastoma.* Biomaterials Science, 2019. doi: 10.1039/c8bm01553h

simultaneous cytotoxicity, antigenicity, and adjuvanticity to generate robust and persistent antitumor immune responses against neuroblastoma.

4.2 Introduction

The design of nanoimmunotherapies capable of triggering effective antitumor responses and immunity requires an understanding of how these therapies are causing tumor cell death, as well as upregulating an immune response. To engineer a nanoimmunotherapy, we not only ought to understand how the CpG coating was affecting the intrinsic properties and photothermal capabilities of the Pussian blue nanoparticles (**Chapter 2**), but we also have to understand the effects of CpG coating and photothermal therapy on the induction of ICD, DC activation and antigen presentation, and T cell proliferation. Our nanoimmunotherapy serves as a dual treatment modality, where tumors are killed by ablation and enhancement of the immune response through the delivery of both antigens and adjuvants locally. CpG is a novel adjuvant that enhances DC function and their ability to prime T cells. The addition of CpG enhances the antigen-uptake activity of DCs, leading to the CD8+ T cell activation and tumor cell death.

Tumors that maintain an immunosuppressive environment, including neuroblastoma, exhibit antigen-presentation impairment; this ability plays a role in tumor antigen tolerance [120, 121]. Several studies show vaccine adjuvant depots can break immune tolerance to tumors antigens and improve antigen presentation [56, 96].

Since CpG-PBNP-PTT introduces the immune system to cancer antigens by means of the dying tumor cells, the addition of CpG onto the particles will make DCs better antigen-presenting cells, allowing for an upregulation of a tumor-specific immune response.

The efficacy of nanoimmunotherapies relies heavily in not only the activation of DCs, but also in the ability of T cells to recognize peptides derived from proteins in any cellular compartment. Given the emerging view that cancer patients contain tumor-reactive T cells that are naturally tolerant to their cancer, a central question in immunotherapy is whether T cells can be activated and expanded to induce clinically useful antitumor responses, especially important for metastaic tumors, where a systemic approach is needed. Even low affinity T cells can potentially discharge their effector function in properly activated [122]. We believe that our nanoimmunotherapy, by inducing tumor debulking, as well as introducing both antigens and adjuvants together, has the capacity of creating strong T cell antitumor responses. Local modification of the primary tumor environment should result in robust systemic antitumor T cell responses. Improved treatment outcomes will manifest in a disruption of the immunosuppressive tumor environment via the increase in the number of tumor-antigen-specific T cells.

A step toward achieving this goal is to ensure that CpG-PBNP-PTT-treated tumors are undergoing ICD – a cell death mechanism that engages the immune system [98, 103]. Immunogenicity of cell death is marked by release of antigens and exogenous adjuvants – such as DAMPS - by dying tumor cells. Along with photothermal heating-induced cell death, our CpG-PBNP-PTT is accompanied by surface calreticulin

exposure, ATP secretion, and HMGB1 release. These cues are important for eliciting a potent antitumor immune response.

By increasing both the antigenicity (by means of the dying tumor cells, and induction of ICD), as well as adjuvanticity (through the addition of CpG), this combination treatment allows for a response that leads to long-term survival and immune memory. Photothermal immunotherapy using CpG-PBNPs therefore has a potential of greatly improving the treatments and responses of cancers.

4.3 Materials and Methods

4.3.1 Antibodies

Fluorescent antibodies against HMGB1 and calreticulin were purchased from Abcam (Cambridge, UK). Lipopolysaccharide (LPS) was purchased from Thermo Fisher Scientific (Carlsbad, CA, USA).

4.3.2 Cells

For *ex vivo* studies, splenic DCs were supplemented with RPMI 1640 medium (Lonza Bioscience, Manchester UK), supplemented with 10% FBS (Corning Inc., Corning, NY, USA), 2 mM L-glutamine (Gibco), 55 μM β-mercaptoethanol (Sigma-Aldrich) 1× non-essential amino acids (Fisher Scientific, Waltham, MA, USA), 10 mM HEPES (Fisher Scientific), and 0.5% penicillin/streptomycin (Gibco).

4.3.3 Animals

All animal studies were approved by the Institutional Animal Care and Use Committee of the George Washington University, Washington, DC, USA (Protocol # A396) and the University of Maryland, College Park, MD, USA. The studies were conducted to ensure humane care of the animals as per the institutional IACUC guidelines. For the DC activation studies, female C57BL/6J mice were obtained from Jackson Laboratory (Bar Harbor, ME, USA). For T cell proliferation studies, female OT-I mice (C57BL/6-Tg(TcraTcrb)1100Mjb/K) were purchased from Jackson Laboratory. For *in vivo* studies, five week old, female A/J mice were purchased from Jackson Laboratory. The animals were acclimated for 3-4 days prior to tumor inoculation.

4.3.4 *Ex vivo* DC studies

DCs were isolated from the spleens of naïve C57BL/6J mice using a CD11c positive magnetic isolation kit, according to the manufacturer's instructions (Miltenyi Biotec GmbH, Bergisch Gladbach, Germany). Cells were plated (10^5 cells/well) in RPMI 1640 media described above. Samples, which were added in triplicate, included media, LPS (1 μg/mL), CpG (40, 10 and 1 μg/mL), PBNPs (1 – 0.25 mg/mL, in 2× dilutions), and CpG PBNPs (1 – 0.25 mg/mL, in 2× dilutions). Cultures were incubated for 24 hours, then collected by centrifugation (800 ×g, 5 minutes), washed twice in FACS buffer, and blocked with anti-CD16/CD32 (BD Biosciences, Franklin Lakes, NJ, USA). The cells were finally stained for 20 minutes at room temperature using monoclonal

antibodies against the surface activation markers CD40, CD80, and CD86 (BD Biosciences). After staining, cells were washed twice and resuspended in FACS buffer containing DAPI for analysis by flow cytometry (CantoII, BD Biosciences). All flow cytometry data were collected and analyzed using FlowJo software (Tree Star Inc., Ashland, OR, USA).

4.3.5 *Ex vivo* T cell proliferation studies

$CD11c^+$ DCs from naïve C57BL/6J mice were isolated and treated as described above for DC activation studies. All treatment groups received either free Trp2 peptide (1.25 ng/well) or no Trp2. After 48 h of culture, Trp2-specific $CD8^+$ T cells were isolated by negative magnetic separation (StemCell Technologies, Vancouver, Canada) from the spleens of Trp2 transgenic mice (A gift from Dr. Giorgio Trinchieri, NCI, NIH). Isolated $CD8^+$ T cells were stained with eFluor 647 proliferation dye (10 nM) and washed 3 times, then 3×10^5 labeled T cells were added to the DC cultures. After another 48 hours of co-culture, cells were washed and blocked, as described above. Cells were then stained with anti-CD8 (BD Biosciences, Franklin Lakes, NJ, USA) for 20 min at room temperature, washed, and resuspended in DAPI in FACS buffer for analysis by flow cytometry.

4.3.6 ICD marker analysis

In vitro CpG-PBNP-PTT and PBNP-PTT was performed as described above (using equivalent concentrations of nanoparticles or controls with/without

laser irradiation).[62] Cell suspensions were then washed and stained with fluorescent antibodies against HMBG1 (intracellular) and calreticulin (extracellular), and flow cytometry was performed. Flow cytometry was performed on the FACSCaliber (BD Biosciences), and analysis was done using the FlowJo software. For intracellular ATP presence, cells were washed after *in vitro* PTT and the CellTiter-Glo luminescent cell viability assay was performed.

4.3.7 *In vivo* studies

For establishing a murine neuroblastoma model, one million Neuro2a cells suspended in phosphate-buffered saline (PBS) were injected subcutaneously in the shaved backs of 4-6 week old female A/J mice, as previously described.[19, 62] All the treatments commenced after the tumors reached a diameter of at least 5 mm (~60 mm^3). Mice were anesthetized prior to and during treatment using 5% isoflurane. Tumor-bearing mice were divided into five groups (n=10 mice/ group): 1) Vehicle (no treatment, injected intratumorally with 50 µL PBS on day 0), 2) Free CpG (10 µg CpG injected intratumorally on days 0, 2, and 5), 3) CpG-PBNPs (2 µg conjugated on the PBNPs; injected intratumorally on days 0, 2, and 5), 4) PBNP-PTT (50 µL of 1 mg/mL PBNPs intratumorally, irradiated at 0.75 W for 10 minutes), and 5) CpG-PBNP-PTT nanoimmunotherapy (50 µL of 1 mg/mL CpG-PBNPs, 2 µg bound CpG, irradiated at 0.75 W for 10 minutes, CpG-PBNPs boosts were given (without PTT) on days 2 and 5). Temperatures reached during PTT were measured using the i7 FLIR thermal imaging camera (Arlington, VA). Tumor growth was

monitored following inoculation and treatments by routine caliper measurements.

4.3.8 Animal exclusion and euthanasia criteria

Animals were excluded from the study if their tumors failed to grow after Neuro2a inoculation. This exclusion occurred infrequently because greater than 95% of injected mice developed tumors. A tumor size of 15 mm diameter in any dimension was designated as the endpoint and mice were euthanized at that time. Euthanasia was achieved through cervical dislocation after CO_2 narcosis. If the tumor impaired mobility of the animal, became ulcerated or appeared infected, or if the mice displayed any signs of distress such as assuming a sick mouse posture, the mice were immediately removed from the study and euthanized. All these steps were conducted in accordance with the approved IACUC protocols.

4.3.9 Statistical analysis

Statistical significance was determined from a two-tailed Student's t test and values with $p < 0.05$ qualified as statistically significant. Survival results were analyzed according to a Kaplan-Meier curve. The log-rank test was used to determine statistically significant differences in survival between the various groups.

4.4 Results

4.4.1 CpG-PBNPs activate DCs and cause CD8+ T cell proliferation *ex vivo*

To test the immunostimulatory properties of the CpG-PBNPs, we measured their ability to activate DCs and T cells compared to free CpG, PBNPs without CpG, and other controls *ex vivo* (**Figures 4.1** and **4.2**). First, we cultured splenic DCs with CpG-PBNPs or PBNPs at different concentrations (diluted 1x – 4x; 1-0.25 mg/mL), free CpG (low, medium, high concentrations; 1-40 μg/mL), LPS, or media, and assessed DC activation by measuring expression of common DC surface activation markers: CD80, CD86, and CD40. Untreated DCs served as a negative control, while LPS and free CpG were employed as positive controls. The concentration of free CpG added to the DCs (e.g. 1×; 40 μg/mL) was equivalent to the amount of CpG bound on 1 mg/mL CpG-PBNPs (40 μg CpG/mg of nanoparticle). Flow cytometry analysis demonstrated increased activation of DCs by CpG-PBNPs compared to uncoated PBNPs as measured by their increased CD80, CD86, and CD40 expression levels (**Figures 4.1A** and **4.2A**). DC activation was also observed to be dose-dependent, increasing with higher concentrations of CpG-PBNPs. In contrast, DC activation with varying concentrations of PBNPs was constant at levels similar to those observed for the untreated DCs (media; negative control). Furthermore, the CD80/86 activation levels with the various doses of CpG-PBNPs were similar to those observed for free CpG. Importantly, the percentage of CD11c+ live cells were similar across all treatment groups indicating biocompatibility of our

nanoparticles (**Figure 4.2B**). These findings demonstrate that the CpG-PBNPs can activate DCs, as a result of the CpG coating.

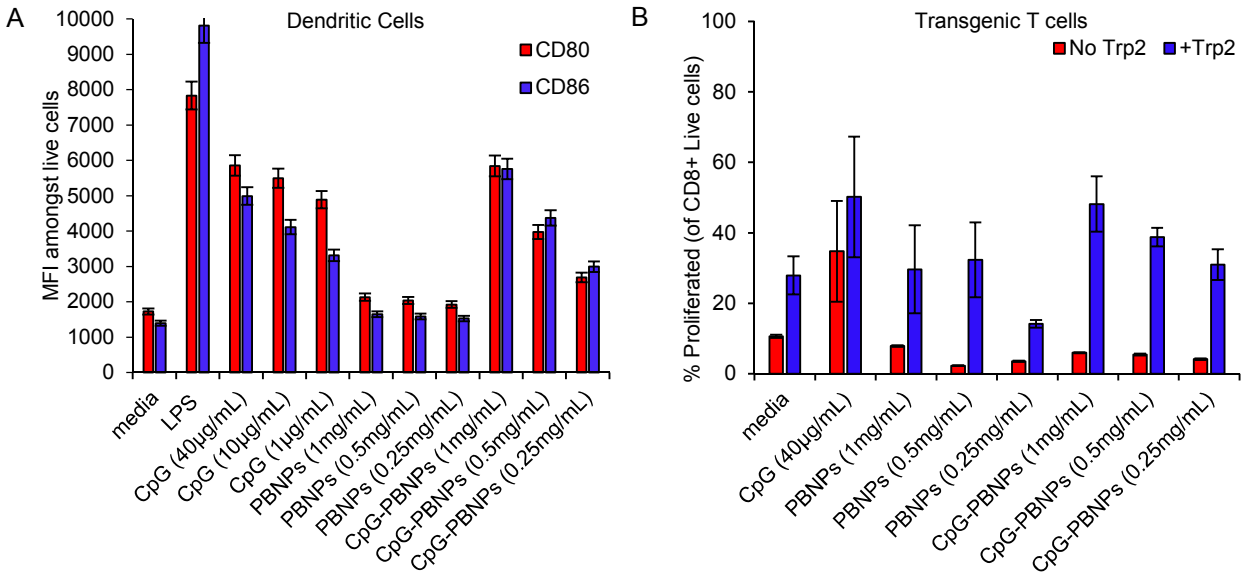

Figure 4.1. Immunostimulatory properties of CpG-PBNPs. (A) Activation of dendritic cells (DCs) upon co-culture with CpG-PBNPs compared to free CpG, PBNPs, and media controls measured by flow cytometry. CD80 (red) and CD86 (blue) MFI of live CD11c+ positive cells (1 – 0.25 mg/mL). CpG concentrations are as follows: 40 µg/mL, 10 µg/mL, and 1 µg/mL. LPS concentration was 1 µg/mL (* significant difference relative to media-treated DCs for both CD80 and CD86 expression, $p < 0.05$). (B) Percent proliferation of CD8+ T cells co-cultured with DCs activated with CpG-PBNPs and controls (free CpG, PBNPs, and media) (1 – 0.25 mg/mL). Groups were treated with and without the antigen Trp2 (1.25 ng/well). (* significant difference relative to media-treated DCs in the presence of Trp2; $p < 0.05$; n.s., not significant relative to media-treated DCs in the presence of Trp2, $p > 0.05$)

In addition to the above studies, we tested the ability of the CpG-PBNPs to activate T cells. For these studies, we utilized Trp2 as a model antigen, expressed in several murine and human cancers, to test T cell activation in context of DC activation (via the CpG-PBNPs) and antigen-presentation (via the added Trp2) It is important to note here that while Trp2 is not expressed in neuroblastoma, it serves as a useful and well-characterized model antigen to test

the immunostimulatory properties of the CpG-PBNPs. DCs that were activated by the same groups used in **Figure 4.1A** were co-cultured with Trp2-specific CD8+T cells (**Figures 4.2C** and **D**), in the presence of the Trp2 peptide (1.25 ng/well). We observed that when DCs activated by CpG-PBNPs were co-cultured with CD8+T cells in the presence of Trp2, their proliferation was increased compared to DCs activated with PBNP (at the same concentration) as measured by the T cell proliferation assay (**Figure 4.1B**). Furthermore, DCs activated with CpG-PBNPs were able to activate CD8+ T cells in a manner similar to DCs activated with free CpG (% proliferated was ~50% for both the 1 mg/mL CpG-PBNPs and the 40 μg/mL free CpG treatments). Overall, these results demonstrate the potential of the CpG-PBNPs to increase DC activation and T cell proliferation, which is important for overcoming tumor-mediated immunosuppression, and improving antitumor immune responses of a therapy.

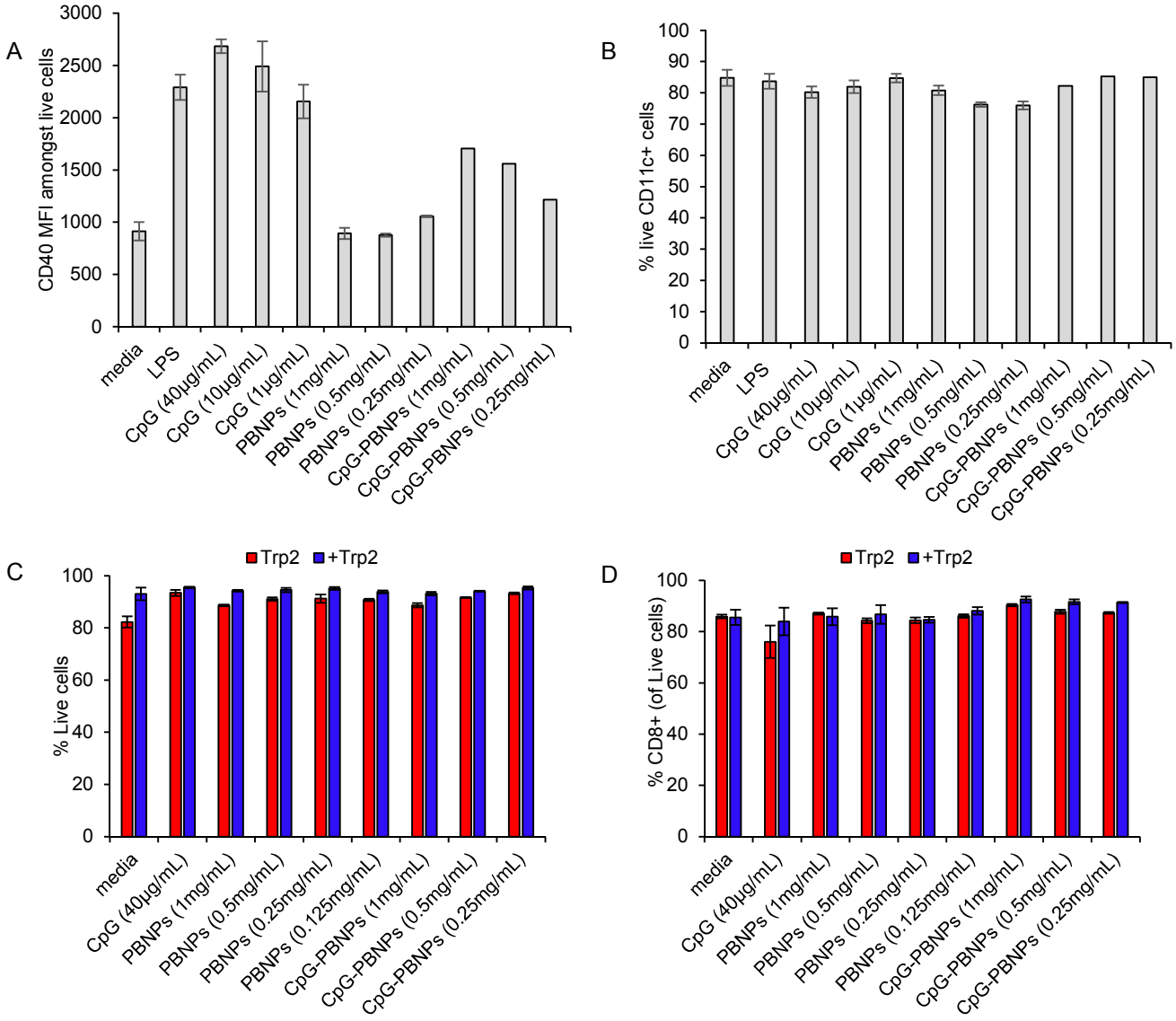

Figure 4.2 Immunostimulatory properties of CpG-PBNPs. (A) CD40 MFI amongst CD11c+ positive cells. (B) % live CD11c+ positive cells treated with varying concentrations (1 – 0.25 mg/mL) CpG-PBNPs and controls (Free CpG, PBNPs. (C) % live cells treated with varying concentrations (1x-4x; 1 – 0.25mg/mL) CpG-PBNPs and controls (Free CpG, PBNPs) with and without the antigen Trp2. (D) % CD8+ positive cells treated with varying concentrations (1 – 0.25 mg/mL) CpG-PBNPs and controls (media, free CpG, PBNPs).

4.4.2 CpG-PBNP-PTT elicits ICD in Neuro2a cells *in vitro*

As part of our multimodal therapy strategy, the CpG-PBNPs should not only activate DCs and T cells (via the CpG coating), but also cause trigger tumor cell death in a manner that engages the immune system (after PTT). These combined effects facilitate improved antigen processing and presentation, leading to enhanced antitumor effects [96]. Previously, we demonstrated the PBNP-PTT elicits ICD as measured by its biochemical correlates (released ATP and HMGB1, and increased surface calreticulin) [62]. Here, we verify whether CpG-PBNP-PTT elicits ICD in Neuro2a cells. Specifically, we assessed the expression of ICD markers (ATP, HMGB1, and calreticulin) on Neuro2a cells treated with CpG-PBNP-PTT (**Figure 4.3**). CpG-PBNP-PTT caused a decrease in intracellular ATP levels in Neuro2a cells (similar to PBNP-PTT), which was lower than the ATP levels observed in Neuro2a cells treated with the vehicle, laser alone, PBNPs, or CpG-PBNPs (**Figure 4.3A**). CpG-PBNP-PTT also triggered a significant increase in surface calreticulin expression (similar to PBNP-PTT) relative to the aforementioned treatment groups (**Figure 4.3B**). Finally, CpG-PBNP-PTT caused a significant decrease in intracellular HMGB1 levels (>40% decrease; similar to PBNP-PTT) compared to the other treatment groups. These findings suggest the CpG-PBNP-PTT is able to effectively elicit ICD in treated Neuro2a cells thus priming a favorable antitumor immune response via this endogenous adjuvant release.

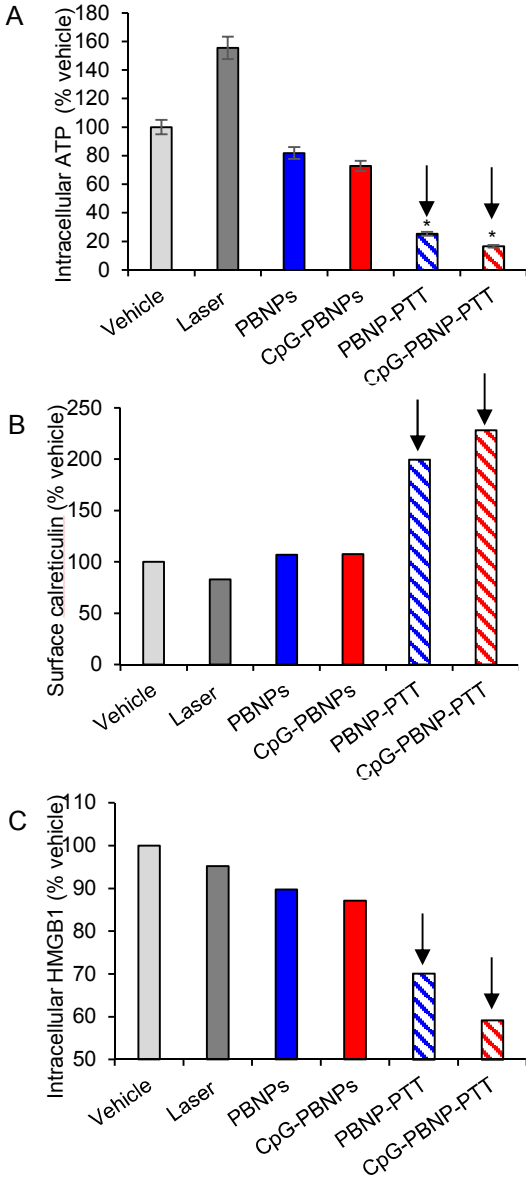

Figure 4.3. Induction of immunogenic cell death (ICD) by CpG-PBNP-PTT *in vitro*. (A) Intracellular ATP in the various treatment groups (as a % of the vehicle-treated group) (* significant difference relative to vehicle; $p < 0.05$). (B) Surface calreticulin expression in the various treatment groups (as a % of the vehicle-treated group). (C) Intracellular HMGB1 in the various treatment groups (as a % of the vehicle-treated group). All groups had concentrations of nanoparticles at 0.05 mg/mL. PTT groups were treated with a laser power of 0.75W for 10 minutes. Arrows denote the treatment groups where all 3 markers of ICD are expressed/present. Panels B and C were analyzed using flow cytometry and the trends in ICD markers were consistent across at least three separate studies.

4.4.3 CpG-PBNP-PTT nanoimmunotherapy results in complete tumor regression and long-term survival in a mouse model of neuroblastoma

Building on our findings described above, we next tested if the increased antigenicity and adjuvanticity elicited by CpG-PBNP-PTT generated anti-tumor immunity in a syngeneic murine model of neuroblastoma. Neuro2a neuroblastoma tumor-bearing mice were divided into five treatment groups (n = 10/group; **Figure 4.4A**): 1) Vehicle (PBS), 2) Free CpG, 3) CpG-PBNPs, 4) PBNP-PTT, and 5) CpG-PBNP-PTT. The average final tumor temperatures achieved during PTT measured by the thermal imaging camera was ~60 ^{o}C (**Figure 4.4B**), which corresponded to the temperature range needed to elicit ICD in Neuro2a-bearing mice[62]. CpG-PBNP-PTT resulted in complete tumor regression in the majority of treated mice (7/10) compared to mice in the four other treatment groups (0/10 each in the vehicle-treated, Free CpG-treated, and the PBNP-PTT-treated groups, and 1/10 in the CpG-PBNPs-treated group; **Figure 4.5**). More importantly, CpG-PBNP-PTT resulted in long-term survival (survival >60 days post-treatment) in 70% of the treated tumor-bearing mice, which was significantly higher than the long-term survival observed in tumor-bearing mice in all other treatment groups (**Figure 4.4C**; $p < 0.05$; log-rank test). Taken together, these data suggest the importance of increasing tumor antigenicity and adjuvanticity via the CpG-PBNP-PTT nanoimmunotherapy in conferring complete tumor-regression, and long-term survival in the mouse model of neuroblastoma.

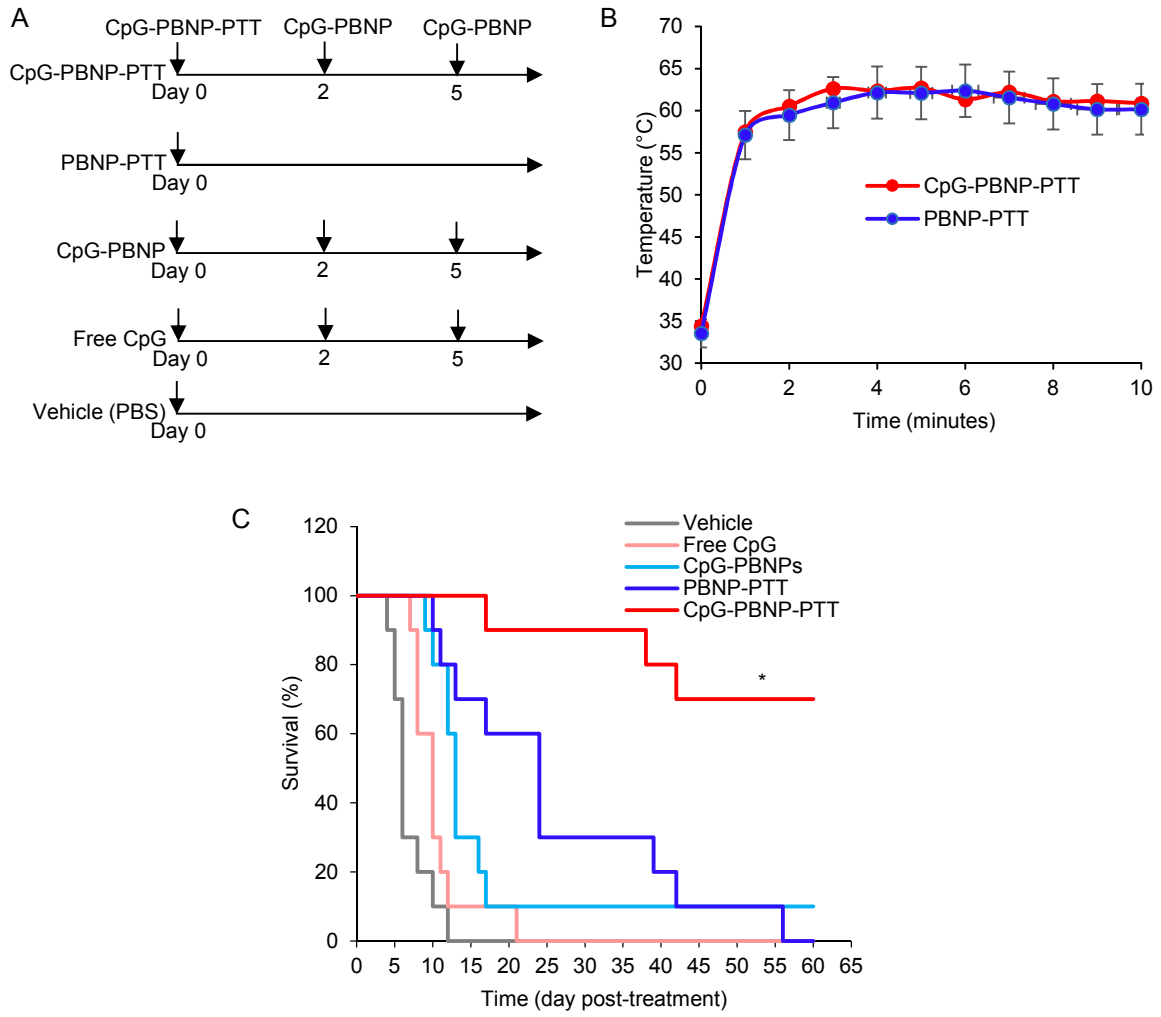

Figure 4.4. Effect of the CpG-PBNP-based nanoimmunotherapy on tumor regression and long-term survival in the Neuro2a neuroblastoma mouse model. (A) Overview of the treatments. Mice bearing ~5 mm diameter Neuro2a neuroblastoma tumors were treated with CpG-PBNP-PTT and corresponding controls. The PTT-treated groups received 50 µL of 1 mg/mL CpG-PBNPs or PBNPs intratumorally (i.t.), and were irradiated by an 808 nm laser at 0.75 W for 10 minutes. Additionally, the CpG-PBNP-PTT received two boosters with CpG-PBNP on Days 2 and 5. The CpG-PBNP-treated groups received 2 µg of conjugated CpG per dose by i.t. injection (Days 0, 2, and 5). CpG-treated groups received 10 µg of free CpG per dose by i.t. injection (Days 0, 2, and 5). (B) Temperature-time profiles of Neuro2a bearing mice treated intratumorally with 1mg/mL CpG-PBNPs (red) or PBNPs (blue) and irradiated with a NIR laser at 0.75 W for 10 minutes. (C) Kaplan-Meier survival plots of neuroblastoma tumor-bearing mice that were treated with CpG-PBNP-PTT, PBNP-PTT, Free CpG-PBNPs, Free CpG, or vehicle. Mice receiving CpG-PBNP-PTT showed significantly higher long-term survival (>100 days) compared with mice in the other groups (* significant difference compared to all other groups, $p < 0.05$, long-rank test, n=10/group).

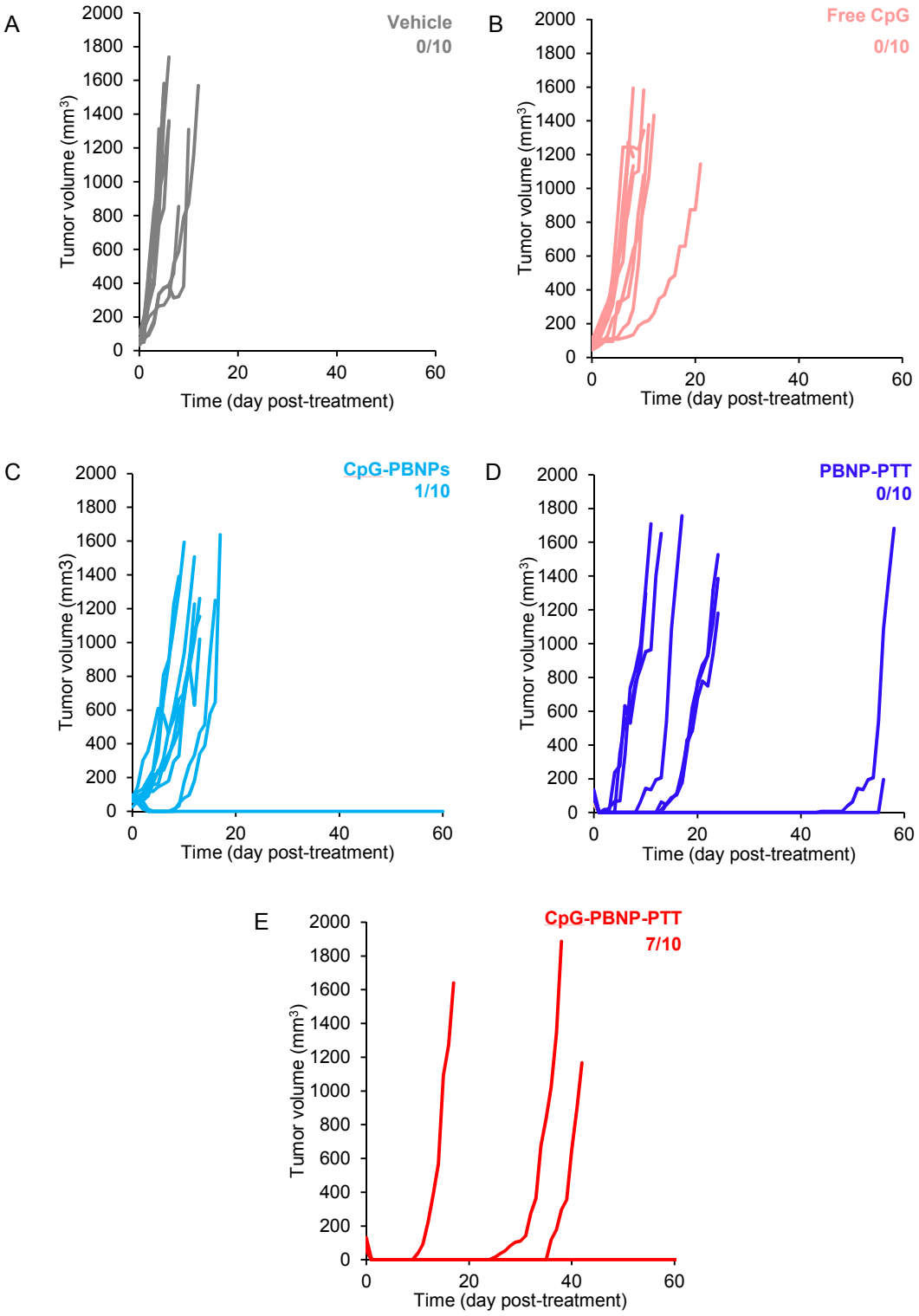

Figure 4.5. Tumor growth curves for individual mice in the various treatment groups: (A) Vehicle, (B) CpG-treated, (C) CpG-PBNP-treated, (D) PBNP-PTT-treated, (E) CpG-PBNP-PTT-treated. Each line represents tumor growth measured in one mouse (numbers in parentheses in each panel A-E indicate number of long-term surviving mice in each group i.e. >60 day survival).

4.5 Discussion

Understanding the responses to the immune system after a cancer therapy can elucidate factors that are important when engineering a combination nanoimmunotherapy. Successful engagement of the immune system after CpG-PBNP-PTT treatment should be manifested by an upregulation of an immune response that is characterized by ICD of neuroblastoma cells, increased DC activation and tumor antigen-presentation, as well as T cell activation and proliferation. When the immune response is upregulated after PTT, it results in stronger antitumor immune responses that will lead to better and more aggressive treatments for neuroblastoma patients. After engineering and characterizing the stability of our CpG-PBNPs for PTT and depot for CpG (Chapter 2), we then sought to understand the effects of our therapy in the activation of DCs and T cells, as well as the ability of CpG-PBNP-PTT to elicit ICD in neuroblastoma cells.

We first studied the ability of our nanoimmunotherapy to activate APCs, particularly DCs, to process and present tumor antigens to immune effector cells (e.g. T cells). Several published studies have reported antigen-presentation impairment in immunosuppressive tumor environments, including neuroblastoma. Since our PBNPs are biofunctionalized with the TLR agonist CpG, it helps to function as a signal that break immune tolerance to tumor antigens. The CpG coating on the CpG-PBNPs was able to increase activation of DC and the proliferation of CD8+ T cells in the presence of a model Trp2 antigen *ex vivo* (**Figure 4.1**). Increasing antigen presentation and activation of

antigen-specific T cell responses is crucial in overcoming tumor-mediated immunosuppression.

The ability of a cancer therapy to elicit ICD has emerged as an important consideration in the design of the next generation of antitumor regimens [98, 100], wherein the applied therapy not only kills tumor cells but simultaneously converts them into a tumor-specific therapeutic vaccine. Therefore, we tested the ability of PTT to elicit ICD in treated Neuro2a cells *in vitro*, since this is critical for the success of our nanoimmunotherapy. The CpG-PBNPs were able to elicit ICD in treated Neuro2a neuroblastoma cells as evidenced by the concurrent surface calreticulin exposure, ATP secretion, and HMGB1 release. (**Figure 4.3**), effects important in initiating a robust antitumor immune response.

Although our study focused on the effects of CpG-PBNP-PTT on tumor cell death, antigenicity, and adjuvanticity, one cannot discount the importance of evaluating the effects of our therapy on other immune cell subsets, including NK cells, macrophages (M1 and M2 phenotypes), and suppressor cells (Tregs, MDSCs) to get a more complete picture of the associated effects of our therapy. These studies are either ongoing or will be undertaken by our group in the near future.

When we studied the effects of our nanoimmunotherapy on killing tumor cells by increasing the antigenicity and adjuvanticity in the local tumor area, we see that PBNP-PTT and CpG act synergistically to create better responses. The CpG-PBNP-PTT nanoimmunotherapy was able to elicit complete tumor regression and long-term survival in a majority (70%) of Neuor2a tumor-bearing

mice (**Figure 4.4**). We attribute the significantly higher long-term survival benefit in the nanoimmunotherapy-treated mice to the priming of an immune response by PTT (increased antigenicity), which is complemented by a reversal of DC exhaustion and immunosuppression by CpG (increased adjuvanticity). While these results are extremely encouraging, additional studies need to be performed in animal models of disseminated neuroblastoma to better mimic neuroblastoma risk groups associated with a poor prognosis (high-risk neuroblastoma), and these are the focus of several ongoing studies.

Chapter 5: CpG-PBNP-PTT elicits antitumor immunity against long-term rechallenge and distal disease[4]

5.1 Abstract

Neuroblastoma is the most common type of pediatric cancer and the most common type of extracranial solid tumor in children. About 50% of patients present with metastatic or distal tumors at initial diagnosis, decreasing the survival rate to 30-40% of patients. Therefore, in order to test whether a neuroblastoma therapy will be successful, we need to test not only the effect of the treatment on treating primary cancers, but also its effect on treating distal and metastatic tumors. Motivated by this need, we monitored the ability of surviving mice treated with CpG-PBNP-PTT to reject tumor rechallenge as well as the abscopal effect of our nanoimmunotherapy on mice with synchronous Neuro2a tumors (wherein the primary tumor is treated with CpG-PBNP-PTT + anti-CTLA-4, and a distal tumor remains untreated). We found that long-term surviving, CpG-PBNP-PTT-treated animals reject Neuro2a rechallenge, suggesting this therapy generates immunological memory. Furthermore, when administered in a syngeneic, distal Neuro2a-based, murine model of neuroblastoma, CpG-PBNP-PTT + anti-CTLA-4 results in complete tumor regression of both primary and secondary tumors in 50% of the mice compared to the controls. Our findings point to the importance of simultaneous cytotoxicity, antigenicity, and adjuvanticity to

[4] This chapter was adapted from Cano-Mejia, J. et al, *Prussian blue nanoparticle-based antigenicity and adjuvanticity trigger robust antitumor immune responses against neuroblastoma.* Biomaterials Science, 2019. doi: 10.1039/c8bm01553h

generate robust and persistent antitumor immune responses against recurring and distal neuroblastoma.

5.2 Introduction

Neuroblastomas account for 97% of all neuroblastic tumors, are clinically heterogeneous, vary in location, histopathologic appearance, and biological characteristics. They are most remarkable for their broad spectrum of clinical behavior, which can range from spontaneous regression, to maturation to a benign ganglioneuroma, or aggressive disease with metastatic dissemination leading to death [4]. The survival of patients with disseminated or metastatic neuroblastoma, when they are more than one year of age, is less than 10% with conventional therapy [1, 2]. This is why the ideal neuroblastoma therapy would be the one that not only effectively eradicates primary tumors, but also treats disseminated and metastatic cancers through an activation of an immune response cascade.

Of emerging interest in this field is the effects of PTT on the immune system. This is because generating a favorable antitumor response by PTT has the potential to effect robust and persistent treatment outcomes that are not limited to localized treatment sites, but can extend to more distant sites of tumor dissemination [20, 23, 123].

Successfully engaging the immune system should result in immunological memory against target cells, which should manifest as efficient protection against future tumor rechallenge. In the case of neuroblastoma, antigen-specific central memory T cells generated following a successful nanoimmunotherapy should be

capable of rapidly eliminating recurrent tumors. We study this effect by rechallenging treated surviving mice with neuroblastoma cells, and look at tumor rejection.

Not only are recurring tumors a major challenge when treating patients with neuroblastoma, but distal and metastatic tumors are also a major consideration when engineering cancer treatments for patients. This is why an emerging objective of PTT is maximizing an "abscopal effect", whereby local administered PTT causes shrinkage of non-treated, disseminated tumors, in addition to tumors directly in the treatment zone [124, 125]. We have shown that CpG-PBNP-PTT causes tumor cell death through ablation of the tumor, and an upregulation of an anti-tumor immune response. In order to treat distal tumors, we introduce a third component of our ensemble, which comprises of systemic administration of the immune checkpoint inhibitor, anti-CTLA-4. These antibodies reverse exhaustion of T cells and unleash their potent antitumor effects [34, 51, 125-128]. Our nanoimmunotherapy ensemble approach using CpG-PBNP-PTT to elicit ICD and release DAMPS from dying tumor cells, locally delivering TLR agonists which improve APC processing and presentation, and administering checkpoint inhibitors to reverse T cell immunosuppression, helps overcome immune evasion mechanisms employed by immunosuppressive tumors, increasing the benefits of these cancer immunotherapies to a larger proportion of patients.

5.3 Materials and Methods

5.3.1 Animals

All animal studies were approved by the Institutional Animal Care and Use Committee of the George Washington University, Washington, DC, USA (Protocol # A396). The studies were conducted to ensure humane care of the animals as per the institutional IACUC guidelines. Five-week old, female A/J mice were purchased from Jackson Laboratory. The animals were acclimated for 3-4 days prior to tumor inoculation.

5.3.2 Mouse rechallenge

Surviving mice that were treated with our CpG-PBNP-PTT were rechallenged 60-90 days after treatment with one million Neuro2 cells suspended in phosphate-buffered saline in the saved backs, as previously described. Age-matched untreated naïve mice were also inoculated and used as controls. Tumor growth was monitored following inoculation and treatments by routine caliper measurements.

5.3.3 Synchronous neuroblastoma mouse model

For establishing the syngeneic synchronous neuroblastoma mouse model, bilateral subcutaneous injections of one million Neuro2a cells (ATCC) were conducted into the shaved backs of 4-6 week old female A/J mice.

5.3.4 *In vivo* PTT studies

For the *in vivo* PTT studies, neuroblastoma (Neuro2a) tumor-bearing mice were treated when one of the tumors reached a diameter or at least 5 mm

(~60 mm^3 volume) measured using calipers. The biggest tumor was then designated the "primary tumor", and the bilateral untreated tumor was the "secondary tumor". Mice were anesthetized prior to and during treatment using 5% isoflurane. Tumor-bearing mice were divided into five groups (n=8-9 mice/ group): 1) Vehicle (no treatment, injected Vehicle (no treatment, injected intratumorally with 50 μL PBS on day 0), 2) PBNP-PTT (50 μL of 1 mg/mL PBNPs intratumorally, irradiated at 0.75 W for 10 minutes), 3) CpG-PBNP-PTT (50 μL of 1 mg/mL CpG-PBNPs, 2 μg bound CpG, irradiated at 0.75 W for 10 minutes, CpG-PBNPs boosts were given (without PTT) on days 2 and 5), 4) PBNP-PTT + anti-CTLA-4 (50 μL of 1 mg/mL PBNPs intratumorally, irradiated at 0.75 W for 10 minutes, anti-CTLA-4 injections of 150 μg on days 1, 5, an 8), 5) CpG-PBNP-PTT + anti-CTLA-4 ((50 μL of 1 mg/mL CpG-PBNPs, 2 μg bound CpG, irradiated at 0.75 W for 10 minutes, CpG-PBNPs boosts were given intratumorally (without PTT) on days 2 and 5, anti-CTLA-4 injections of 150 μg intraperitoneally on days 1, 5, an 8). Temperatures reached during PTT were measured using the i7 FLIR thermal imaging camera (Arlington, VA). Tumor growth was monitored following inoculation and treatments by routine caliper measurements. Surviving mice were rechallenged with Neuro2a cells at day 65 as described above.

5.3.5 Animal exclusion and euthanasia criteria

Animals were excluded from the abscopal effect study if both tumors failed to grow after Neuro2a inoculation. This exclusion occurred infrequently because greater

than 95% of injected mice developed tumors. A tumor size of 15 mm in diameter in any dimension was designated as the endpoint of mice with one tumor, and a tumor size of 13 mm in diameter in any dimension was designated as the endpoint of mice with two tumors. Euthanasia was achieved through cervical dislocation after CO_2 narcosis. If the tumor impaired mobility of the animal, became ulcerated or appeared infected, or if the mice displayed any signs of distress such as assuming a sick mouse posture, the mice were immediately removed from the study and euthanized. All these steps were conducted in accordance with the approved IACUC protocols.

5.3.6 Statistical analysis

Statistical significance was determined from a two-tailed Student's t test and values with $p < 0.05$ qualified as statistically significant. Survival results were analyzed according to a Kaplan-Meier curve. The log-rank test was used to determine statistically significant differences in survival between the various groups.

5.4 Results

5.4.1 Long-term surviving mice treated with CpG-PBNP-PTT exhibit protection against tumor rechallenge

An ideal tumor therapy is one that not only effectively eradicates tumors but prevents recurrence after successful elimination from the body. Therefore, we next investigated whether our nanotherapy consisting of CpG-PBNP-PTT conferred protection in long-term surviving mice that were rechallenged with the original tumor cells (Neuro2a) (**Figure 5.1**). Our studies consisted of two groups: 1) naïve group: where untreated mice were challenged with 10^6 Neuro2a cells, and 2) rechallenged group: where long-term surviving mice previously treated with our nanoimmunotherapy (CpG-PBNP-PTT) were rechallenged with 10^6 Neuro2a cells after 60-90 days of tumor-free survival (n = 7/group). Remarkably, all of the CpG-PBNP-PTT-treated, long-term surviving mice exhibited protection against the tumor rechallenge, and these mice rapidly eliminated the rechallenged tumors (**Figure 5.1**). Further, the rechallenged mice survived for 90 days post tumor rechallenge compared with naïve control mice that had to be euthanized due to high tumor burden 12-14 days post-challenge. These data suggest the potential of CpG-PBNP-PTT in conferring immunological memory and protection in long-term surviving mice against tumor rechallenge / recurrence.

5.4.2 Abscopal effect in mice treated with CpG-PBNP-PTT + anti-CTLA-4 eliminate distal tumors

Given the high prognosis of disseminated disease in neuroblastoma patients, we then sought to study the effects of our nanoimmunotherapy in treating mice with distal Neuro2a tumors. We developed a bilateral subcutaneous tumor mouse model in which the treated tumors on one side of the mouse represented the primary tumor, and the untreated tumor represented distal, metachronous, or metastatic tumors. We tested the abscopal effect of our therapy by treating the "primary tumor" with CpG-PBNP-PTT + anti-CTLA-4 or respective controls, and looking at the tumor progression or regression of the untreated "secondary tumor". To test the efficacy of our therapy, Neuro2a tumor-bearing mice were divided into five groups (**Figure 5.2A**): 1) CpG-PBNP-PTT + anti-CTLA-4-treated, 2) PBNP-PTT + anti-CTLA-4-treated, 3) CpG-PBNP-PTT-treated, 4) PBNP-PTT-treated, and 5) Vehicle (PBS) ($n \geq 3$/group). PTT-treated mice reached tumor temperatures averaging 65 °C (**Figure 5.2B**). Our nanoimmunotherapy resulted in significant tumor regression and slower tumor growth of the distal tumors compared with untreated mice. Remarkably, mice treated with CpG-PBNP-PTT + anti-CTLA-4 resulted in complete tumor regression of both primary and secondary tumor (**Figure 5.3**), and long-term survival in 50% of the treated mice (at 60 days post-treatment, **Figure 5.2C**). The long-term tumor-free survival was significantly higher (50% survival) than that observed (at 60 days post-treatment) for mice treated with PBNP-PTT + anti-CTLA-4 (25% survival), CpG-PBNP-PTT (0% survival), PBNP-PTT (0% survival), and vehicle (0% survival). Additionally, to understand the antitumor and memory responses generated by our therapy, we

rechallenged long-term surviving mice with 10^6 Neuro2a cells 65 days post-treatment. Our studies consisted of three groups: 1) naïve group: where untreated mice were challenged with 10^6 Neuro2a cells, 2) PBNP-PTT + anti-CTLA-4 rechallenged group: where long-term surviving mice previously treated with PBNP-PTT + anti-CTLA-4 were rechallenged with 10^6 Neuro2a cells after at least 90 days of tumor-free survival (n = 1 for this study), and 3) CpG-PBNP-PTT + anti-CTLA-4: where long-term surviving mice previously treated with CpG- PBNP-PTT + anti-CTLA-4 were rechallenged with 10^6 Neuro2a cells after at least 90 days of tumor-free survival (n = 2 for this study). Impressively, all of the rechallenged mice (both PBNP-PTT + anti-CTLA-4 -treated, and CpG-PBNP-PTT + anti-CTLA-4 -treated) exhibited protection against the tumor rechallenge, and these mice rapidly eliminated the rechallenged tumors (**Figure 5.2D**), compared with control mice that quickly succumbed to their disease by day 7. These data suggest the potential of combination nanoimmunotherapies consisting of photothermal therapy as well as immunotherapies that target both DC activation (CpG), and T cell activation (anti-CTLA-4) in treating disseminated neuroblastoma, as well as conferring immunological memory to combat recurring disease.

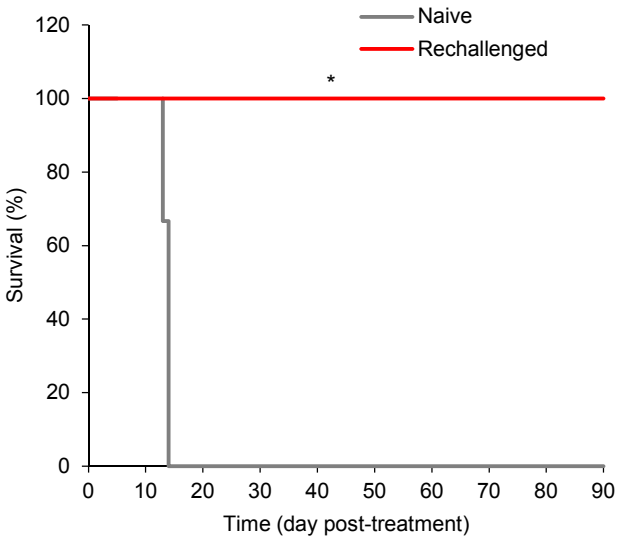

Figure 5.1. Effect of the CpG-PBNP-based nanoimmunotherapy on Neuro2a rechallenge of surviving mice. Long-term surviving mice rechallenged with Neuro2a cells 60-90 days after treatment showed complete tumor rejection (* significant difference compared to naïve mice, $p < 0.05$, n>=7/group).

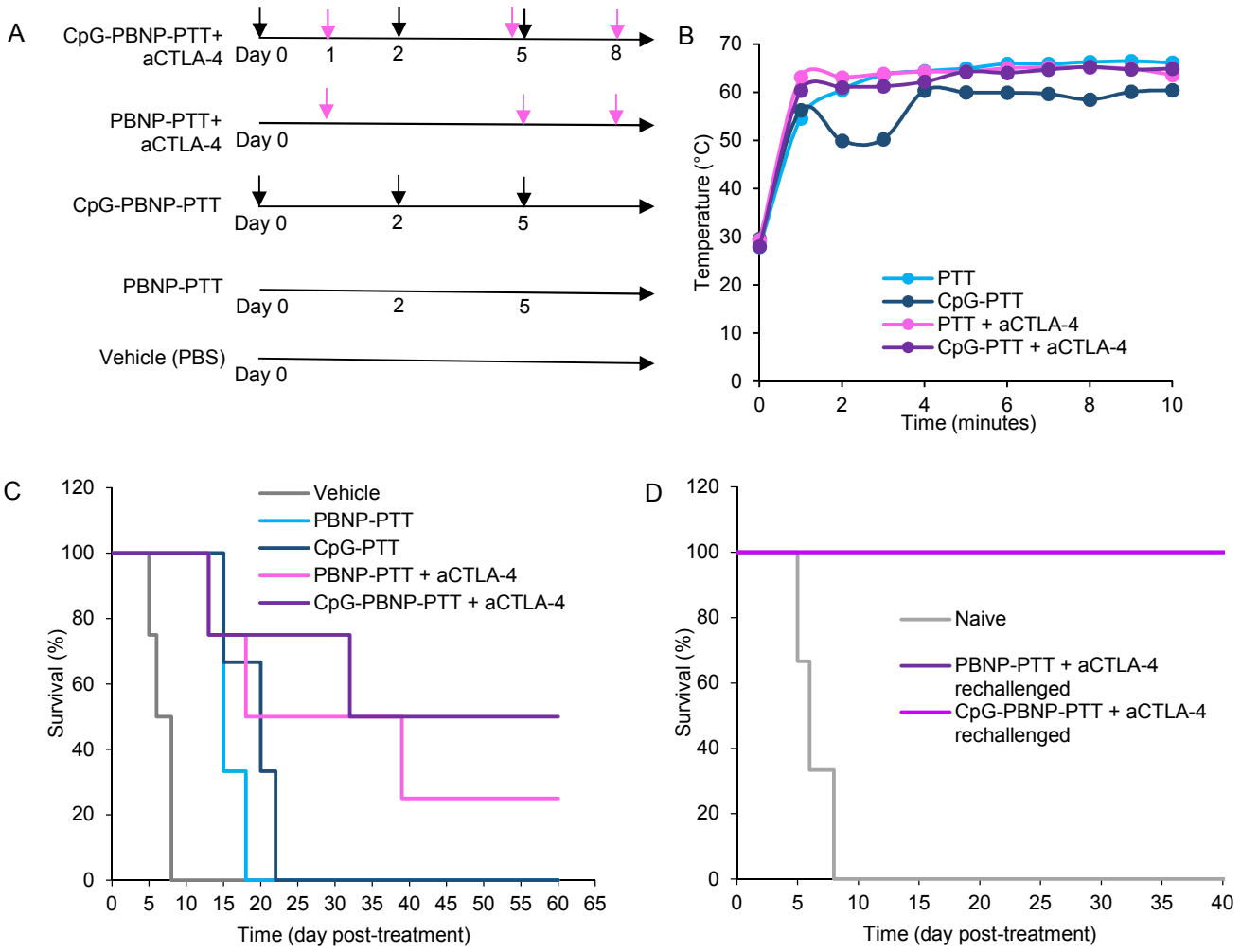

Figure 5.2. Effect of the CpG-PBNP-based nanoimmunotherapy on tumor regression and long-term survival in the distal Neuro2a neuroblastoma mouse model. (A) Overview of the treatments. Mice bearing ~5 mm diameter Neuro2a neuroblastoma tumors were treated with CpG-PBNP-PTT + anti-CTLA-4 and corresponding controls. The PTT-treated groups received 50 µL of 1 mg/mL CpG-PBNPs or PBNPs intratumorally (i.t.), and were irradiated by an 808 nm laser at 0.75 W for 10 minutes. Additionally, the CpG-PBNP-PTT received two boosters with CpG-PBNP on Days 2 and 5 i.t. (black arrows). The groups that received anti-CTLA-4 got 150 µg of antibody on days 1, 5, and 8 intraperitoneally (i.p) (pink arrows) (B) Temperature-time profiles of Neuro2a bearing mice treated intratumorally with 1mg/mL CpG-PBNPs or PBNPs and irradiated with a NIR laser at 0.75 W for 10 minutes. (C) Kaplan-Meier survival plots of neuroblastoma tumor-bearing mice that were treated with PBNP-PTT, CpG-PBNP-PTT, PBNP-PTT + anti-CTLA-4, CpG-PBNP-PTT + anti-CTLA-4, or vehicle. Mice receiving CpG-PBNP-PTT + anti-CTLA-4 showed significantly higher long-term survival compared with mice in the other groups. (D) Long-term surviving mice rechallenged with Neuro2a cells 65 days after treatment showed complete tumor rejection (* significant difference compared to naïve mice, $p < 0.05$, n>=3/group).

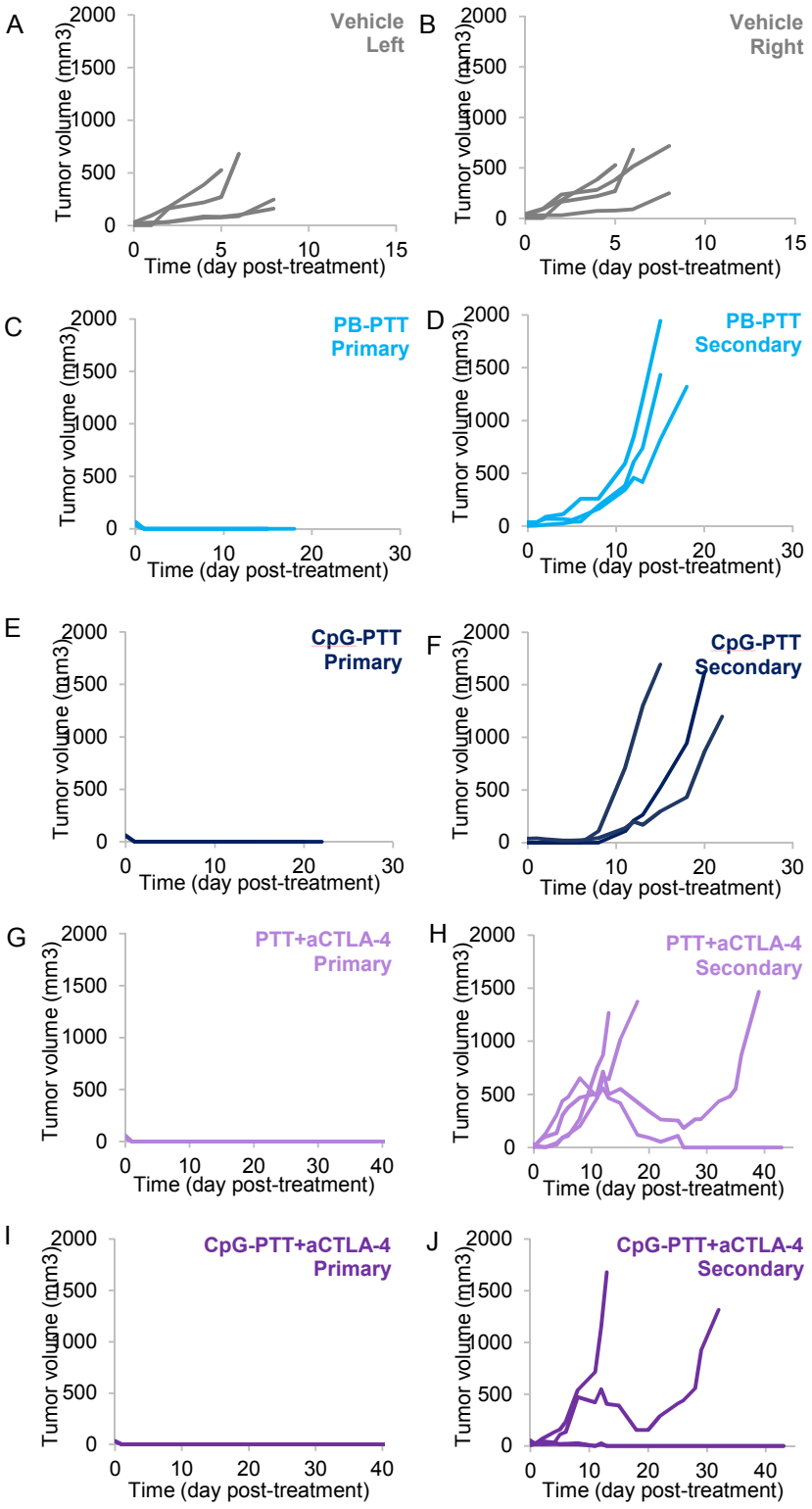

Figure 5.3. Tumor growth curves for individual mice in the various treatment groups: (A,B) Vehicle, (C,D) PBNP-PTT-treated, (E,F) CpG-PBNP-PTT-treated, (G,H) PBNP-PTT + anti-CTLA-4 - treated, (I,J) CpG-PBNP-PTT + anti-CTLA-4 -treated. Each line represents tumor growth measured in one mouse

5.5 Discussion

The goal of our nanoimmunotherapy is to design an enhanced therapeutic, that is capable of eliciting maximal long-term antitumor efficacy. A successful therapy is one that leads to tumor elimination, and should both target active disease and prevent immune escape leading to relapse or metastases. There is great motivation for more cross-disciplinary research, which can leverage new immunotherapy discoveries to address current limitations and boost the application of photothermal therapy for the treatment of both local and distal or metastatic disease. As such, this work pursues nanoparticle-based photothermal therapy and CpG adjuvant immunotherapy as two synergistic strategies to generate enhanced therapies for the treatment of neuroblastoma.

Metastasis accounts for over 90% of cancer-related deaths. In the case of neuroblastoma, 50% of patients present with distal or metastatic disease at initial diagnosis, making the survival rate only 30%. Hence, boosting photothermal immunotherapy-induced abscopal response rates could substantially impact patient care far beyond the patients who now benefit from heat therapies or immunotherapies alone. To test the long-term immune responses of our nanoimmunotherapy, we studied the effects of CpG-PBNP-treated mice in generating a memory response by rechallenging these mice with Neuro2a. We also studied the abscopal effects of our therapy by using a synchronous distal tumor model of neuroblastoma, wherein we treated one tumor with CpG-PBNP-PTT + anti-CTLA-4, and observed the other tumor's progression or regression.

The CpG-PBNP-PTT nanoimmunotherapy was able to elicit complete tumor regression, long-term survival (Chapter 4), and protection against tumor rechallenge in a majority of Neuro2a tumor-bearing mice (**Figure 5.1**). To further elucidate the long-term memory and abscopal effects of our therapy, we tested our nanoimmunotherapy in a mouse model of disseminated neuroblastoma. In this model, a mouse had two synchronous subcutaneous Neuro2a tumors wherein the primary tumor was treated with CpG-PBNP-PTT + anti-CTLA-4, and a distal tumor receives no treatment. We chose to add anti-CTLA-4 to our treatment to further upregulate the immune response generated by CpG-PBNP-PTT and boost memory T cell responses. By administering targeted blockades to receptors such as CTLA-4, T cells specifically are free to respond to co-stimulation, and this elicit enhanced antitumor efficacy. Another advantage to using checkpoint inhibitors as a therapeutic tool is that they do not need to be tailored to every patient – rather they mechanistically prevent the suppression of already present immune cells, and allow a patient's own endogenous immune system to effectively neutralize the malignancies. We found that when Neuro2a-bearing mice were treated with CpG-PBNP-PTT + anti-CTLA-4, there was an abscopal effect that was able to eliminate an untreated, secondary, distal tumor. Similar to immune reactions against antigens from bacteria or viruses, the abscopal effect requires priming of immune cells against tumor antigens. Local irradiation of a tumor may lead to immunogeneic forms of cell death and liberation of tumor cell-derived antigens. These antigens can be recognized by antigen presenting cells within the tumor (DCs and macrophages). Cytotoxic T cells which recognize these tumor antigens may in turn be primed by the tumor-antigen presenting cells. In contrast to the local effect of irradiation on the tumor

cells, these cytotoxic T cells circulate through the blood stream and are thus able to destroy tumor cells in distant parts of the body which were not irradiated.

Abscopal effects of photothermal therapy are often blocked by the immunosuppressive environment inside the irradiated tumor which prevents effective T cell priming. This explains why the effect is so rarely seen in patients receiving heat therapy (such as hyperthermia or radiotherapy) alone. In contrast, the combination of immunomodulatory drugs such as TLRs and checkpoint inhibitors can partially reconstitute systemic anti-tumor immune reactions induced after local tumor PTT. While these studies represent a good start, a thorough characterization of the underlying immune effects contributed by both CpG-PBNP-PTT and anti-CTLA-4 (innate and adaptive) that drive the antitumor responses of our combination therapy is warranted, and is the focus of ongoing work in our group.

Finally, long-term surviving mice treated with CpG-PBNP-PTT + anti-CTLA-4 exhibited protection against tumor rechallenge indicating the development of immunity against these tumors in photothermal immunotherapy-treated mice (**Figure 5.2C**). Similarly, further studies are necessary to elucidate the underlying immunological mechanisms that elicit these protective responses. **Figure 5.4** provides a hypothesized mechanism of action of our nanoimmunotherapy in treating neuroblastoma. The biofunctionalized PBNPs ablate the primary tumor, releasing tumor antigens, dancer signals, and cancer adjuvants, simultaneously. These antigens released by dying cells are captured by DCs, processed into peptides and presented to CD4+Th cells. Furthermore, after/during PTT, the CpG is uptaken in the endosomes of DCs. The presence of the PTT-generated adjuvants and CpG therefore improves tumor

antigen presentation, while also delivering an immunostimulatory adjuvant for improved responses. Once activated, effector T cells may help generate an immune response through the activation of cytotoxic CD8+T cells that can eradicate tumors. Additionally, tumor-infiltrating B cells may help present tumor-associated antigens for the induction of a CD4+Th cell-mediated cellular immunity. The combination of ablation, improved antigen presentation, and CD4+/CD8+ T cell activation, result in the elimination of the primary tumor as well as distal tumors

To conclude, our study points to the important role that CpG-PBNPs may play in the upcoming years in immunoengineering, where the nanoparticles are used to engineer a suitable immune response to treat advanced cancers such as high-risk neuroblastoma, improving the outlook for these patients.

Chapter 6: Proposed future work

The results presented in this dissertation involve designing nanoimmunotherapies with PBNPs for the treatment of neuroblastoma. We immunoengineered this strategy by utilizing the photothermal properties of PBNPs to induce ICD and an upregulation of an immune response locally, and that response was then complimented by immunotherapies that improved antigen presentation and T cell activation. In order to move towards a therapy that can be used in patients, we are currently working on strategies that improve and enhance both our treatment modality as well as the neuroblastoma tumor models used. Specifically, we are working on: 1) Improving the delivery of our laser by designing an interstitial photothermal therapy system (iPTT); and 2) Developing and testing a new mouse model of neuroblastoma utilizing TH-MYCN transgenic mice and neuroblastoma cells that more likely resemble human neuroblastoma. These new studies will improve the research presented by moving towards more clinically-relevant strategies.

6.1 Engineering an iPTT treatment for enhanced heating capabilities

Neuroblastoma is a type of cancer that forms in certain types of nerve tissues. It most frequently starts from one of the adrenal glands, but can also develop or spread to the neck, chest, abdomen, or spine [4]. Since neuroblastoma is not a surface tumor, for those tumors located deep underneath the tissue surface, an interstitial laser delivery is would be more advantageous than superficial illumination for PTT. Currently, nanoparticle-based PTT utilizes nanoparticle-assisted noninvasive laser irradiation to

achieve selective photothermal interaction [18, 19, 31, 62]. Previously, we have used PBNP-PTT, where the procedure requires a laser to be held over the treatment site with PBNPs injected intratumorally [18, 19]. However, photothermal therapy faces difficulties treating deeper tumors or tumors with heavily pigmented overlying skin due to the limitation of light penetration in tissue. Pigmented skin and the normal tissue between the treatment surface and the tumor absorb most of the incident light, limiting photothermal interaction in the target tissue [129]. Increasing the irradiation power will cause more damage to the healthy tissue, minimizing the therapeutic effects. In the interest of expanding PTT beyond surface treatments, we aim to develop an interstitial photothermal therapy using PBNPs (iPTT). When the laser light is directed into the target tissue through an interstitial fiber, surface damage can be avoided and deep tumors can be reached. This is especially important in treating deep tumors such as neuroblastoma. However, appropriate thermal interaction is still crucial in order to achieve a long-term, systemic effect for cancer treatment. Therefore, we are currently determining the conditions (nanoparticle concentration, laser power, and exposure time) to determine effective temperature regimes for iPTT. We also tested our iPTT in an *in vivo* model of neuroblastoma, and studied its effect on tumor heating capabilities.

6.1.1 Materials and Methods

iPTT system

We developed an iPTT system using a catheter-based laser with a spherical light diffuser (SD, Medlight SA, Switzerland). A standard optical connector allowed coupling of the device with a 808 nm NIR laser (Laserglow Technologies, Canada). A

3 meters glass optical fiber guides the light from the proximal to the distal end of the device. The distal extremity is an illumination tip which isotropically emits the light transmitted by the optical fiber.

iPTT *in vitro*

We first tested the heating capabilities of iPTT compared to PTT *in vitro*. We utilized 1.75 mL microcentrifuge tubes (ThermoFisher Scientific, Waltham, MA) filled with 200uL of PBNPs (1 mg/mL), and tested the effect of laser power on heating capabilities. The PBNPs were irradiated for 10 minutes using PTT (surface light illumination) or iPTT (spherical light diffuser submerged in the PBNPs). The laser powers ranged from 80 – 200 mW. Prior to actual power outputs for various power settings were determined using a spherical power meter (ILX Lightware OMM-6810B, Newport Corporations, USA).

PTT *in vivo*

For the *in vivo* PTT studies, neuroblastoma (Neuro2a) tumor-bearing mice were treated when the mice had tumors of at least ~15 mm in diameter, measured using calipers. PTT was conducted as described previously. Briefly, mice were anesthetized prior to and during treatment using 2–5% isoflurane. The tumors were then i.t. injected with 50 μL of PBNPs resuspended in Milli-Q water (1 mg/mL), and the tumor are was irradiated with an 808 nm NIR laser from Laserglow Technologies (Toronto, ON, Canada) at 200 mW for 10 minutes. The temperatures reached during PTT were measured using a FLIR thermal camera (Arlington, VA).

iPTT *in vivo*

Mice were be anesthetized prior to and during treatment using 2–5% isoflurane. The tumors were then i.t. injected with 50 μL of PBNPs resuspended in Milli-Q water (1 mg/mL). iPTT was conducted by inserting the spherical diffuser directly into the middle of the tumor using a 20-gauge needle after PBNP injection. Mice were intratumorally irradiated for 10 minutes at 200 mW. To acquire temperature data, thermocouple needles were sterilized and insterted into the tumor next to the spherical light diffuser.

6.1.2 Results and discussion

iPTT results in better heating capabilities than PTT *in vitro*

To assess the effect of using a spherical light diffuser on photothermal heating properties compared to surface light delivery (PTT), we conducted iPTT vs PTT studies as a function of different laser powers *in vitro*. We see that the photothermal heating effect was laser-power dependent, with the temperatures increasing as the laser power increased (**Figure 6.1**). However, iPTT is able to cause higher temperature increases at the same laser power compared to PTT (14-25 °C higher, 80 – 200 mW respectively) (**Figure 6.1**). The improved heating capabilities of iPTT could be due to the fact that the spherical laser diffuser distributes NIR light more evenly across the nanoparticle solution compared to the surface laser used in PTT. This leads to better temperature distributions and higher temperatures.

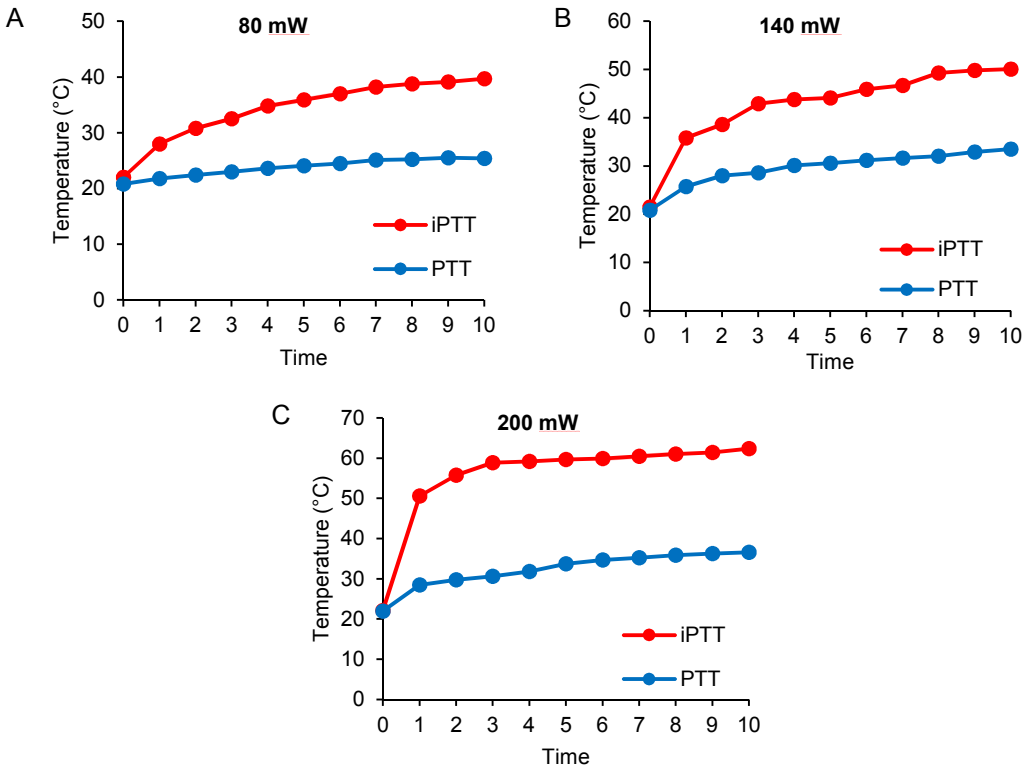

Figure 6.1. Heating capabilities of of PTT vs iPTT *in vitro*. Photothermal heating curves (time-temperature profiles) of 200uL of 1 mg/mL PBNPs in water using NIR laser powers at (A) 80 mW, (B) 140 mW, and (C) 200 mW. Laser power was delivered using an 808 nm NIR laser (PTT; blue), or an 808 nm NIR laser through a spherical diffuser (iPTT; red).

iPTT results in better heating capabilities than PTT *in vivo*

Building on our *in vitro* findings described above, we next tested if iPTT could cause ablative tumor temperatures *in vivo* compared to PTT as a step toward illustrating the photothermal treatment capabilities of iPTT (**Figure 6.2**). Since we saw ablative temperatures (~60 °C) being reached at 200 mW using iPTT, we decided to use this laser power *in vivo*. It is important to note that this laser power is much lower than the 0.75 W we currently use for PTT. This elucidates the efficacy of iPTT in delivering

and distributing NIR light. The final tumor temperatures achieved during iPTT measured by a needle thermocouple was ~56 ^{o}C, which corresponds to the temperature range needed to elicit tumor cell death and ICD in Neuro2a-bearing mice. However, when mice were treated with the same laser power but in a PTT setting, final tumor temperatures reached a temperature of only ~32 ^{o}C (**Figure 6.3**). These findings show the potential of iPTT to be used for deep tumors, where tumors are evenly irradiated from the inside out at lower laser powers. This eliminates any previously described concerns of PTT such as depth of tumor and pigmentation of the skin. Taken together, these data suggest the effectiveness of iPTT for the design of enhanced nanoimmunotherapies for the treatment of neuroblastoma.

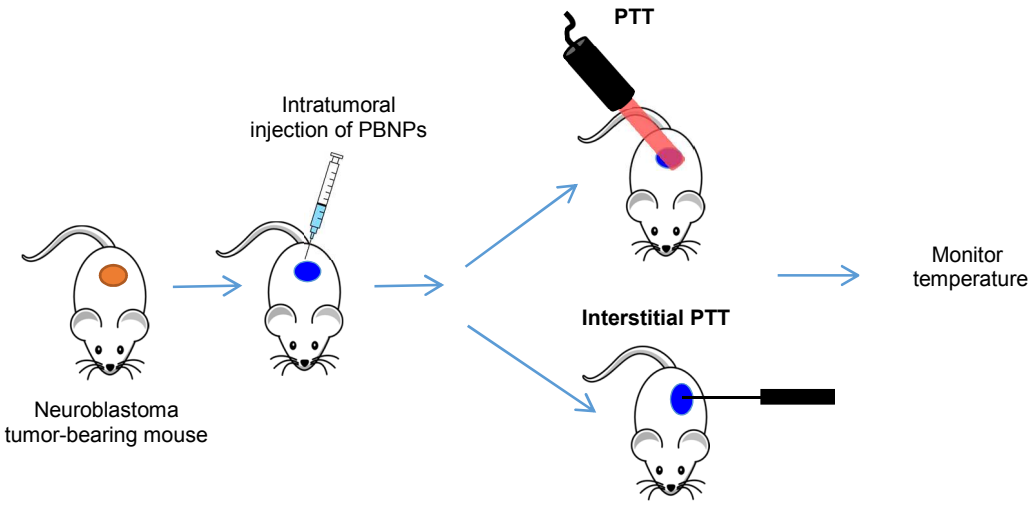

Figure 6.2. Schematic illustration of PTT vs iPTT *in vivo* pilot study. Neuroblastoma tumor-bearing mice were intratumorally injected with 1 mg/mL PBNPs and treated with PTT or iPTT using an 808 nm NIR laser at a power of 200 mW for 10 minutes.

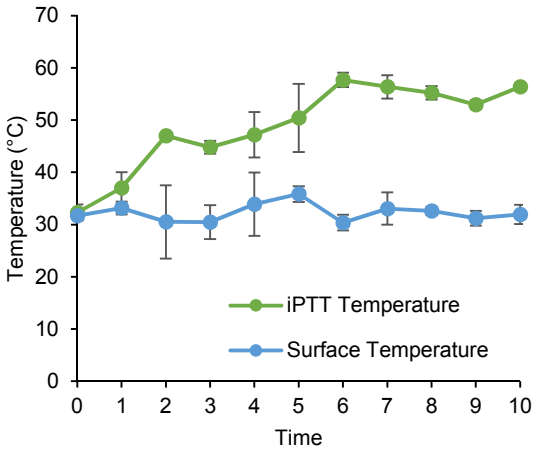

Figure 6.3. Heating capabilities of PTT vs iPTT *in vivo*. Photothermal heating curves (time-temperature profiles) of mice treated with iPTT or PTT. Mice bearing ~17 mm Neuro2a neuroblastoma tumors were treated with iPTT or PTT for 10 minutes after intratumoral (i.t) injection of PBNPs (50 uL of 1 mg/mL); laser power: 200 mV (n=3/group).

6.1.3 Conclusions and future directions

NIR laser delivery and temperature increase in tumor tissue during PTT is a significant factor in determining the outcomes and successes of the treatment. Therefore, we propose the design of an iPTT system where the laser is delivered through a spherical diffuser for better delivery of NIR light. The pilot studies described above elucidate the efficacy of using iPTT for nanoimmunotherapies. Future studies will focus on finding the optical temperature range for both tumor ablation and immunological stimulation both *in vitro* and *in vivo*. We will determine the characteristics of temperature increase in target tissue and the temperature profiles at varying distances from the spherical diffuser during interstitial laser irradiation. The development of an iPTT treatment using PBNPs has a high clinical relevance since it

has the potential to provide novel and more effective therapies for neuroblastoma cancer patients.

6.2 Developing a better neuroblastoma tumor model

One drawback in the development of novel nanoimmunotherapies for neuroblastoma is the lack of suitable autologous mouse models. Currently, we use the most common neuroblastoma mouse model which grows Neuro2a cells in A/J mice, for which only limited immunological tools are available due to the A/J genetic background. Neuro2a cells do not express the tumor antigen GD2 (disialoganglioside). The tumor antigen GD2 is expressed on the surface of virtually all human neuroblastoma cells and has been shown to be an effective target for immunotherapy [130-132]. The absence of murine neuroblastoma cell lines expressing significant amounts of GD2 has hindered the development of autologous murine neuroblastoma tumor models. Additionally, the role of adaptive immune effector cells in the anti-neuroblastoma immune response remains to be elucidated. Human neuroblastoma cells have been reported to express low levels of MHC Class I. Therefore, neuroblastoma cells may be poorly recognized by tumor-specific T cells [133]. However, there cells are also shown to upregulate MHC Class I molecules upon inflammation, especially following exposure to interferon□γ (IFN□γ) [134]. Since our nanoimmunotherapies take advantage of the immune response elicited after PTT and upregulates it [19, 62], we need neuroblastoma tumor models that correctly reflect the responses that human neuroblastoma will have to our therapies.

Weiss et al. [135, 136] generated a TH-MYCN transgenic mouse that spontaneously develop neuroblastoma. These neuroblastoma tumors have strong histological and genetic similarities with human neuroblastoma [137-139]. Kroesen et al.[140] derived the transgenic cell line 9464D from spontaneous neuroblastoma tumors arising in in C57BI/6 TH-MYCN mice. They contain the human MYCN transgene and express the corresponding human *MYCN* transcript. Similar to human neuroblastoma cells, syngeneic TH-MYCN-derived 9464D cells endogenously express the tumor antigen GD2 and low levels of MHC Class I [140]. Therefore the transplantable TH-MYCN model represents a relevant model for the development of novel immunocombinatorial approaches for neuroblastoma patients.

The goal of this study is to develop and characterize a 9464D neuroblastoma tumor model in our lab, and test the efficacy of our nanoimmunotherapies in treating neuroblastoma in this new model.

6.2.1 Materials and Methods

9464D cells

The transgenic cell line 9464D was derived from spontaneous tumors from TH-MYCN transgenic mice on C57B1/6 background and were a kind gift from Dr. Carol Thiele (National Cancer Institute, NIH, Bethesda). 9464D cell line cultured in Dulbecco's-modified Eagle (DMEM) medium containing 10% FCS, 1% nonessential amino acids, 0.5% AA and 0.05% β-mercaptoethanol (complete medium).

Real-time PC

Tumors were harvested from 9464D induced mice and total RNA was extracted using RNeasy (Qiagen) kit following the manufacturer's protocol. RNA concentration was measured by (NanoDrop), and 0.5 µg RNA was reverse transcribed to cDNA using the iScript™ cDNA Synthesis Kit (Bio-Rad). Real-time RT–PCR was performed using the iQ™ SYBR® Green Supermix on ABI prism 7900 HT sequence detection system (Applied Biosystems, Foster City, CA, USA). Thermal cycling conditions were 95°C for 3 min and then 40 cycles of 95°C for 15 s and 58°C for 45 s. Melting curve analysis confirmed that only a single product was amplified. The following primers were used:

Porphobilinogen deaminase (PBGD):

forward (5'CCTACCATACTACCTCCTGGCTTTAC-3');

reverse (5'-TTTGGGTGAAAGACAACAGCAT-3');

hMYCN:

forward (5,CGACCACAAGGCCCTCAGTA-3,);

reverse (5'-CAGCCTTGGTGTTGGAGGAG-3');

GD2-synthase:

forward (5'-CCAAGGAGCCGAGTACAACAT-3');

reverse (5'-GTAGGGTAAAAGCGTCGGATG-3');

Survivin:

forward (5'-CTGCTTTAAGGAATTGGAAGGCT-3');

reverse (5'-CTGACGGGTAGTCTTTGCAGT-3');

S100A6:

forward (5'-TGGCTCCAAGCTGCAGG-3');

reverse (5'CCCAGGAAGGCGACATACTC-3');

ODC:

forward (5' GCACATCCAAAGGCAAAGTTG-3');

reverse (5'-CAAACTTAACACTGAGGCGACAGA-3');

PBGD served as a reference gene. mRNA expression was determined relative to PBGD expression using the formula: $2^{(CT\ index-CT\ PBGD)}$. Mean relative expression levels were determined by triplicate measurements.

GD2 expression on 9464D cells

9464D and Neuro2a cells were sorted for GD2 expression. Cells were stained with anti-CD-2 or isotype control and sorted using a BD Biosciences FACSCaliber (Franklin Lakes, NJ), and analysis was done using FlowJo (Ashland, OR) software.

***In vitro* PBNP-PTT**

In vitro PBNP-PTT was performed using an 808 nm NIR laser from Laserglow Technologies (Toronto, ON, Canada). Either 50,000 Neuro2a neuroblastoma cells were seeded overnight in 96-well plates, or ten million Neuro2a cells were suspended in 1 mL PBS in a 1.7 mL micorcentrifuge tube. Varied concentrations of PBNPs were added to the cells, and the cells were then illuminated by the NIR laser. Power was confirmed by a power meter (Thorlabs, Newton, NJ). Temporal temperature measurements were taken using a thermal camera (FLIR, Arlington, VA).

CEM43 calculations

Thermal doses administered to the various groups was expressed in terms of CEM43 (cumulative equivalent minutes at 43 ^{o}C). CEM43 was calculated as described previously in Chapter 3.

ICD marker analysis

In vitro PBNP-PTT was performed as described above. Cell suspensions were then washed and stained with fluorescent antibodies against HMGB1 (intracellular) and calreticulin (extracellular) and flow cytometry was performed. Antibodies were purchased from Abcam (Cambridge, UK), flow cytometry was performed on the BD Biosciences FACSCaliber (Franklin Lakes, NJ), and analysis was done using FlowJo (Ashland, OR) software. For intracellular ATP presence, cells were washed after *in vitro* PBNP-PTT and the ATP-based CellTiter-Glo (Promega, Madison, WI) Luminescent Cell Viability Assay was performed.

***In vivo* study**

2 million 9464D cells in 100 μL PBS were subcutaneously injected into the backs of previously shaven C57B1/6 mice. Treatment began when tumor volumes reached ~60 mm^3. Mice were anesthetized prior to and during treatment using 5% isoflurane. Tumor-bearing mice were divided into three groups (n=5 mice/ group): 1) Vehicle (no treatment) 2) PBNP-PTT (50 μL of 1 mg/mL PBNPs intratumorally, irradiated at 0.75 W for 10 minutes), and 3) CpG-PBNP-PTT nanoimmunotherapy (50 μL of 1 mg/mL CpG-PBNPs, 2 μg bound CpG,

irradiated at 0.75 W for 10 minutes, CpG-PBNPs boosts were given (without PTT) on days 2 and 5). Temperatures reached during PTT were measured using the i7 FLIR thermal imaging camera (Arlington, VA). Tumor growth was monitored following inoculation and treatments by routine caliper measurements.

6.2.2 Results and discussion

Characterization of TH-MYCN-derived 9464D neuroblastoma cell lines

To characterize the neuroblastoma phenotype of the 9464D cell lines, the expression of several neuroblastoma-associated genes was determined by quantitative RT-PCR. *Survivin*, an antiapoptotic gene highly expressed in neuroblastoma was detected [141, 142]. *S100A6*, which is expressed by more differentiated human neuroblastoma cells could also be detected in the cell line [143]. Ornithine decarboxylase (ODC) is correlated with MYCN expression in tumors from TH-MYCN mice and is expressed by the TH-MYCN-derived cell line [144, 145]. *GD2 synthase* one of the key enzymes in the production of GD2 [146, 147], was also expressed on the surface of 9464D cells. (**Figure 6.4A**). It is important to note that we have not yet characterized these genes in the Neuro2a cell line. These studies are important in determining the efficacy of 9464D cell line in mimicking human neuroblastoma, and it is currently being studied in the lab.

After gene characterization of the 9464D cell lines, we then looked at the expression of GD2. The tumor antigen GD2 is expressed on the surface of virtually all human

neuroblastoma cells and has been shown to be an effective target for immunotherapy [132, 147]. The absence of murine neuroblastoma cell lines expressing significant amounts of GD2 has hampered the development of autologous murine neuroblastoma tumor models. Strikingly, 9464D cells, but not Neuro2a cells, expressed significant amounts of GD2 on their cell surface (**Figure 6.4B**). Based on these data, we decided to use 9464D cells for further studies as they not only endogenously express the tumor antigen GD2, but also express other immunological relevant genes.

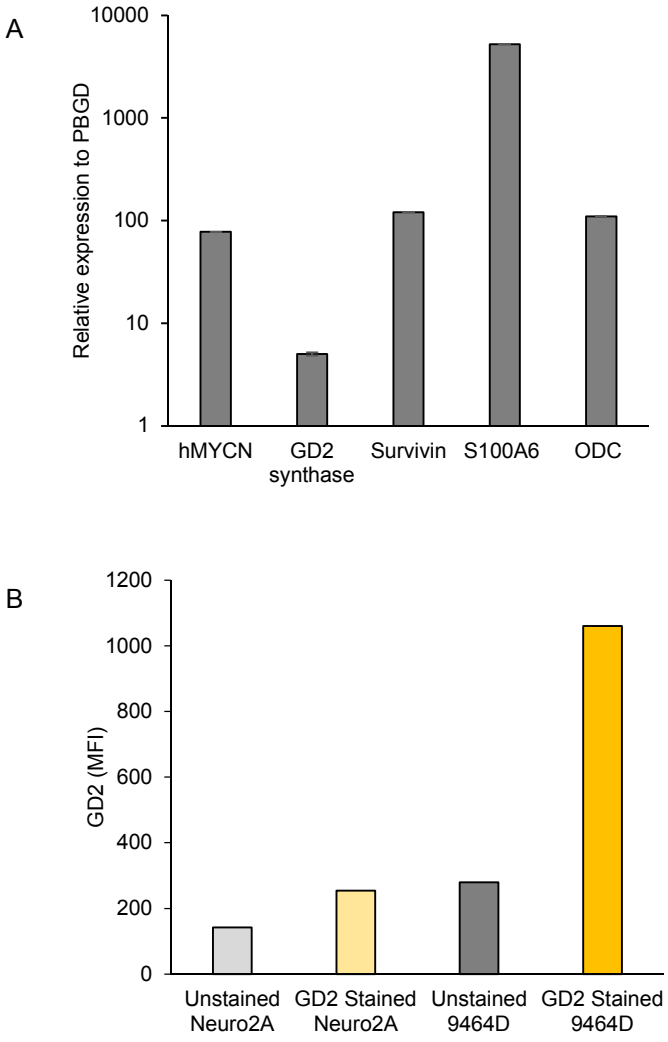

Figure 6.4. Characterization of 9464D cells. A) Expression of neuroblastoma-associated genes in the MYCN transgenic cell line 9464D. Total RNA was isolated and reverse transcribed to cDNA. Quantitative expression was determined for hMYCN (the human *MYCN* cDNA transgene used in the TH-MYCN transgenic mouse), *GD2 synthase*, *survivin*, *S100A6*, and *ODC* and related to the expression of the household gene PBGD. B) GD2 is greatly expressed in 9464D cells compared to Neuro2a cells.

Photothermal heating capabilities of 9464D cells after PBNP-PTT

To assess the photothermal heating properties of 9464D cells, we conducted photothermal heating studies *in vitro* as a function of laser power. The photothermal heating effect was laser power-dependent (**Figure 6.5A**). The temperatures increased with increasing laser power (0.2 – 1.5 W) reaching a maximum temperature around 76 ^{o}C at 10 minutes at a concentration of 1.5 mg/mL PBNPs. Thermal doses administered to the various groups was also expressed in terms of CEM43. CEM43 analysis allows for a generalizable comparison of biological effect across different thermal therapies and serves as an objective metric for thermal injury [98]; it has been used extensively in the literature for measuring the effects of heat on different tissues [100-102]. We have measured the thermal doses of 9464D cells in terms of CEM43 (**Figure 6.5B**), to further study thermal effects to tumor regression and survival in the future. These results show that 9464D can be subjected to photothermal therapy, and reach temperatures that are ideal for the induction of ICD and cell killing. We will further characterize the photothermal therapies by studying cell death after killing, as well as iPTT in a 9464D model of neuroblastoma.

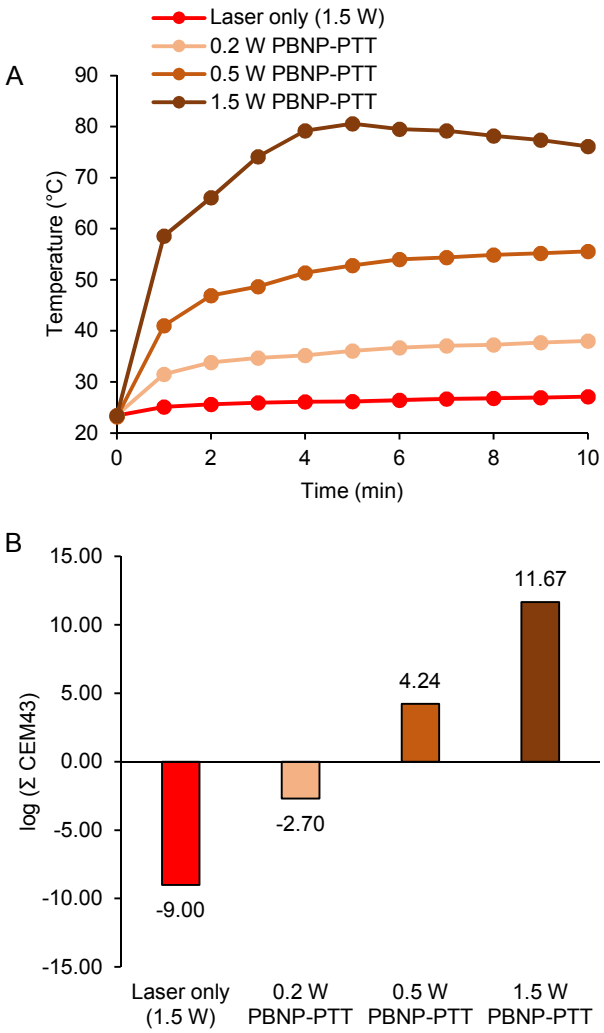

Figure 6.5. Heating capabilities of 9464D cells after PBNP-PTT. A) Photothermal heating curves (temperature-time profiles) of 1.5 mg/mL PBNPs using varying NIR laser powers (0.2 – 1.5 W) for 10 minutes. B) Thermal dose after PBNP-PTT described in terms of cumulative equivalent minutes at 43 ^{o}C; a thermal dose parameter (CEM43).

ICD marker analysis of 9464D cells after PBNP-PTT

The induction of ICD is crucial for the success of our nanoimmunotherapies. Therefore, we next studied the effects of PBNP-PTT in eliciting ICD in 9464D cells. We have demonstrated that PBNP-PTT elicits ICD in Neuro2a cells as measured by its biochemical correlates (released ATP, and HMtGB1, and increased surface calreticulin) [62]. Here, we verify whether PBNP-PTT elicits ICD in 9464D cells. Our pilot studies show that two out of three ICD markers are met after PTT (**Figure 6.6**). PBNP-PTT caused a decrease in intracellular ATP levels in 9464D at higher temperatures. PTT also triggered a significant increase in surface calreticulin expression relative to controls. However, PBNP-PTT did not cause a decrease in intracellular HMGB1 levels compared to other treatment groups. We have seen this trend in other cancer models such as B16F10 melanoma, which use C57B1/6 mice. It is important to note that the 9464D model uses a black mouse model (C57B1/6 mice), compared to the Neuro2a mode, which uses a white mouse (A/J). Since different cells can absorb different amounts of light due to the pigmentation, induction of ICD in the 9464D model might require different thermal doses. Further studies need to be conducted to determine the optimal nanoparticle concentration, laser power, and thermal dose in the 9464D model of neuroblastoma to reach ideal tumor ablative temperatures as well as an upregulation of an antitumor immune response. To complement current PTT-stimulated release of DAMPs, we are currently working on synthesizing HMGB1-coated PBNPs to ensure that PTT induces the release and expression of HMGB1 to induce ICD (**Appendix 8**). If we find that several temperature regimes cause the

induction of 2/3 ICD markers, we can use these DAMPs-coated PBNPs to exogenously deliver HMGB1 and cause a synthetic ICD that will be further complemented by the various immunotherapies of our nanoimmunotherapy.

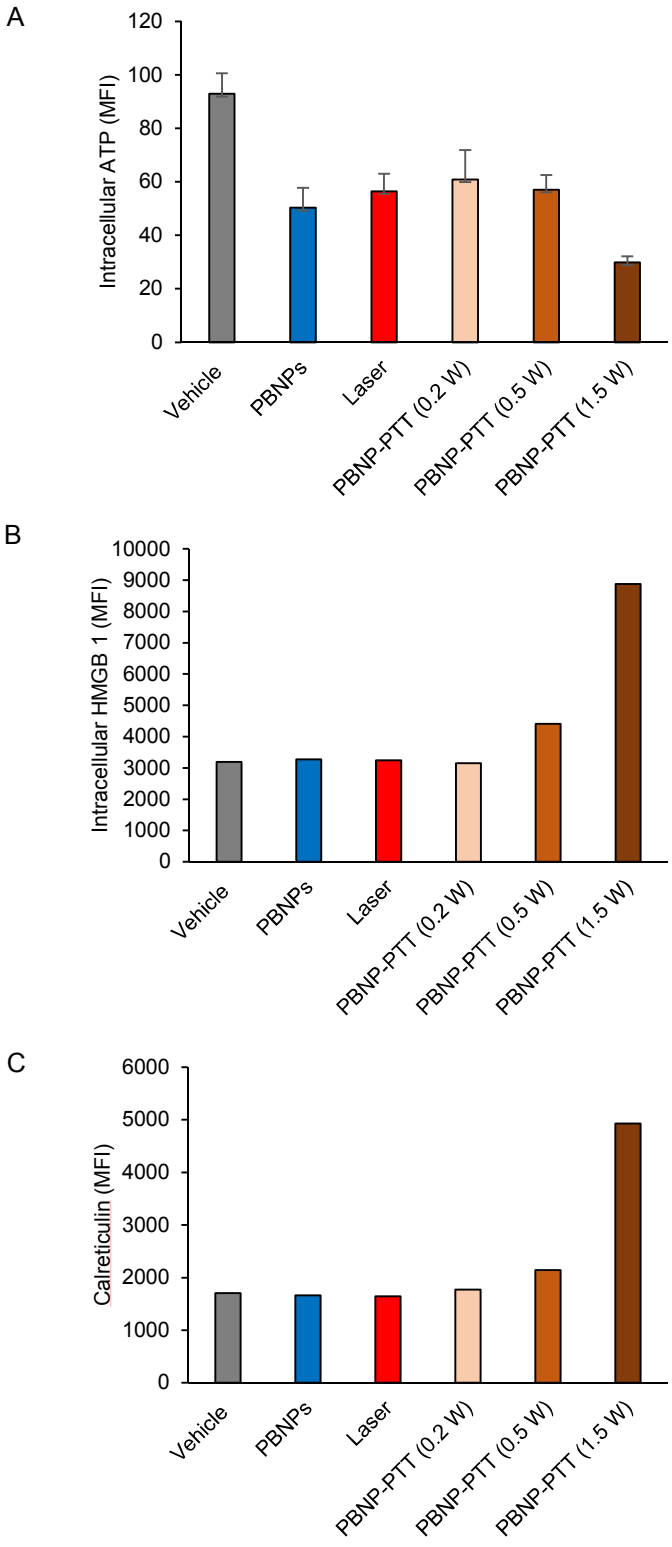
A
Intracellular ATP (MFI)
120
100
80
60
40
20
0
Vehicle
PBNPs
Laser
PBNP-PTT (0.2 W)
PBNP-PTT (0.5 W)
PBNP-PTT (1.5 W)
B
Intracellular HMGB 1 (MFI)
10000
9000
8000
7000
6000
5000
4000
3000
2000
1000
0
Vehicle
PBNPs
Laser
PBNP-PTT (0.2 W)
PBNP-PTT (0.5 W)
PBNP-PTT (1.5 W)
C
Calreticulin (MFI)
6000
5000
4000
3000
2000
1000
0
Vehicle
PBNPs
Laser
PBNP-PTT (0.2 W)
PBNP-PTT (0.5 W)
PBNP-PTT (1.5 W)

Figure 6.6. Induction of immunogenic cell death (ICD) by PBNP-PTT in 9464D cells. A) Intracellular ATP in the various treatment groups (as a % of the vehicle-treated group). (B) Intracellular HMGB1 in the various treatment groups (as a % of the vehicle-treated group). (C) Surface calreticulin expression in the various treatment groups (as a % of the vehicle-treated group). Vehicle groups were treated with 10 μL of distilled water. All groups had concentration of nanoparticles of 1.5 mg/mL.

CpG-PBNP-PTT in the 9464D mouse model of neuroblastoma

Building on our findings described above, we next tested if CpG-PBNP-PTT generated tumor death and survival in the 9464D model of neuroblastoma. 9464D neuroblastoma tumor-bearing mice were divided into three treatment groups (n=5/group; **Figure 6.7**): 1) Untreated, 2) PBNP-PTT, and 3) CpG-PBNP-PTT. The average final tumor temperatures achieved during PTT measured by the thermal imaging camera was ~118 ^{o}C (**Figure 6.7A**), which corresponds to the temperature range needed to elicit tumor cell death in tumor-bearing C57B1/6 mice (data not shown). CpG-PBNP-PTT resulted in complete tumor regression in all the treated mice (5/5) compared to mice in the PBNP-PTT group (3/5) and untreated group (0/5) (**Figure 6.7 B-E**). Since this pilot study only included PTT-treated groups, we are currently working on repeating this study, and also including representative controls (laser, PBNPs, CpG-PBNPs). We will also test our nanoimmunotherapy (CpG-PBNP-PTT + anti-CTLA-4) in a distal and metastatic model of 9464D neuroblastoma.

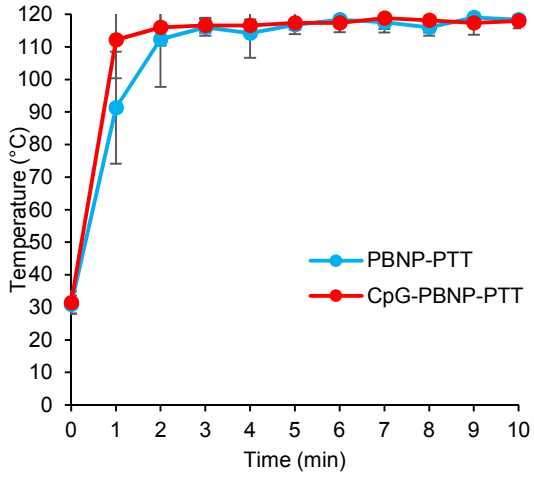
Temperature (°C)
Time (min)
PBNP-PTT
CpG-PBNP-PTT

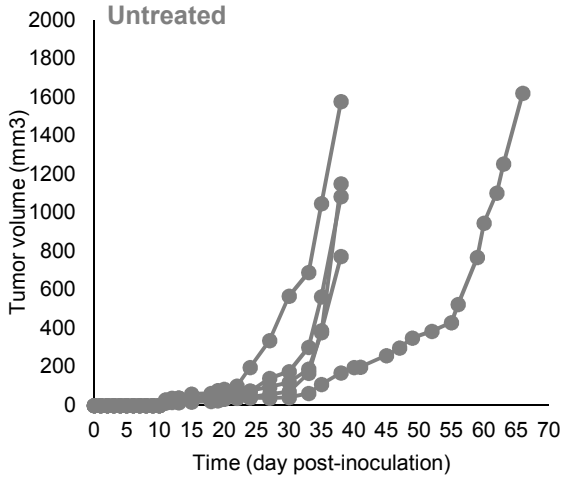
Untreated
Tumor volume (mm3)
Time (day post-inoculation)

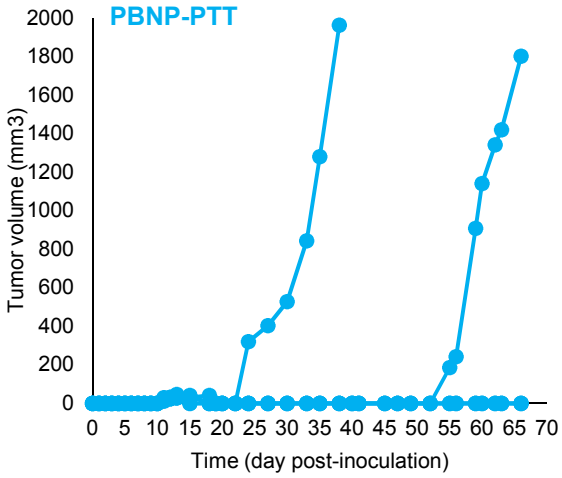
PBNP-PTT
Tumor volume (mm3)
Time (day post-inoculation)

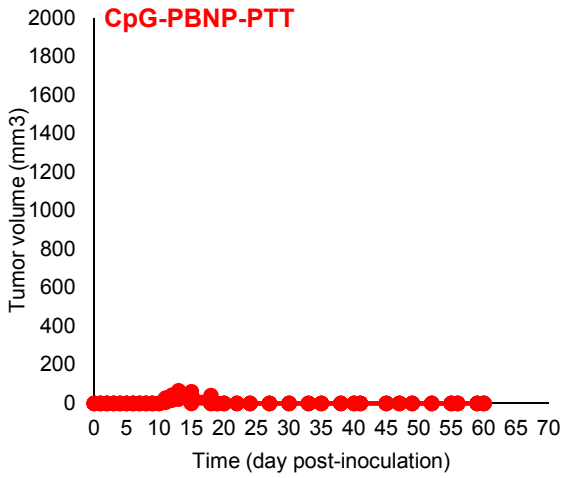
CpG-PBNP-PTT
Tumor volume (mm3)
Time (day post-inoculation)

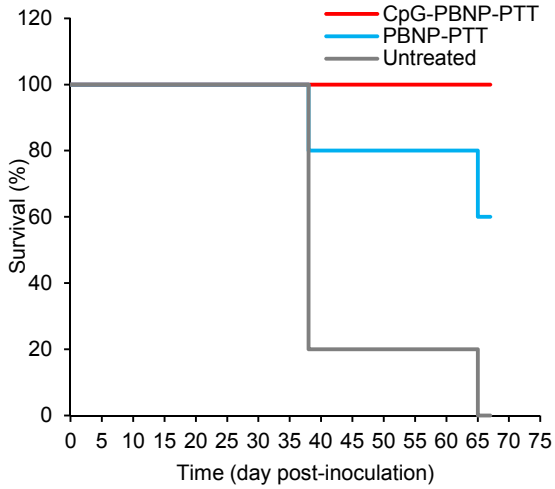
CpG-PBNP-PTT
PBNP-PTT
Untreated
Survival (%)
Time (day post-inoculation)

Figure 6.7. Effect of CpG-PBNP-based nanoimmunotherapy on tumor regression and survival in the 9464D neuroblastoma mouse model. Mice bearing ~5 mm diameter 9464D neuroblastoma tumors were treated with CpG-PBNP-PTT and corresponding controls. The PTT-treated groups received 50 μL of 1 mg/mL CpG-PBNPs or PBNPs intratumorally (i.t.), and were irradiated by an 808 nm laser at 0.75 W for 10 minutes. Additionally, the CpG-PBNP-PTT received two boosters with CpG-PBNP on Days 2 and 5 i.t. (A) Temperature-time profiles of 9464D bearing mice treated intratumorally with 1mg/mL CpG-PBNPs or PBNPs and irradiated with a NIR laser at 0.75 W for 10 minutes. (B-D) Tumor growth curves for individual mice in the various treatment groups. Each line represents tumor growth measured in one mouse (E) Kaplan-Meier survival plots of 9464D tumor-bearing mice that were treated with PBNP-PTT, CpG-PBNP-PTT, or left untreated. Mice receiving CpG-PBNP-PTT showed significantly higher long-term survival compared with the other groups. Ongoing study.

6.2.3 Conclusions and future directions

Utilizing neuroblastoma mouse models that more likely resemble human neuroblastoma is crucial for the development of effective nanoimmunotherapies. We are currently working on testing the effects of our nanoimmunotherapy on TH-MYCN-derived 9464D neuroblastoma cell lines. Pilot studies show that this cell lines express GD2, an important neuroblastoma marker that determines the efficacy of immunotherapies, as well as various genes expressed in human neuroblastoma. We show that we are able to heat 9464D using PBNP-PTT, leading to thermal doses that are conductive to ICD and tumor cell death. Lastly, when testing our nanoimmunotherapy in a 9464D mouse model of neuroblastoma, we see that mice treated with CpG-PBNP-PTT result in tumor regression and long-term survival. Future studies will focus on further characterization of the 9464D cells before and after PTT to determine the changes in cell phenotype and cell death after treatment. The immune effects after nanoimmunotherapy (immune cell infiltration, DC activation, T cell

proliferation, immune memory) will also be studied. The development of a more significant neuroblastoma model, and the understanding of the immune effects generated after nanoimmunotherapies is crucial for the advancement of more effective treatments for neuroblastoma.

6.3 Nanoimmunotherapies for the treatment of metastatic neuroblastoma

Despite a significant improvement in understanding and treating primary neuroblastoma tumors, metastasis remains the leading cause of death in this cancer[148]. Therefore, a successful cancer treatment must not only treat the primary tumor, but also create sufficient responses against metastases. In response to this need, we are planning studies that study the efficacy of our nanoimmunotherapy in treating metastatic tumors using a metastatic model of neuroblastoma. Briefly, this study will be conducted similar to studies in Chapter 5, i.e. identical groups and treatment methods. Importantly, these studies will be performed in experimental models of metastatic neuroblastoma using Neuro2a or 9464D cells. These models of experimental metastases will contain a "primary" tumor and metastasized disease. The primary tumors will be established by subcutaneous injection of Neuro2a or 9464D cells. For metastasis, tumor cells will be intravenously injected in mice, as previously described in literature [149]. In this model metastatic nodules typically appear in the abdomen. The progression of these metastases will be monitored by whole animal bioluminescence imaging. The primary tumor will be CpG-PBNP-PTT +/- anti-CTLA-4-treated and the metastatic nodules will be left untreated. Based on our preliminary

data, we anticipate that mice in the nanoimmunotherapy-treated group will exhibit slower tumor growth and significantly longer survival compared with the untreated mice due to the increased tumor cell death by ablation and upregulation of an immune response (**Figure 6.8**). The findings of these studies will be crucial in designing future studies in orthotopic models of neuroblastoma [140, 150] where PBNP-PTT will be administered interstitially.

6.4 Statement of cancer relevance

The work presented in this dissertation designed a novel, safe, and effective treatment for neuroblastoma, which is a common childhood malignancy with a dismal prognosis, and a leading cause of cancer-related deaths in children. This research contributes new methodology, novel insights, and effective therapeutic nanoimmunotherapies for the nanotechnology, cancer biology, and immunology fields. The findings presented in this dissertation will advance insights into the design of novel nanoimmunotherapies, which combine the complementary advantages of nanomedicine and immunotherapy, for the treatment of cancer. The approaches investigated in this project, which comprises the use of nanoparticles to administer interstitial photothermal therapy while simultaneously serving as a local depot for cancer adjuvants in combination with TLRs and checkpoint inhibitors, will likely be applicable to other solid tumors, both pediatric and adult, with a propensity to dissipate early in their clinical course. Successful completion of this project will offer a novel option for the treatment of high-risk neuroblastoma and will open the way to generating

data essential to our overall goal: *translation of the study to the design and conduct of future clinical trials*

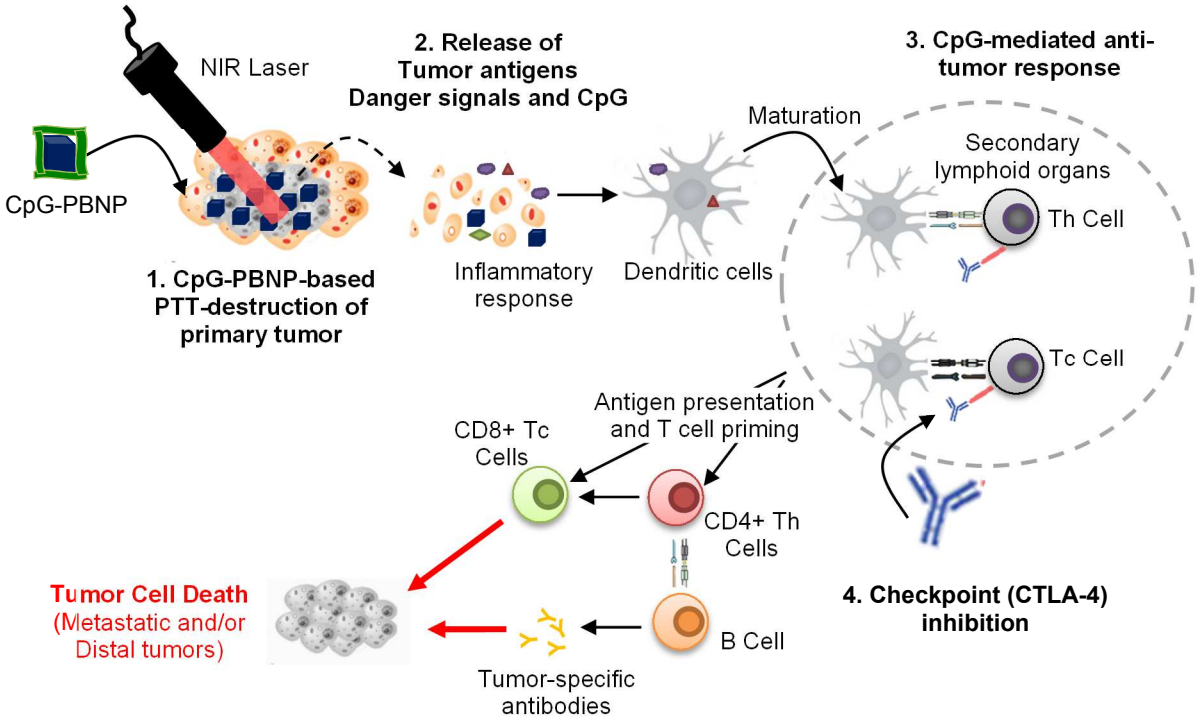

Figure 6.8: A hypothesized mechanism of action of the CpG-PBNP-PTT + anti-CLTA-4 nanoimmunotherapy is presented. 1) PTT-based destruction of tumors in a minimally invasive manner, 2) Release of tumor antigens and danger signals post-PTT providing an immunostimulatory, multi-antigen local effect, and 3) the use of CpG-PBNPs that improves the uptake and antigen presentation of DCs to T cells, activating them and unleashing a potent antitumor immune response. 4) I.p (systemically) administered anti-CTLA-4 reverses immunosuppression, unleashing the antitumor immune responses of endogenous immune cells, particularly T cells. The above processes combine to yield improved tumor responses and development of immunity against tumor rechallenge and distal tumors in a mouse model of neuroblastoma.

Appendix

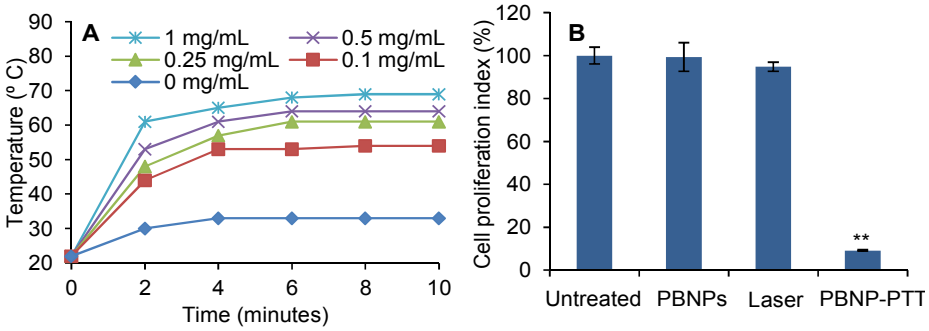

Appendix 1: PBNPs work as effective PTT agents. A) Photothermal heating of varying concentrations of PBNPs irradiated with a 808 nm NIR laser for 10 minutes at 1.875 W/cm^2 showing heating of the nanoparticles. B) PTT with 0.05 mg/mL PBNPs + 1.875 W/cm^2 laser fluence (using 808nm laser) results in significantly decreased proliferation of Neuro2a cells relative to controls using nanoparticles alone, laser alone, and left untreated (**$p<0.01$).

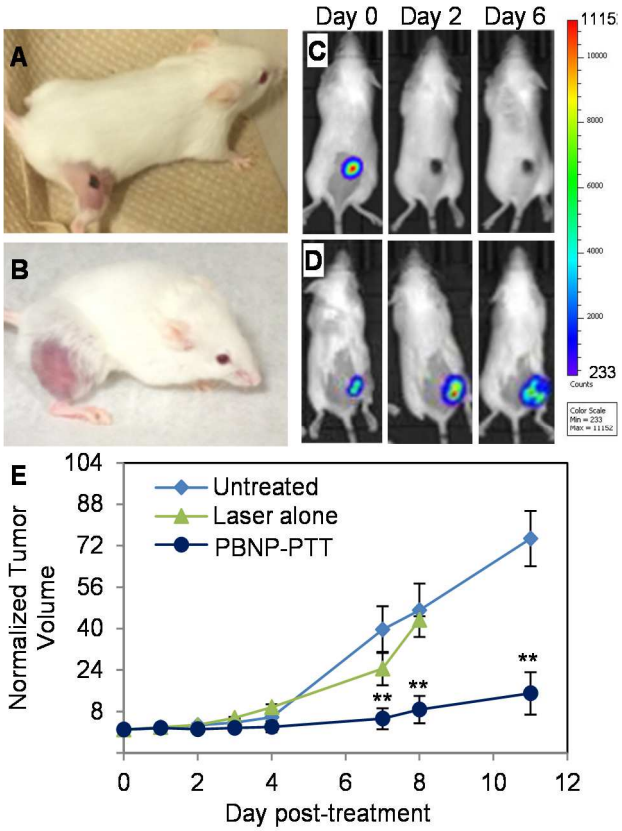

Appendix 2: Effect of PBNP-PTT on Neuro2a tumor growth. Representative photographs of Neuro2a tumor-bearing mice treated with: A) PBNP-PTT and B) remaining untreated. Representative, temporal images (Day 0, 2, and 6) of bioluminescent Neuro2a tumor-bearing mice that are C) PBNP-PTT treated and D) untreated (Scale bar = tumor bioluminescence intensity; p/s/cm^2/sr). E) Normalized tumor volume showing a marked reduction in Neuro2a tumor growth rate in PBNP-PTT treated mice relative to Untreated and Laser alone controls (**indicates significant decrease; $p< 0.001$).

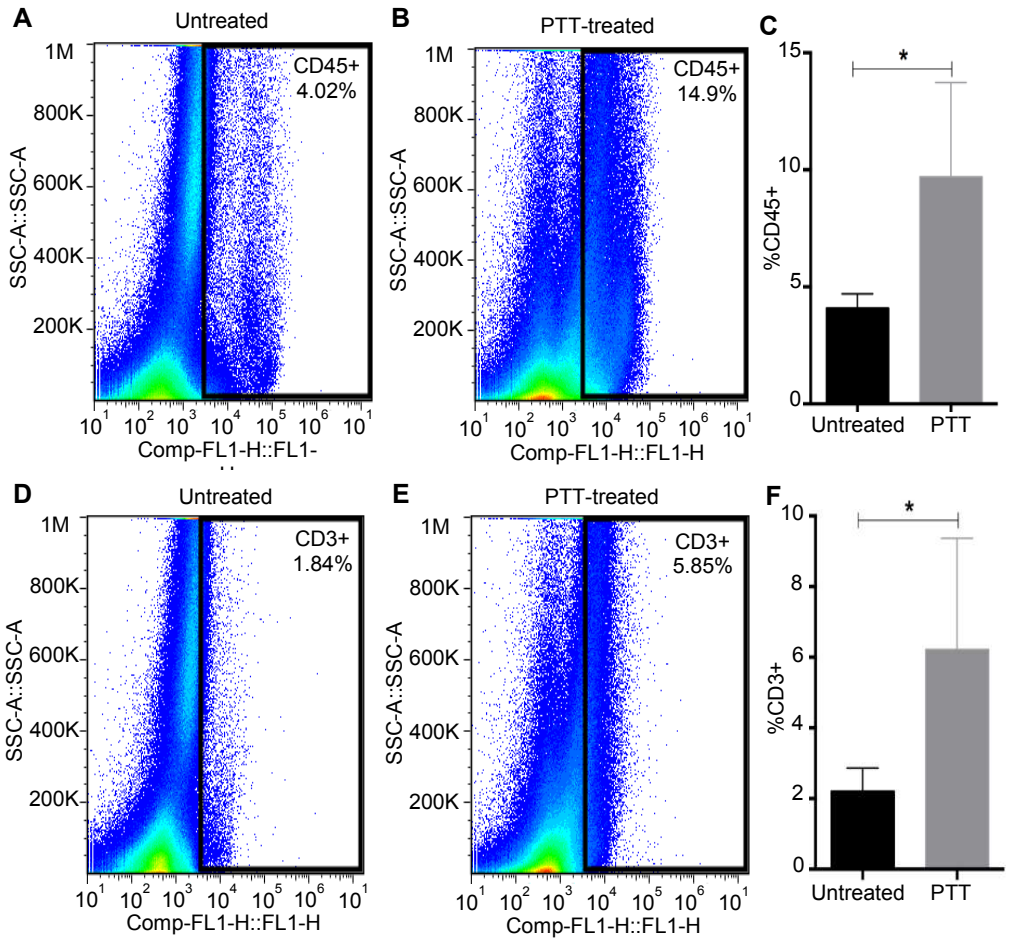

Appendix 3. Immunostimulatory effects of PBNP-based PTT. Representative scatter plots of CD45+ cells in tumors of: A) Untreated and B) PTT-treated mice. C) %CD45+ cells in the tumors of untreated and PTT-treated mice showing significantly higher percentage of CD45+ cells in tumors of PTT-treated vs. untreated mice (p=0.0294). Representative scatter plots of CD3+ cells in tumors of: D) Untreated and E) PTT-treated mice. F) %CD3+ cells in the tumors of untreated and PTT-treated mice showing significantly higher percentage of CD3+ cells in tumors of PTT-treated vs. untreated mice (p=0.0424).

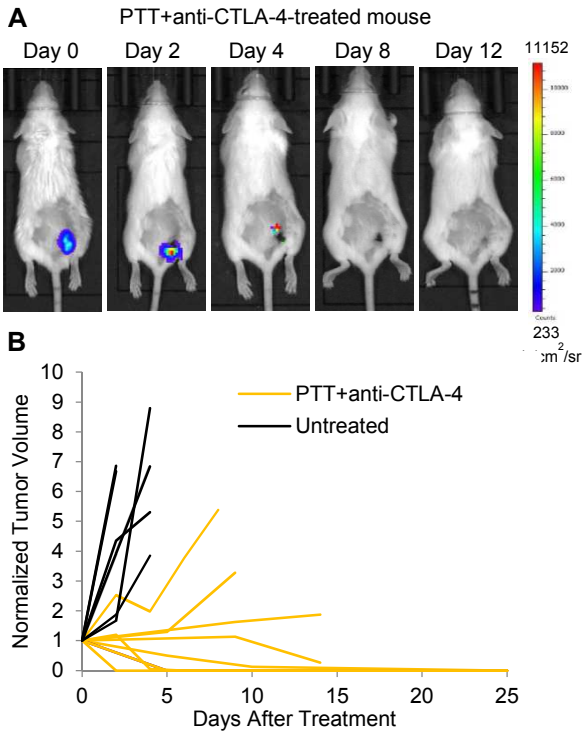

Appendix 4. Effect of photothermal immunotherapy (PTT+anti-CTLA-4 therapy) on tumor regression and long-term survival in the neuroblastoma mouse model. A) Representative image of a long-term surviving mouse treated with PTT+anti-CTLA-4 showing complete tumor regression (scale bar = bioluminescent intensity; p/s/cm^2/sr). B) Normalized tumor growth curves for tumor-bearing mice treated with PTT+anti-CTLA-4 (violet) or left untreated (black). C) Kaplan-Meier survival plots of neuroblastoma mice that were treated with PTT+anti-CTLA-4, anti-CLTA-4 alone, PTT alone, or untreated. Mice receiving photothermal immunotherapy showed significantly higher long-term survival (> 100 days) compared with mice in the other groups (log-rank test; $p<0.05$).

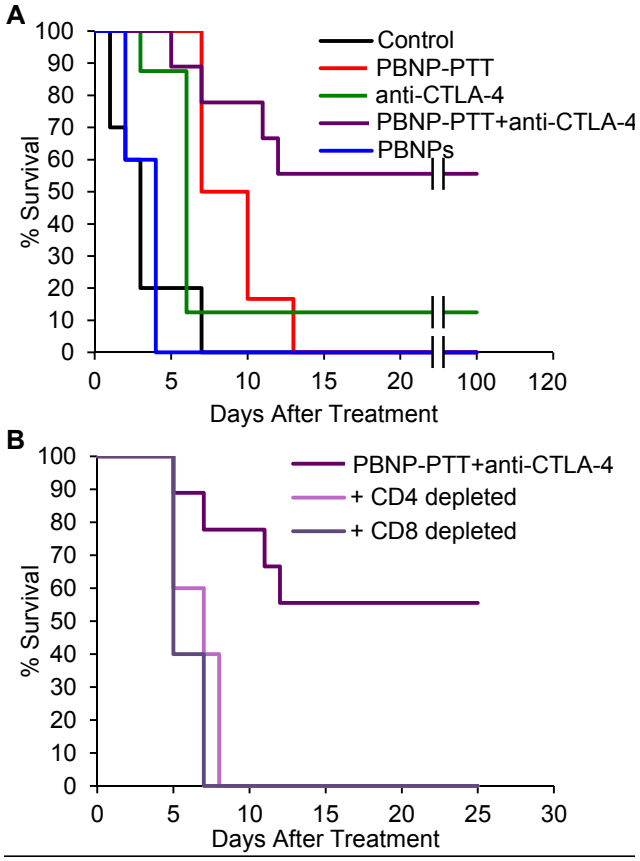

Appendix 5: Effect of PBNP-PTT+anti-CTLA-4 nanoimmunotherapy on tumor regression and long-term survival in a mouse model of neuroblastoma. A) Kaplan-Meier survival plots of Neuro2a tumor-bearing mice that were treated with PBNP-PTT + anti-CTLA-4, anti-CTLA-4 alone, PBNP-PTT alone, PBNPs alone, or untreated. Mice receiving PBNP-PTT + anti-CTLA-4 showed significantly higher long-term survival (<100 days) compared with mice in the other groups (log-rank test $p<0.05$, $n>=5$ per group). B) Kaplan-Meier survival plots of Neuro2a tumor-bearing mice depleted in CD4+ and CD8+ T cells. Depletion of CD4+ and CD8+ T cells (n=5 per group) effectively abrogated the therapeutic responses of the PBNP-PTT + anti-CTLA-4 nanoimmunotherapy (log-rank test, $p<0.005$).

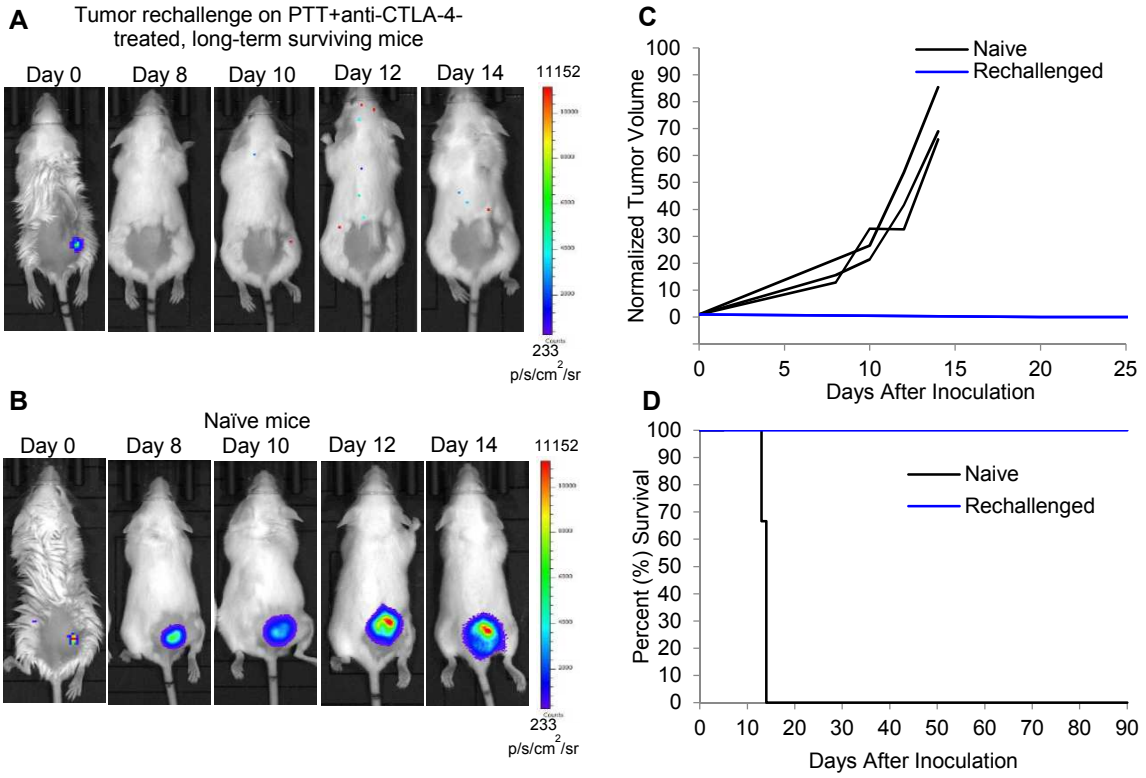

Appendix 6. Effect of tumor rechallenge in combination photothermal immunotherapy-treated, long-term surviving mice. (A-B) Representative images showing protection against tumor rechallenge in A) photothermal immunotherapy-treated mice and B) tumor progression in naïve, untreated mice (scale bars = bioluminescent intensity; p/s/cm^2/sr). C) Tumor growth curves after challenge with 10^6 Neuro2a cells in untreated mice (naïve, black ; n=3) and long-term surviving photothermal immunotherapy-treated mice (rechallenged, blue ; n=3) showing protection in the rechallenged group compared to progression in the naïve group. D) Kaplan-Meier survival plots showing significantly higher long-term survival in the rechallenged group compared to naïve mice (log-rank test, $p<0.05$).

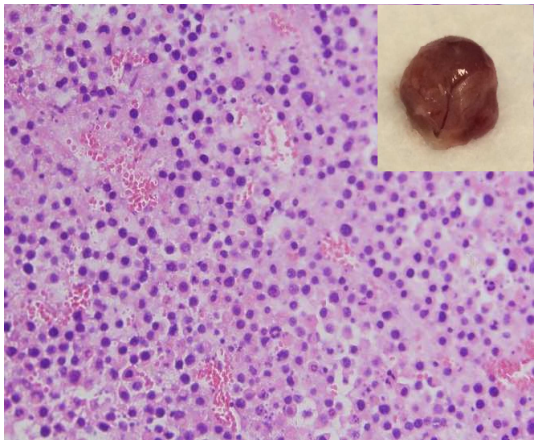

Appendix 7: Representative image of an H&E stained tumor excised from a Neuro2a tumor-bearing mouse. Inset: representative photograph of a tumor excised from a tumor-bearing mouse. Both images demonstrate that the tumors are well vascularized and not a loose collection of tumor cells.

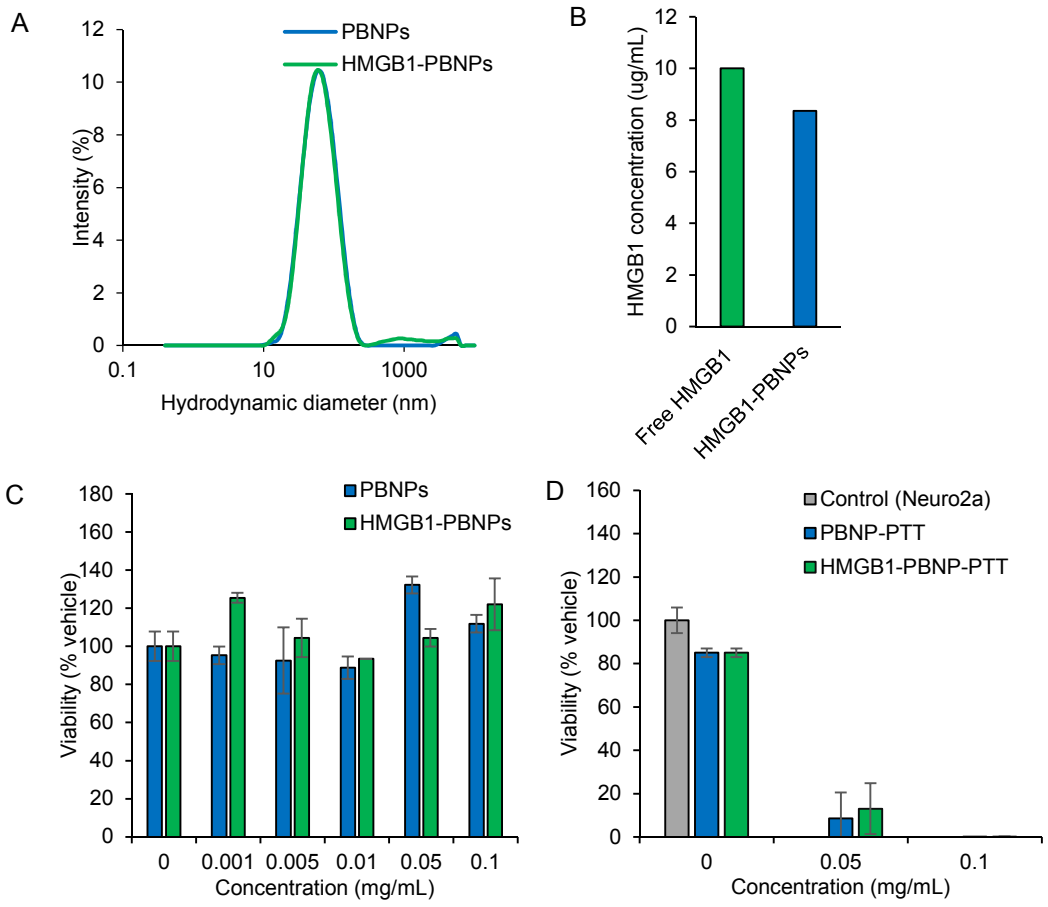

Appendix 8: Synthesis and characterization of HMGB1-coated PBNPs. (A) Dynamic light scattering (DLS). (B) HMGB1 encapsulation onto the PBNPs, showing 81% encapsulation efficiency. (C) Cytotoxicity of varying concentrations (0.001-0.1 mg/mL) PBNPs and HMGB1-PBNPs on Neuro2a cells, measured by a cell viability assay. (D) Cytotoxicity of 50,000 Neuro2a cells after PBNP-PTT or HMGB1-PBNP (nanoparticle concentration was 0.05 – 0.1 mg/mL, 0.75 W laser, 10 minutes).

Publications, Presentations and Awards

Accepted publications

Cano-Mejia J, Bookstaver ML, Sweeney EE, Jewell CM, Fernandes R (2019) "Prussian blue nanoparticles-based antigenicity and adjuvanticity trigger robust antitumor immune responses against neuroblastoma" *Biomaterials Science.* DOI: 10.1039/C8BM01553H.

Sweeney EE*, **Cano-Mejia J***, Fernandes R (2018) "Photothermal therapy generates a window of immunogenic cell death in neuroblastoma" *Small.* Vol. 14. No. 20, e1800678
*authors contributed equally

Cano-Mejia J, Sweeney EE, Burga RA, Fisher JP, Bollard CM, Cruz CRY, Fernandes R (2017) "Prussian blue nanoparticle-based photothermal therapy combined with checkpoint inhibition for photothermal immunotherapy of neuroblastoma" *Nanomedicine NBM.* Vol. 13, No. 2, 771-781.

Vojtech JM, **Cano-Mejia J**, Dumont MF, Sze RW, Fernandes R (2015) "Biofunctionalized Prussian Blue Nanoparticles for Multimodal Molecular Imaging Applications" *J. Vis. Exp.* Vol. 1, No. 98, e52621

Presentations

April 2019: Prussian blue nanoparticles-based antigenicity and adjuvanticity trigger robust antitumor immune responses against neuroblastoma" *Society for Thermal Medicine.* St. Pete Beach, FL. Oral Presentation.

October 2018. Engineered CpG-loaded Prussian blue nanoparticles as nanoimmunotherapy agents for neuroblastoma. *Biomedical Engineering Society Conference (BMEs).* Atlanta, GA. Oral Presentation.

May 2018. CpG-loaded Prussian blue nanoparticles as nanoimmunotherapy agents for neuroblastoma. *Society for Thermal Medicine.* Tucson, AZ. Oral Presentation.

April 2018. CpG-loaded Prussian blue nanoparticles as nanoimmunotherapy agents for cancer. *GW Cancer Center Retreat.* Washington D.C. Poster Presentation

April 2018. CpG-loaded Prussian blue nanoparticles as nanoimmunotherapy agents for cancer. *GW Research Day*, Washington D.C. Poster Presentation

May 2017. Prussian blue nanoparticle-based photothermal therapy combined with checkpoint inhibition for photothermal immunotherapy of neuroblastoma. *Society for Thermal Medicine.* Cancun, Mexico. Oral Presentation, Session Co-Chair.

April 2017. CpG-loaded Prussian blue nanoparticles as nano-immunotherapy agents for cancer. *Children's National Medical Center Research and Education Week*. Washington, D.C. Poster Presentation.

November 2016. Prussian blue nanoparticle-based photothermal therapy combined with checkpoint inhibition for photothermal immunotherapy of neuroblastoma. *Joseph E. Robert, Jr. Center for Surgical Care Research Day.* Washington, DC. Oral Presentation.

October 2016. Prussian blue nanoparticle-based photothermal therapy combined with checkpoint inhibition for photothermal immunotherapy of neuroblastoma. *Biomedical Engineering Society Conference (BMEs).* Minneapolis, Minnesota. Oral Presentation.

September 2016. Prussian blue nanoparticle-based photothermal therapy combined with checkpoint inhibition for photothermal immunotherapy of neuroblastoma. *14th International Nanomedicine and Drug Delivery Symposium (NanoDDS).* Baltimore, MD. Poster Presentation

April 2016. Prussian blue nanoparticle-based photothermal therapy combined with checkpoint inhibition for photothermal immunotherapy of neuroblastoma. *Children's National Medical Center Research and Education Week.* Washington, DC. Poster Presentation.

October 2015. Prussian blue nanoparticles for photothermal immunotherapy of advanced cancers. Tampa, FL. Poster Presentation

April 2015. Engineered Prussian blue nanoparticles for photothermal immunotherapy of neuroblastoma. *Children's National Medical Center Research and Education Week.* Washington, DC. Poster Presentation.

Awards and Honors

GW Cancer Center Retreat (2018)

First place for the poster "CpG-loaded Prussian blue nanoparticles as nanoimmunotherapy agents for cancer"

$2,000 towards conference of choice.

Society for Thermal Medicine Co-Chair (2017)

Selected as co-chair for the "Photodynamic and Novel Combination Therapies" session for the 2017 Society for Thermal Medicine conference.

Society for Thermal Medicine Young Investigator Award (2017)

National Science Foundation (NSF) LSAMP Bridge to the Doctorate Fellowship (2014-2015)

$30,000 yearly student stipend and tuition remission.

References

1. Siegel, R.L., K.D. Miller, and A. Jemal, *Cancer statistics, 2019.* CA Cancer J Clin, 2019. **69**(1): p. 7-34.
2. Ward, E., et al., *Childhood and adolescent cancer statistics, 2014.* CA Cancer J Clin, 2014. **64**(2): p. 83-103.
3. Pinto, N.R., et al., *Advances in Risk Classification and Treatment Strategies for Neuroblastoma.* J Clin Oncol, 2015. **33**(27): p. 3008-17.
4. Brodeur, G.M., et al., *Neuroblastoma*, in *Principles and Practice of Pediatric Oncology*, P.A. Pizzo and D.G. Poplack, Editors. 2010, Wolters Kluwer Health/Lippincott Williams & Wilkins: Philadelphia, PA. p. 886-922.
5. Bellanti, F., B. Kågedal, and O. Della Pasqua, *Do pharmacokinetic polymorphisms explain treatment failure in high-risk patients with neuroblastoma?* Eur J Clin Pharmacol, 2011. **67 Suppl 1**: p. 87-107.
6. Pugh, T.J., et al., *The genetic landscape of high-risk neuroblastoma.* Nat Genet, 2013. **45**(3): p. 279-84.
7. Lawrence, M.S., et al., *Mutational heterogeneity in cancer and the search for new cancer-associated genes.* Nature, 2013. **499**(7457): p. 214-8.
8. Pistoia, V., et al., *Immunosuppressive microenvironment in neuroblastoma.* Front Oncol, 2013. **3**: p. 167.
9. Rabinovich, G.A., D. Gabrilovich, and E.M. Sotomayor, *Immunosuppressive strategies that are mediated by tumor cells.* Annu Rev Immunol, 2007. **25**: p. 267-96.
10. Beatty, G.L. and W.L. Gladney, *Immune escape mechanisms as a guide for cancer immunotherapy.* Clin Cancer Res, 2015. **21**(4): p. 687-92.
11. Schumacher, T.N. and R.D. Schreiber, *Neoantigens in cancer immunotherapy.* Science, 2015. **348**(6230): p. 69-74.
12. Gubin, M.M., et al., *Tumor neoantigens: building a framework for personalized cancer immunotherapy.* J Clin Invest, 2015. **125**(9): p. 3413-21.
13. London, W.B., et al., *Clinical and biologic features predictive of survival after relapse of neuroblastoma: a report from the International Neuroblastoma Risk Group project.* J Clin Oncol, 2011. **29**(24): p. 3286-92.
14. von Stedingk, K., D. Gisselsson, and D. Bexell, *Multidimensional intratumour heterogeneity in neuroblastoma.* Oncotarget, 2019. **10**(1): p. 3-5.
15. Layer, J.P., et al., *Amplification of N-Myc is associated with a T-cell-poor microenvironment in metastatic neuroblastoma restraining interferon pathway activity and chemokine expression.* Oncoimmunology, 2017. **6**(6): p. e1320626.
16. Quezada, S.A., et al., *Shifting the equilibrium in cancer immunoediting: from tumor tolerance to eradication.* Immunol Rev, 2011. **241**(1): p. 104-18.
17. Koebel, C.M., et al., *Adaptive immunity maintains occult cancer in an equilibrium state.* Nature, 2007. **450**(7171): p. 903-7.

18. Hoffman, H.A., et al., *Prussian blue nanoparticles for laser-induced photothermal therapy of tumors.* RSC Advances, 2014. **4**(56): p. 29729-29734.
19. Cano-Mejia, J., et al., *Prussian blue nanoparticle-based photothermal therapy combined with checkpoint inhibition for photothermal immunotherapy of neuroblastoma.* Nanomedicine Nanotechnol Biol Med, 2017. **13**(2): p. 771-781.
20. Guo, L., et al., *Combinatorial photothermal and immuno cancer therapy using chitosan-coated hollow copper sulfide nanoparticles.* ACS Nano, 2014. **8**(6): p. 5670-81.
21. Wang, C., et al., *Immunological responses triggered by photothermal therapy with carbon nanotubes in combination with anti-CTLA-4 therapy to inhibit cancer metastasis.* Adv Mater, 2014. **26**(48): p. 8154-62.
22. Chen, W., et al., *Combining photothermal therapy and immunotherapy against melanoma by polydopamine-coated Al2O3 nanoparticles.* Theranostics, 2018. **8**(8): p. 2229-2241.
23. Bear, A.S., et al., *Elimination of metastatic melanoma using gold nanoshell-enabled photothermal therapy and adoptive T cell transfer.* PLoS One, 2013. **8**(7): p. e69073.
24. Iyer, A.K., et al., *Exploiting the enhanced permeability and retention effect for tumor targeting.* Drug Discov Today, 2006. **11**(17-18): p. 812-8.
25. Greish, K., *Enhanced permeability and retention (EPR) effect for anticancer nanomedicine drug targeting.* Methods Mol Biol, 2010. **624**: p. 25-37.
26. Faustino, P.J., et al., *Quantitative determination of cesium binding to ferric hexacyanoferrate: Prussian blue.* J Pharm Biomed Anal, 2008. **47**(1): p. 114-25.
27. Dumont, M.F., et al., *Biofunctionalized Gadolinium-Containing Prussian Blue Nanoparticles as Multimodal Molecular Imaging Agents.* Bioconjug Chem, 2014. **25**(1): p. 129-137.
28. Dumont, M.F., et al., *Manganese-containing Prussian blue nanoparticles for imaging of pediatric brain tumors.* Int J Nanomed, 2014. **9**: p. 2581-2595.
29. Verzijl, J.M., et al., *In vitro cyanide release of four prussian blue salts used for the treatment of cesium contaminated persons.* J Toxicol Clin Toxicol, 1993. **31**(4): p. 553-62.
30. Kale, S.S., et al., *Composite iron oxide-Prussian blue nanoparticles for magnetically guided T1-weighted magnetic resonance imaging and photothermal therapy of tumors.* Int J Nanomedicine, 2017. **12**: p. 6413-6424.
31. Vojtech, J.M., et al., *Biofunctionalized prussian blue nanoparticles for multimodal molecular imaging applications.* J Vis Exp, 2015(98): p. e52621.
32. den Brok, M.H., et al., *In situ tumor ablation creates an antigen source for the generation of antitumor immunity.* Cancer Res, 2004. **64**(11): p. 4024-9.
33. Couzin-Frankel, J., *Breakthrough of the year 2013. Cancer immunotherapy.* Science, 2013. **342**(6165): p. 1432-3.
34. Mulder, W.J.M. and S. Gnjatic, *Cancer Immunotherapy from Local to Global.* Nature Nanotechnology, 2017. **12**(9): p. 840-841.

35. Hodi, F.S., et al., *Improved survival with ipilimumab in patients with metastatic melanoma.* N Engl J Med, 2010. **363**(8): p. 711-23.
36. Larkin, J., et al., *Combined Nivolumab and Ipilimumab or Monotherapy in Untreated Melanoma.* N Engl J Med, 2015. **373**(1): p. 23-34.
37. McArthur, H.L. and D.B. Page, *Immunotherapy for the treatment of breast cancer: checkpoint blockade, cancer vaccines, and future directions in combination immunotherapy.* Clin Adv Hematol Oncol, 2016. **14**(11): p. 922-933.
38. Postow, M.A., et al., *Nivolumab and ipilimumab versus ipilimumab in untreated melanoma.* N Engl J Med, 2015. **372**(21): p. 2006-17.
39. Wolchok, J.D., et al., *Nivolumab plus ipilimumab in advanced melanoma.* N Engl J Med, 2013. **369**(2): p. 122-33.
40. Leach, D.R., M.F. Krummel, and J.P. Allison, *Enhancement of antitumor immunity by CTLA-4 blockade.* Science, 1996. **271**(5256): p. 1734-6.
41. Peggs, K.S., et al., *Blockade of CTLA-4 on both effector and regulatory T cell compartments contributes to the antitumor activity of anti-CTLA-4 antibodies.* J Exp Med, 2009. **206**(8): p. 1717-25.
42. Peggs, K.S., et al., *Principles and use of anti-CTLA4 antibody in human cancer immunotherapy.* Curr Opin Immunol, 2006. **18**: p. 206-213.
43. Iwai, Y., et al., *Cancer immunotherapies targeting the PD-1 signaling pathway.* J Biomed Sci, 2017. **24**(1): p. 26.
44. Dudley, M.E. and S.A. Rosenberg, *Adoptive-cell-transfer therapy for the treatment of patients with cancer.* Nat Rev Cancer, 2003. **3**(9): p. 666-75.
45. Rosenberg, S.A., et al., *Adoptive cell transfer: a clinical path to effective cancer immunotherapy.* Nat Rev Cancer, 2008. **8**(4): p. 299-308.
46. Knochelmann, H.M., et al., *CAR T Cells in Solid Tumors: Blueprints for Building Effective Therapies.* Front Immunol, 2018. **9**: p. 1740.
47. Pardoll, D.M., *Cancer vaccines.* Nat Med, 1998. **4**(5 Suppl): p. 525-31.
48. Adams, S., *Toll-like receptor agonists in cancer therapy.* Immunotherapy, 2009. **1**(6): p. 949-64.
49. Krieg, A.M., *Toll-like receptor 9 (TLR9) agonists in the treatment of cancer.* Oncogene, 2008. **27**(2): p. 161-7.
50. Melisi, D., et al., *Toll-Like Receptor 9 Agonists for Cancer Therapy.* Biomedicines, 2014. **2**(3): p. 211-228.
51. Michot, J.M., et al., *Immune-related adverse events with immune checkpoint blockade: a comprehensive review.* Eur J Cancer, 2016. **54**: p. 139-48.
52. Goldberg, M.S., *Immunoengineering: how nanotechnology can enhance cancer immunotherapy.* Cell, 2015. **161**(2): p. 201-4.
53. Carpentier, A.F., et al., *Oligodeoxynucleotides containing CpG motifs can induce rejection of a neuroblastoma in mice.* Cancer Res, 1999. **59**(21): p. 5429-32.
54. Lee, B.L. and G.M. Barton, *Trafficking of endosomal Toll-like receptors.* Trends Cell Biol, 2014. **24**(6): p. 360-9.
55. Pilon-Thomas, S., et al., *Immunostimulatory effects of CpG-ODN upon dendritic cell-based immunotherapy in a murine melanoma model.* J Immunother, 2006. **29**(4): p. 381-7.

56. Bourquin, C., et al., *Targeting CpG oligonucleotides to the lymph node by nanoparticles elicits efficient antitumoral immunity.* J Immunol, 2008. **181**(5): p. 2990-8.
57. Han, Q., et al., *CpG loaded MoS2 nanosheets as multifunctional agents for photothermal enhanced cancer immunotherapy.* Nanoscale, 2017. **9**(18): p. 5927-5934.
58. Tao, Y., et al., *Engineered, self-assembled near-infrared photothermal agents for combined tumor immunotherapy and chemo-photothermal therapy.* Biomaterials, 2014. **35**(24): p. 6646-56.
59. Tao, Y., et al., *Immunostimulatory oligonucleotides-loaded cationic graphene oxide with photothermally enhanced immunogenicity for photothermal/immune cancer therapy.* Biomaterials, 2014. **35**(37): p. 9963-71.
60. Yang, L., et al., *Therapeutic injection of C-class CpG ODN in draining lymph node area induces potent activation of immune cells and rejection of established breast cancer in mice.* Clin Immunol, 2009. **131**(3): p. 426-37.
61. Fu, G., et al., *Prussian blue nanoparticles operate as a new generation of photothermal ablation agents for cancer therapy.* Chem Commun 2012. **48**: p. 11567–11569.
62. Sweeney, E.E., J. Cano-Mejia, and R. Fernandes, *Photothermal Therapy Generates a Thermal Window of Immunogenic Cell Death in Neuroblastoma.* Small, 2018: p. e1800678.
63. Burga, R.A., et al., *Conjugating Prussian blue nanoparticles onto antigen-specific T cells as a combined nanoimmunotherapy.* Nanomedicine (Lond), 2016. **11**(14): p. 1759-67.
64. Sweeney, E.E., et al., *Photothermal therapy improves the efficacy of a MEK inhibitor in neurofibromatosis type 1-associated malignant peripheral nerve sheath tumors.* Sci Reports, 2016. **6**: p. 37035.
65. Sabel, M.S., et al., *Immunologic response to cryoablation of breast cancer.* Breast Cancer Res Treat, 2005. **90**(1): p. 97-104.
66. Wu, F., L. Zhou, and W.R. Chen, *Host antitumour immune responses to HIFU ablation.* Int J Hyperthermia, 2007. **23**(2): p. 165-71.
67. Pan, J., et al., *Antigen-Directed Fabrication of a Multifunctional Nanovaccine with Ultrahigh Antigen Loading Efficiency for Tumor Photothermal-Immunotherapy.* Adv Mater, 2018. **30**(8).
68. Du, G., et al., *Intradermal vaccination with hollow microneedles: A comparative study of various protein antigen and adjuvant encapsulated nanoparticles.* J Control Release, 2017. **266**: p. 109-118.
69. Chiu, Y.C., et al., *Modular Vaccine Design Using Carrier-Free Capsules Assembled from Polyionic Immune Signals.* ACS Biomater Sci Eng, 2015. **1**(12): p. 1200-1205.
70. Chiu, Y.C., et al., *Assembly and Immunological Processing of Polyelectrolyte Multilayers Composed of Antigens and Adjuvants.* ACS Appl Mater Interfaces, 2016. **8**(29): p. 18722-31.
71. Hess, K.L., et al., *Polyplexes assembled from self-peptides and regulatory nucleic acids blunt toll-like receptor signaling to combat autoimmunity.* Biomaterials, 2017. **118**: p. 51-62.

72. Hotaling, N.A., et al., *Biomaterial Strategies for Immunomodulation.* Annu Rev Biomed Eng, 2015. **17**: p. 317-49.
73. Song, C., R. Griffin, and H.J. Park, *Influence of Tumor pH in Therapeutic Response*, in *Cancer Drug Discovery and Development: Cancer Drug Resistance*, B.T.H.P. Inc., Editor 2006: Totowa, NJ. p. 21-42.
74. Meng, F.H., et al., *Intracellular drug release nanosystems.* Materials Today, 2012. **15**(10): p. 436-442.
75. Itaya, K., H. Akahoshi, and S. Toshima, *Electrochemistry of Prussian Blue Modified Electrodes: An Electrochemical Preparation Method.* J Electrochem Soc, 1982. **129**(7): p. 1498-1500.
76. Karyakin, A.A., *Prussian Blue and Its Analogues: Electrochemistry and Analytical Applications.* Electroanal, 2001. **13**(10): p. 813-819.
77. Zhang, P., et al., *Polyelectrolyte Multilayers Assembled Entirely from Immune Signals on Gold Nanoparticle Templates Promote Antigen-Specific T Cell Response.* ACS Nano, 2015. **9**(6): p. 6465-77.
78. De Koker, S., et al., *Polymeric multilayer capsules delivering biotherapeutics.* Adv Drug Deliv Rev, 2011. **63**(9): p. 748-61.
79. DeMuth, P.C., et al., *Polymer multilayer tattooing for enhanced DNA vaccination.* Nat Mater, 2013. **12**(4): p. 367-76.
80. Tostanoski, L.H., et al., *Design of Polyelectrolyte Multilayers to Promote Immunological Tolerance.* ACS Nano, 2016.
81. Zeng, Q., et al., *In Vivo Expansion of Melanoma-Specific T Cells Using Microneedle Arrays Coated with Immune-Polyelectrolyte Multilayers.* ACS Biomater Sci Eng, 2017. **3**(2): p. 195-205.
82. Bookstaver, M.L., et al., *Improving Vaccine and Immunotherapy Design Using Biomaterials.* Trends Immunol, 2018. **39**(2): p. 135-150.
83. Loo, C., et al., *Immunotargeted nanoshells for integrated cancer imaging and therapy.* Nano Lett, 2005. **5**(4): p. 709-11.
84. Roper, D.K., W. Ahn, and M. Hoepfner, *Microscale Heat Transfer Transduced by Surface Plasmon Resonant Gold Nanoparticles.* J Phys Chem C Nanomater Interfaces, 2007. **111**(9): p. 3636-3641.
85. Dickerson, E.B., et al., *Gold nanorod assisted near-infrared plasmonic photothermal therapy (PPTT) of squamous cell carcinoma in mice.* Cancer Lett, 2008. **269**(1): p. 57-66.
86. Lal, S., S.E. Clare, and N.J. Halas, *Nanoshell-enabled photothermal cancer therapy: impending clinical impact.* Acc Chem Res, 2008. **41**(12): p. 1842-51.
87. Cobley, C.M., et al., *Targeting gold nanocages to cancer cells for photothermal destruction and drug delivery.* Expert Opin Drug Deliv, 2010. **7**(5): p. 577-87.
88. Huang, N., et al., *Single-wall carbon nanotubes assisted photothermal cancer therapy: animal study with a murine model of squamous cell carcinoma.* Lasers Surg Med, 2010. **42**(9): p. 638-48.
89. Yu, J.G., et al., *Irradiation-mediated carbon nanotubes' use in cancer therapy.* J Cancer Res Ther, 2012. **8**(3): p. 348-54.

90. Burke, A.R., et al., *The resistance of breast cancer stem cells to conventional hyperthermia and their sensitivity to nanoparticle-mediated photothermal therapy.* Biomaterials, 2012. **33**(10): p. 2961-70.
91. Lv, R., et al., *In Situ Growth Strategy to Integrate Up-Conversion Nanoparticles with Ultrasmall CuS for Photothermal Theranostics.* ACS Nano, 2017. **11**(1): p. 1064-1072.
92. Xu, J., et al., *Integration of IR-808 Sensitized Upconversion Nanostructure and MoS2 Nanosheet for 808 nm NIR Light Triggered Phototherapy and Bioimaging.* Small, 2017. **13**(36).
93. Pattani, V.P., et al., *Role of apoptosis and necrosis in cell death induced by nanoparticle-mediated photothermal therapy.* J Nanopart Res, 2015. **17**: p. 20.
94. Fay, B.L., J.R. Melamed, and E.S. Day, *Nanoshell-mediated photothermal therapy can enhance chemotherapy in inflammatory breast cancer cells.* Int J Nanomedicine, 2015. **10**: p. 6931-41.
95. Chen, Q., et al., *Photothermal therapy with immune-adjuvant nanoparticles together with checkpoint blockade for effective cancer immunotherapy.* Nat Commun, 2016. **7**: p. 13193.
96. Galluzzi, L., et al., *Immunogenic cell death in cancer and infectious disease.* Nat Rev Immunol, 2017. **17**(2): p. 97-111.
97. Galluzzi, L., et al., *Molecular mechanisms of cell death: recommendations of the Nomenclature Committee on Cell Death 2018.* Cell Death Differ, 2018.
98. Kroemer, G., et al., *Immunogenic cell death in cancer therapy.* Annu Rev Immunol, 2013. **31**: p. 51-72.
99. Kepp, O., et al., *Consensus guidelines for the detection of immunogenic cell death.* Oncoimmunology, 2014. **3**(9): p. e955691.
100. Ladoire, S., et al., *Immunogenic cell death-related biomarkers: Impact on the survival of breast cancer patients after adjuvant chemotherapy.* Oncoimmunology, 2016. **5**(2): p. e1082706.
101. Menger, L., et al., *Cardiac glycosides exert anticancer effects by inducing immunogenic cell death.* Sci Transl Med, 2012. **4**(143): p. 143ra99.
102. Angelova, A.L., et al., *Complementary induction of immunogenic cell death by oncolytic parvovirus H-1PV and gemcitabine in pancreatic cancer.* J Virol, 2014. **88**(10): p. 5263-76.
103. Garg, A.D., et al., *Immunogenic cell death.* Int J Dev Biol, 2015. **59**(1-3): p. 131-40.
104. FDA:. *Radiogardase - ferric hexacyanoferrate(ii) capsule: http://www.accessdata.fda.gov/drugsatfda_docs/label/2008/021626s007lbl.pdf.* February 9, 2018].
105. Yang, Y., et al., *Quantitative determination of thallium binding to ferric hexacyanoferrate: Prussian blue.* Int J Pharm, 2008. **353**(1-2): p. 187-94.
106. Burga, R.A., et al., *Conjugating Prussian blue nanoparticles onto antigen-specific T cells as a combined nanoimmunotherapy.* Nanomedicine (Lond), 2016. **11**(14): p. 1759-67.
107. Chakrabarti, L., et al., *Reversible adaptive plasticity: a mechanism for neuroblastoma cell heterogeneity and chemo-resistance.* Front Oncol, 2012. **2**: p. 82.

108. Chakrabarti, L., et al., *A Mechanism Linking Id2-TGFbeta Crosstalk to Reversible Adaptive Plasticity in Neuroblastoma.* PLoS One, 2013. **8**(12): p. e83521.
109. Chakrabarti, L., C. Morgan, and A.D. Sandler, *Combination of Id2 Knockdown Whole Tumor Cells and Checkpoint Blockade: A Potent Vaccine Strategy in a Mouse Neuroblastoma Model.* PLoS One, 2015. **10**(6): p. e0129237.
110. Siegel, R.L., K.D. Miller, and A. Jemal, *Cancer Statistics, 2017.* CA Cancer J Clin, 2017. **67**(1): p. 7-30.
111. Dumont, M.F., et al., *Manganese-containing Prussian blue nanoparticles for imaging of pediatric brain tumors.* Int J Nanomedicine, 2014. **9**: p. 2581-95.
112. Sapareto, S.A. and W.C. Dewey, *Thermal dose determination in cancer therapy.* Int J Radiat Oncol Biol Phys, 1984. **10**(6): p. 787-800.
113. van Rhoon, G.C., et al., *Health Council of The Netherlands: no need to change from SAR to time-temperature relation in electromagnetic fields exposure limits.* Int J Hyperthermia, 2011. **27**(4): p. 399-404.
114. Maguire, P.D., et al., *A phase II trial testing the thermal dose parameter CEM43 degrees T90 as a predictor of response in soft tissue sarcomas treated with pre-operative thermoradiotherapy.* Int J Hyperthermia, 2001. **17**(4): p. 283-90.
115. Yarmolenko, P.S., et al., *Thresholds for thermal damage to normal tissues: an update.* Int J Hyperthermia, 2011. **27**(4): p. 320-43.
116. de Bruijne, M., et al., *Evaluation of CEM43 degrees CT90 thermal dose in superficial hyperthermia: a retrospective analysis.* Strahlenther Onkol, 2010. **186**(8): p. 436-43.
117. Scaffidi, P., T. Misteli, and M.E. Bianchi, *Release of chromatin protein HMGB1 by necrotic cells triggers inflammation.* Nature, 2002. **418**(6894): p. 191-5.
118. Bianchi, M.E., et al., *High-mobility group box 1 protein orchestrates responses to tissue damage via inflammation, innate and adaptive immunity, and tissue repair.* Immunol Rev, 2017. **280**(1): p. 74-82.
119. Dumitriu, I.E., et al., *The secretion of HMGB1 is required for the migration of maturing dendritic cells.* J Leukoc Biol, 2007. **81**(1): p. 84-91.
120. Raffaghello, L., et al., *Multiple defects of the antigen-processing machinery components in human neuroblastoma: immunotherapeutic implications.* Oncogene, 2005. **24**(29): p. 4634-44.
121. Lorenzi, S., et al., *IRF1 and NF-kB restore MHC class I-restricted tumor antigen processing and presentation to cytotoxic T cells in aggressive neuroblastoma.* PLoS One, 2012. **7**(10): p. e46928.
122. Martinez, R.J. and B.D. Evavold, *Lower Affinity T Cells are Critical Components and Active Participants of the Immune Response.* Front Immunol, 2015. **6**: p. 468.
123. Luo, L., et al., *Laser Immunotherapy in Combination with Perdurable PD-1 Blocking for the Treatment of Metastatic Tumors.* ACS Nano, 2018. **12**(8): p. 7647-7662.

124. Min, Y., et al., *Antigen-capturing nanoparticles improve the abscopal effect and cancer immunotherapy.* Nat Nanotechnol, 2017. **12**(9): p. 877-882.
125. Postow, M.A., et al., *Immunologic correlates of the abscopal effect in a patient with melanoma.* N Engl J Med, 2012. **366**(10): p. 925-31.
126. Alexander, W., *The Checkpoint Immunotherapy Revolution: What Started as a Trickle Has Become a Flood, Despite Some Daunting Adverse Effects; New Drugs, Indications, and Combinations Continue to Emerge.* P T, 2016. **41**(3): p. 185-91.
127. Mehta, A., R. Oklu, and R.A. Sheth, *Thermal Ablative Therapies and Immune Checkpoint Modulation: Can Locoregional Approaches Effect a Systemic Response?* Gastroenterology Research and Practice, 2016.
128. Topalian, S.L., C.G. Drake, and D.M. Pardoll, *Immune checkpoint blockade: a common denominator approach to cancer therapy.* Cancer Cell, 2015. **27**(4): p. 450-61.
129. Le, K., et al., *Assessment of thermal effects of interstitial laser phototherapy on mammary tumors using proton resonance frequency method.* J Biomed Opt, 2011. **16**(12): p. 128001.
130. Yu, A.L., et al., *Anti-GD2 antibody with GM-CSF, interleukin-2, and isotretinoin for neuroblastoma.* N Engl J Med, 2010. **363**(14): p. 1324-34.
131. Cheung, N.K., et al., *FCGR2A polymorphism is correlated with clinical outcome after immunotherapy of neuroblastoma with anti-GD2 antibody and granulocyte macrophage colony-stimulating factor.* J Clin Oncol, 2006. **24**(18): p. 2885-90.
132. Yang, R.K. and P.M. Sondel, *Anti-GD2 Strategy in the Treatment of Neuroblastoma.* Drugs Future, 2010. **35**(8): p. 665.
133. Wolfl, M., et al., *Expression of MHC class I, MHC class II, and cancer germline antigens in neuroblastoma.* Cancer Immunol Immunother, 2005. **54**(4): p. 400-6.
134. Prigione, I., et al., *Immunogenicity of human neuroblastoma.* Ann N Y Acad Sci, 2004. **1028**: p. 69-80.
135. Weiss, W.A., et al., *Targeted expression of MYCN causes neuroblastoma in transgenic mice.* EMBO J, 1997. **16**(11): p. 2985-95.
136. Alam, G., et al., *MYCN promotes the expansion of Phox2B-positive neuronal progenitors to drive neuroblastoma development.* Am J Pathol, 2009. **175**(2): p. 856-66.
137. Moore, H.C., et al., *Histological profile of tumours from MYCN transgenic mice.* J Clin Pathol, 2008. **61**(10): p. 1098-103.
138. Hackett, C.S., et al., *Genome-wide array CGH analysis of murine neuroblastoma reveals distinct genomic aberrations which parallel those in human tumors.* Cancer Res, 2003. **63**(17): p. 5266-73.
139. Terrile, M., et al., *miRNA expression profiling of the murine TH-MYCN neuroblastoma model reveals similarities with human tumors and identifies novel candidate miRNAs.* PLoS One, 2011. **6**(12): p. e28356.
140. Kroesen, M., et al., *A transplantable TH-MYCN transgenic tumor model in C57Bl/6 mice for preclinical immunological studies in neuroblastoma.* Int J Cancer, 2014. **134**(6): p. 1335-45.

141. Azuhata, T., et al., *The inhibitor of apoptosis protein survivin is associated with high-risk behavior of neuroblastoma.* J Pediatr Surg, 2001. **36**(12): p. 1785-91.
142. Lamers, F., et al., *Knockdown of survivin (BIRC5) causes apoptosis in neuroblastoma via mitotic catastrophe.* Endocr Relat Cancer, 2011. **18**(6): p. 657-68.
143. Wasik, U., et al., *Influence of S100A6 on CacyBP/SIP Phosphorylation and Elk-1 Transcriptional Activity in Neuroblastoma NB2a Cells.* J Cell Biochem, 2016. **117**(1): p. 126-31.
144. Rounbehler, R.J., et al., *Targeting ornithine decarboxylase impairs development of MYCN-amplified neuroblastoma.* Cancer Res, 2009. **69**(2): p. 547-53.
145. Hogarty, M.D., et al., *ODC1 is a critical determinant of MYCN oncogenesis and a therapeutic target in neuroblastoma.* Cancer Res, 2008. **68**(23): p. 9735-45.
146. Lo Piccolo, M.S., N.K. Cheung, and I.Y. Cheung, *GD2 synthase: a new molecular marker for detecting neuroblastoma.* Cancer, 2001. **92**(4): p. 924-31.
147. Schulz, G., et al., *Detection of ganglioside GD2 in tumor tissues and sera of neuroblastoma patients.* Cancer Res, 1984. **44**(12 Pt 1): p. 5914-20.
148. Ara, T. and Y.A. DeClerck, *Mechanisms of invasion and metastasis in human neuroblastoma.* Cancer Metastasis Rev, 2006. **25**(4): p. 645-57.
149. Su, B., et al., *Systemic TNFalpha gene therapy synergizes with liposomal doxorubicine in the treatment of metastatic cancer.* Mol Ther, 2013. **21**(2): p. 300-8.
150. Stauffer, J.K., et al., *High-throughput molecular and histopathologic profiling of tumor tissue in a novel transplantable model of murine neuroblastoma: new tools for pediatric drug discovery.* Cancer Invest, 2012. **30**(5): p. 343-63.